NOLTR 72-124

REFRACTION OF UNDERWATER EXPLOSION SHOCK WAVES: SARGASSO SEA MEASUREMENTS

By
Robert Thrun

17 JULY 1972

NOL

NAVAL ORDNANCE LABORATORY, WHITE OAK, SILVER SPRING, MARYLAND

NOLTR 72-124

UNCLASSIFIED

Security Classification

DOCUMENT CONTROL DATA - R & D

Security classification of title, body of abstract and indexing annotation must be entered when the overall report is classified)

1 ORIGINATING ACTIVITY (Corporate author)	2a. REPORT SECURITY CLASSIFICATION
Naval Ordnance Laboratory White Oak, Silver Spring, Md. 20910	UNCLASSIFIED 2b. GROUP

3 REPORT TITLE

Refraction of Underwater Explosion Shock Waves: Sargasso Sea Measurements

4 DESCRIPTIVE NOTES (Type of report and inclusive dates)

5 AUTHOR(S) (First name, middle initial, last name)

Robert Thrun

6 REPORT DATE	7a. TOTAL NO OF PAGES	7b. NO. OF REFS
17 July 1972	iii + 66	8

8a. CONTRACT OR GRANT NO	9a. ORIGINATOR'S REPORT NUMBER(S)
b. PROJECT NO NA 002/20	NOLTR 72-124
c.	9b. OTHER REPORT NO(S) (Any other numbers that may be assigned this report)
d.	

10 DISTRIBUTION STATEMENT

Approved for public release; distribution unlimited

11 SUPPLEMENTARY NOTES	12 SPONSORING MILITARY ACTIVITY
	Defense Nuclear Agency Washington, D. C. 20360

13 ABSTRACT

An experiment was conducted in the Sargasso Sea to measure the effect of refraction on underwater explosion shock waves. Sound velocity profiles were measured during the experiment. Eight-lb and 900-lb charges were detonated at precisely controlled depths. The explosion pulses at the close-in (thermocline-related) caustic and at the first convergence zone were measured by a vertical array of gages and recorded. The measured shock wave peak pressures, impulses, and energies are compared with what might be expected under isovelocity conditions. Some of the shock wave pulses and frequency spectra are presented. A considerable enhancement of pressures and energies was observed.

DD FORM 1 NOV 65 1473 (PAGE 1)

S/N 0101-807-6801

UNCLASSIFIED

Security Classification

14 KEY WORDS	LINK A		LINK B		LINK C	
	ROLE	WT	ROLE	WT	ROLE	WT
Underwater Explosions						
Refraction						
Shock Waves						
Sound Velocity						
Frequency Spectra						
Convergence Zones						

NOLTR 72-124

REFRACTION OF UNDERWATER EXPLOSION SHOCK WAVES: SARGASSO SEA MEASUREMENTS

by:
Robert Thrun

ABSTRACT: An experiment was conducted in the Sargasso Sea to measure the effect of refraction on underwater explosion shock waves. Sound velocity profiles were measured during the experiment. Eight-lb and 900-lb charges were detonated at precisely controlled depths. The explosion pulses at the close-in (thermocline-related) caustic and at the first convergence zone were measured by a vertical array of gages and recorded. The measured shock wave peak pressures, impulses, and energies are compared with what might be expected under isovelocity conditions. Some of the shock wave pulses and frequency spectra are presented. A considerable enhancement of pressures and energies was observed.

EXPLOSIONS RESEARCH DEPARTMENT
UNDERWATER EXPLOSIONS DIVISION
NAVAL ORDNANCE LABORATORY
WHITE OAK, SILVER SPRING, MARYLAND

NOLTR 72-124

17 July 1972

Refraction of Underwater Explosion Shock Waves: Sargasso Sea Measurements

This report presents a description and analysis of data obtained by the Naval Ordnance Laboratory in an oceanic experiment on the refraction of underwater explosion shock waves. This analysis was funded by the Defense Atomic Support Agency (now the Defense Nuclear Agency) under its Work Unit NA-002/20. Mention of commercially available equipment does not constitute an endorsement or criticism by the Laboratory.

ROBERT WILLIAMSON II
Captain, USN
Commander

C. J. ARONSON
By direction

CONTENTS

ILLUSTRATIONS

TABLES

REFRACTION OF UNDERWATER EXPLOSION SHOCK WAVES: SARGASSO SEA MEASUREMENTS

1. INTRODUCTION

1.1 Earlier studies have indicated that gradients in sound velocity can influence the propagation of shock waves (references 1, 2, 3, 4). Because of refraction, the pulse shapes (pressure vs time) are considerably distorted from the shapes that would be expected in isovelocity water. The regions of shock wave enhancement are of interest, particularly caustics. Caustics are focal surfaces where the strongest energy focusing occurs.

1.2 In April and May 1966, NOL conducted a series of tests in the Sargasso Sea to investigate caustics in the ocean. Convergence zone caustics were of primary interest. Convergence zones are regions where sound or explosion pulses that propagate along deep ocean paths are bent upward and focused by the sound velocity gradient in the ocean. Some measurements of close-in caustics were also made. These tests were in several ways an extension of tests made in the Dickerson quarry (reference 4). Both series concentrated on measuring shock wave pressure histories at the caustic with a relatively close gage spacing. The two experiments differed in size. The Sargasso Sea experiment had much greater ranges and larger ratios of range to charge dimension. The convergence zone caustic was at a relative minimum in range. (A caustic occurs when the derivative of range along ray paths at a given depth with respect to initial ray angle is zero. This can be either a relative minimum or a relative maximum in range.) The caustics in the quarry and the close-in ocean caustic (due to the surface thermocline) were at relative maxima in range.

1.3 Some theoretical treatments predict that the caustic thickness is dependent on the charge dimensions or, equivalently, the frequency content of the shock wave pulse. The quarry results tended to show this. For this reason, two charge sizes were used in the ocean, 8 pounds and 900 pounds.

2. EXPERIMENTAL PROCEDURE

Most of the details of the experimental setup are described in reference 5. These details will be summarized here. Two ships were involved in the experiment, as shown in Figure 1. The principal task of the M/V OCEANIC was the handling of explosive charges. The USNS LYNCH had equipment to record the shock wave. The ship locations, shot times, charge weights, and depths of bursts for the shots analyzed in this report (duds, equipment checkouts, etc. are omitted) are given in Appendix A.

2.1 GAGES

2.1.1 The gage array consisted of 100 hydrophones spaced along a 200-foot vertical distance. They were spaced every three feet from 0 to 57 feet (measured from the top), every one foot from 57 to 105 feet, and every three feet from 107 to 200 feet.

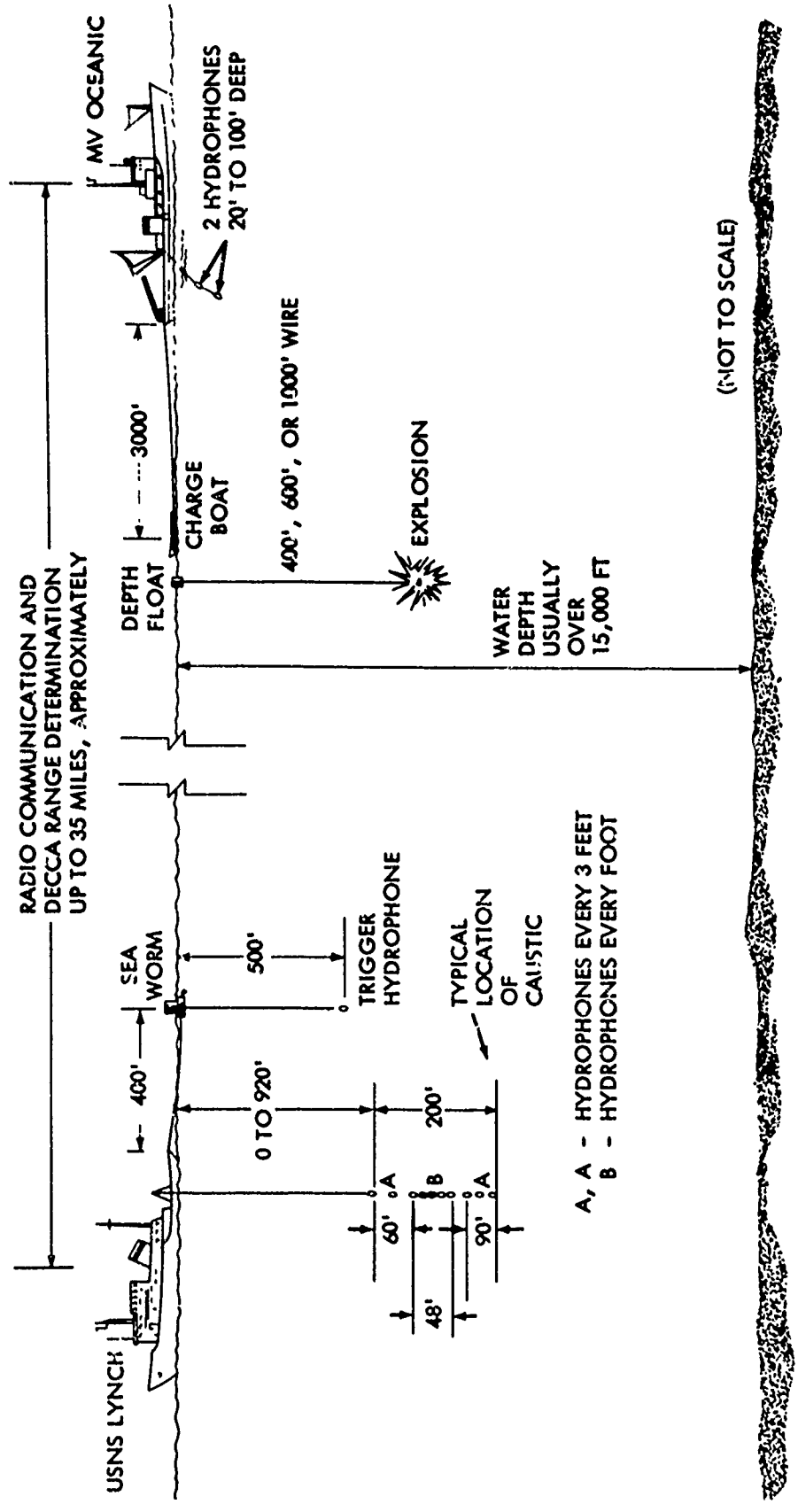

FIG. 1 TYPICAL OPERATING CONDITIONS

2.1.2 The gages were Massa type 201 hydrophones. Each of these was mounted on a gage-signal amplifier (GSA). The primary purpose of the amplifiers was to provide impedance matching between the hydrophones and signal cables. The GSA's also incorporate padding capacitors to reduce the sensitivity of the hydrophones to avoid overloading the recording system. By changing the capacitance in parallel with the hydrophones, the sensitivity could be varied so that 1, 4, 16, or 80 psi would produce a full scale deviation on the recorders. Receipt of the shock wave by a trigger gage positioned in front of the array triggered relays in the GSA's and set the proper gain just before the shock wave was recorded.

2.1.3 Because the type of hydrophone that it was necessary to use to record the low pressures encountered in this experiment was known to have irregularities in its response, every effort was made to obtain as accurate a calibration as possible. The hydrophones were calibrated by a dead weight static-pressure release apparatus before the experiment. After the experiment, the acoustic response under pressure was checked (reference 6). The response varied up to 50% (~2dB) for particular combinations of pressure and frequency, but there was no consistent trend among the samples tested. Most of the hydrophones decreased in sensitivity with increasing hydrostatic pressure, but some increased in sensitivity or remained constant. For a single hydrophone there was no uniform trend with respect to frequency or hydrostatic pressure. The possibility that some of the hydrophones were consistently high or low with respect to neighboring hydrophones was also investigated and was discounted.

2.1.4 The gage signal amplifier cases were a source of ringing for the hydrophones. This was shown in the acoustic response as a sharp drop somewhere between 6000 and 9000 Hz. The unmounted hydrophones had a smoother (but still uneven) response. Attempts to filter out the ringing by computer processing of the digitized signal were unsuccessful.

2.2 RECORDERS

2.2.1 Three different systems were used to record shock wave pressures. The primary recorder was an Ampex FR-600 magnetic tape recorder, which was used on all shots. The FR-600 provided 13 channels of shock wave recording. Oscilloscopes (Tektronix RM 565) were connected in parallel to eight of the FR-600 channels. Nine special recorders, called SPIN DRIFT recorders after the name of the project for which they were originally designed, were used on some shots. These provided up to 11 channels of shock wave recording each.

2.3 DETONATING SYSTEM

2.3.1 Because an accurate hydrostatic pressure triggered detonating system was not available, a special wire controlled firing system was used. A measured length of wire was on a spool attached to the charge. The other end of the wire was attached to a float. When the charge sank to the firing depth and unreeled the wire, tension on the wire pulled a pin on the firing device and fired the charge. Price (reference 5) estimates the depth of burst to be accurate to ±15 feet.

2.4 OPERATIONAL PROCEDURE

2.4.1 The general procedure was as follows: Relatively crude ray tracing calculations were made aboard ship, using the velocity profile measured at the test site, to predict the approximate range to the caustic. The ships separated to the predicted range, eight-pound charges were dropped directly off the OCEANIC, and the shock wave was recorded on the FR-600 aboard the LYNCH. The FR-600 records were promptly played back on a Honeywell Visicorder. From the arrival time differences (see 5.1.1) it was possible to determine the distance from the caustic. The range was then adjusted so the gage string would coincide with the caustic. When it appeared that the range had been adjusted properly, the SPIN DRIFT recorders were used to record an eight-pound shot and obtain a detailed picture of the caustic with this charge size. After this was done successfully, a 900-pound charge was launched, fired, and recorded with all recorders. This procedure was repeated with different combinations of charge and gage depths. Various operational problems, and the fact that the range to the caustic shifted, prevented this procedure from being strictly followed. The conditions for the shots analyzed in this report are shown in Appendix A.

2.5 OTHER INSTRUMENTATION

2.5.1 An ACF (now NUS) TR-4 velocimeter was carried aboard the OCEANIC. Velocimeter casts were taken at night and at times when the use of the velocimeter would not interfere with the dropping of charges. A table of casts from Price's report (reference 5) and the velocity-depth curves are presented in Appendix B. The data were used at sea for making rough predictions of caustic range and are indispensible for any theoretical calculations that are to be compared to the results of this experiment.

2.5.2 There were some velocimeter casts taken from the LYNCH, but they were not used in analyzing the data from the cruise.

2.5.3 Many bathythermograph casts were taken from the LYNCH. These provided information on sound velocity near the surface more frequently than could be measured with the velocimeters. Other instruments used included a Decca Hi-Fix ranging system for precisely determining the distance between ships.

3. SOUND VELOCITY

3.1 SOUND VELOCITY PROFILES

3.1.1 Graphs of the sound velocity profiles measured from the OCEANIC are presented in Appendix C. These are all based on the raw outputs from the velocimeter. The slight corrections for nonlinearity of the velocimeter and the change of density of water were not made. The velocimeter was temperature compensated so no correction had to be made for temperature.

3.1.2 Cast No. 11 was held at 2500 feet, approximately in the middle of the main thermocline, for several hours to observe internal waves. The depth of the velocimeter was varying because of ship motion, at the same time the velocity was varying because of internal waves. To make a correction for ship motion it was assumed that the slope of the thermocline remained constant while it moved up and down (Fig. 2).

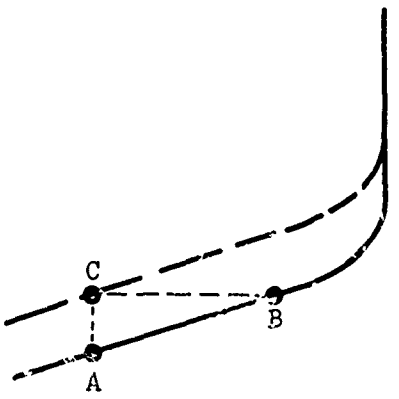

FIG. 2

A and B represent points on the thermocline while it is in the same position. C is a point on the thermocline when it is shifted upward.

R. M. Barash of the Naval Ordnance Laboratory plotted the internal wave by this method. His result is shown in Figure 3.

3.2 PROFILE VARIATIONS

3.2.1 The measured profiles were used for further studies. They were fitted with curves that were used as input to ray tracing programs.

3.2.2 Profile 12, shown in Figure 4, taken immediately after the internal wave measurements, was used for a computational study of the effect of internal waves. The fitted profile had two isovelocity layers placed in such a way that the thermocline could be shifted up or down. With a maximum excursion of 250 feet, the range to the caustic shifted by about 600 feet.

3.2.3 Another computational study was done to get quantitative estimates of the effect of profile detail on the caustic range. Figure 5 shows the two ways in which Profile 21 was varied. The higher minimum velocity, representing an exaggeration of the detail found at the velocity minimum, produced a shift in the caustic range of 150 feet. The entire upper portion of the profile was shifted as shown. This produced a shift in caustic range of 750 feet. The upper portion of the profile did not change by this magnitude during the experiment, but greater changes do occur with the changing seasons over the course of a year.

3.2.4 The slight effect of the variation of the velocity minimum indicates that it is not necessary to fit this portion of the profile precisely. In any case, fitting the fine detail would be difficult. That the ray diagram is not very sensitive to the upper layers should not be entirely unexpected. Most of the ray travel is in the lower layers. For some comparisons of theory with this experiment it is adequate to use a single profile representative of the entire experiment rather than match specific profiles and shots. Profile 21, taken in the middle of the experiment, best represents the mean of several profiles and has been the most frequently used.

4. RAY PATTERN

4.1 Before going into details of shock wave measurements, a general overall description of the ray pattern and the types of pulses to be expected is in order.

4.2 A typical sound velocity profile and ray diagram for the experiment are shown in Figure 6. The shock wave rays that start downward are bent upward by the

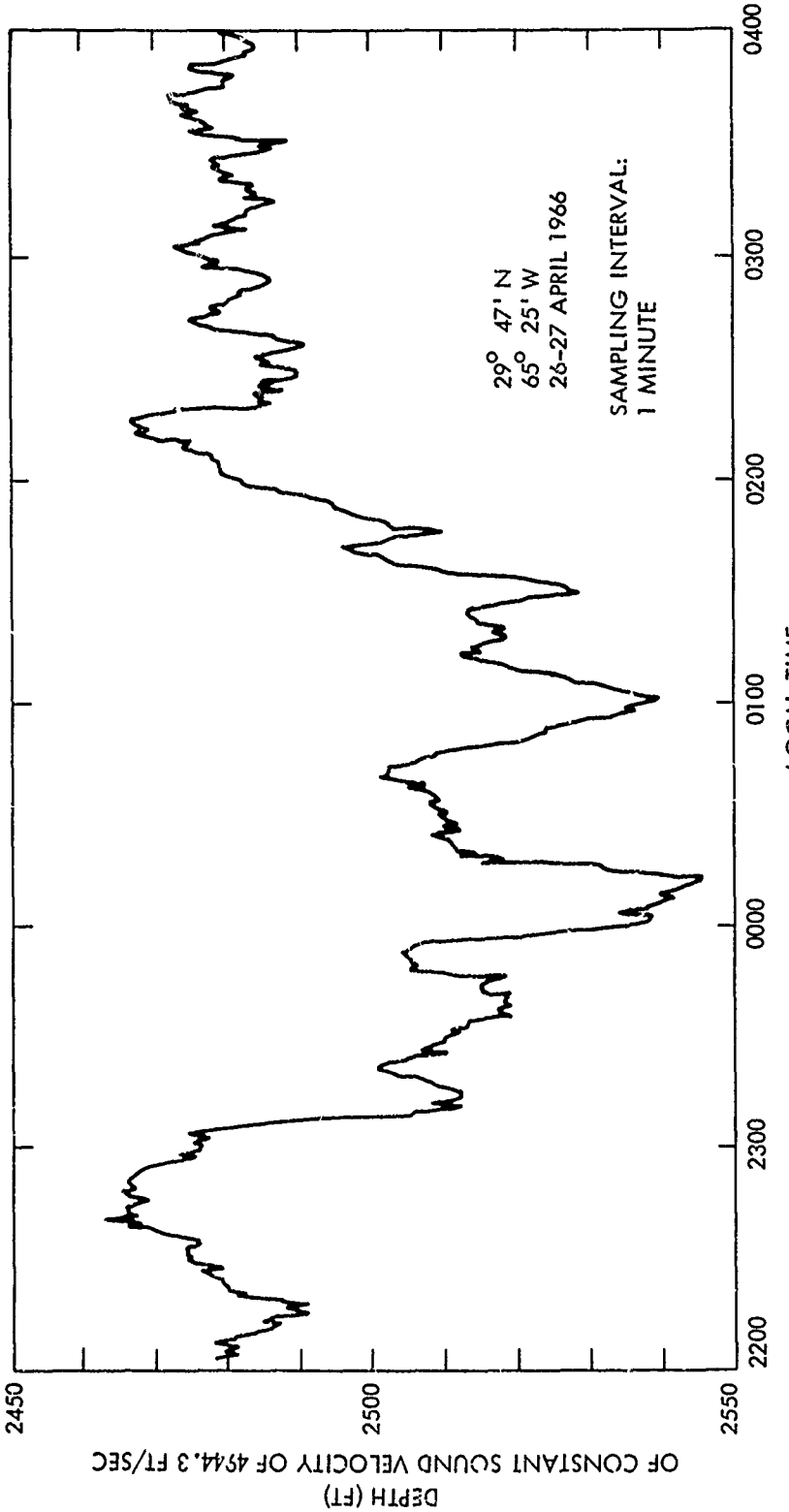

FIG. 3 INTERNAL WAVES - MOVEMENT OF THE THERMOCLINE

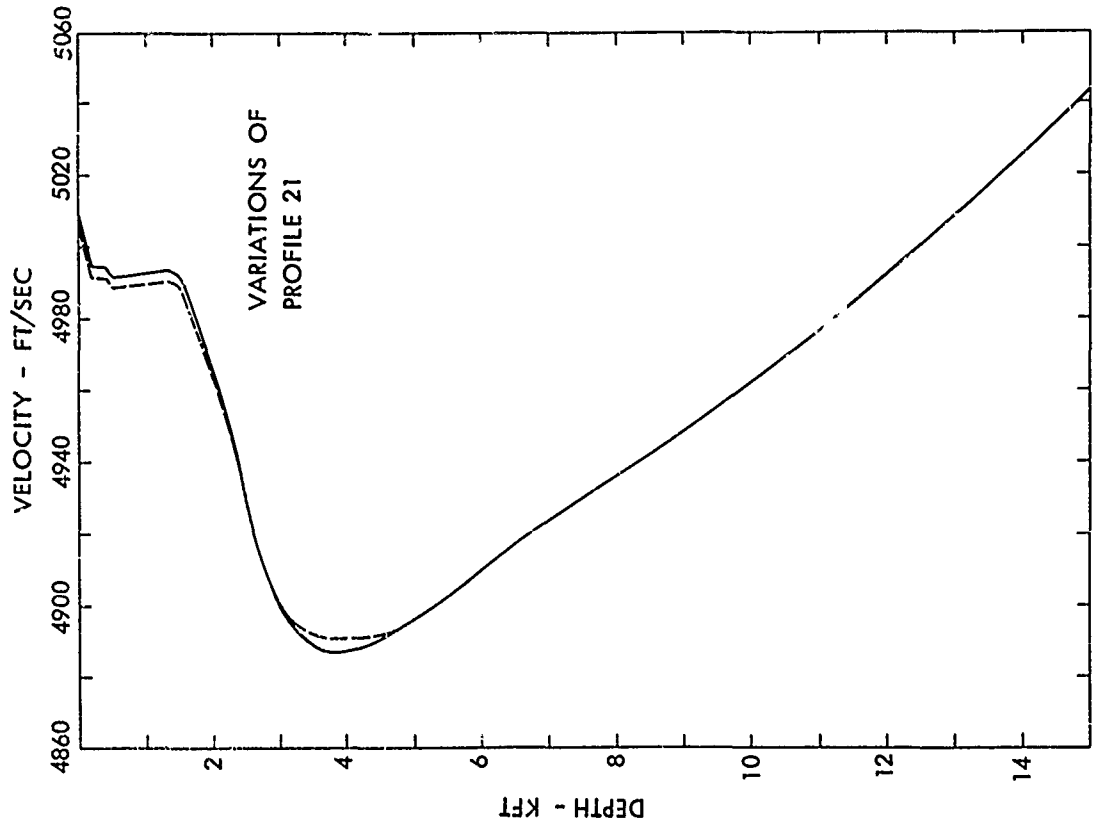

FIG. 5

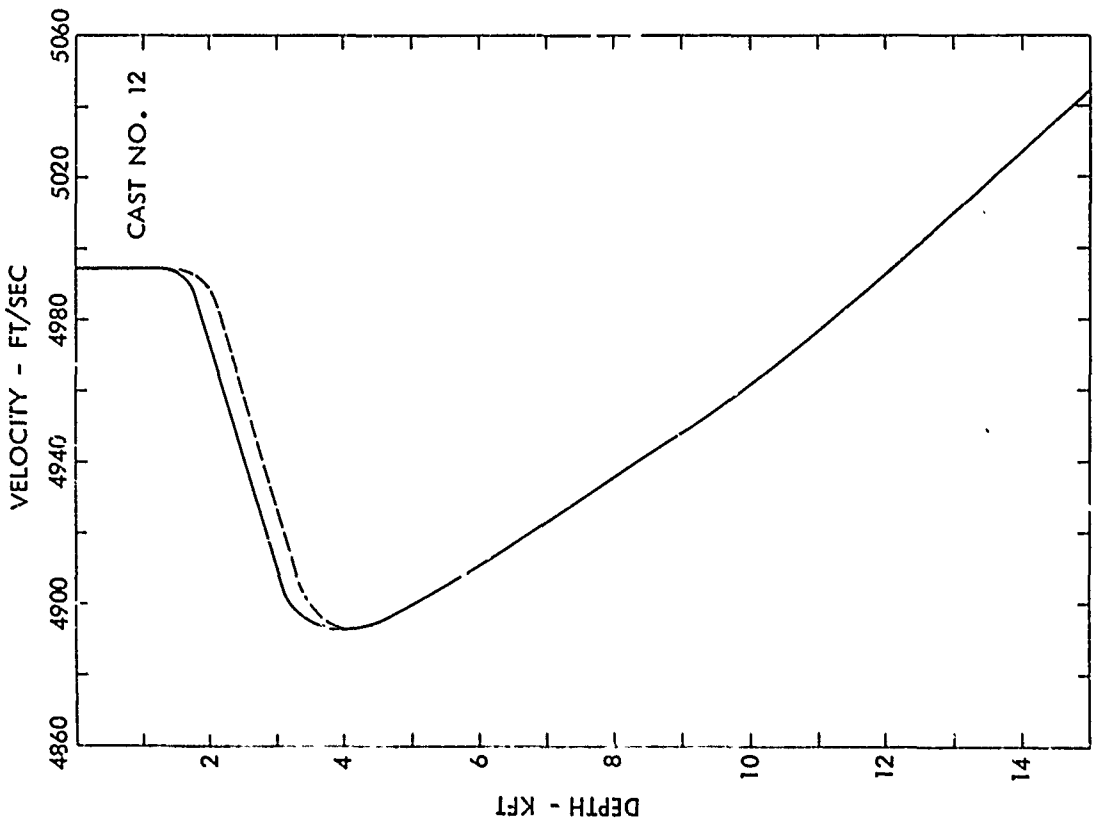

FIG. 4

PROFILE VARIATIONS

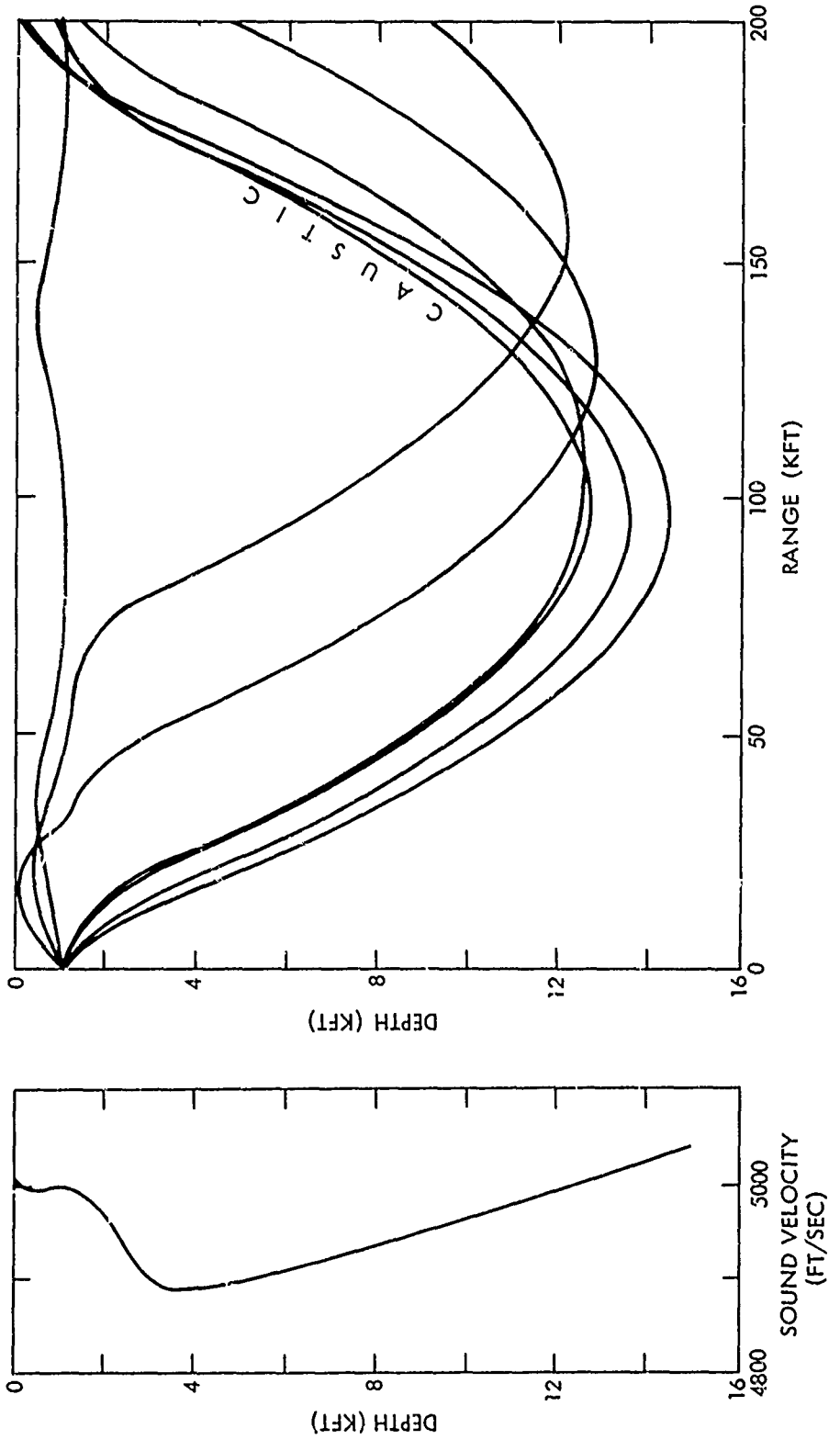

FIG. 6 TYPICAL PROFILE AND RAY PATTERN

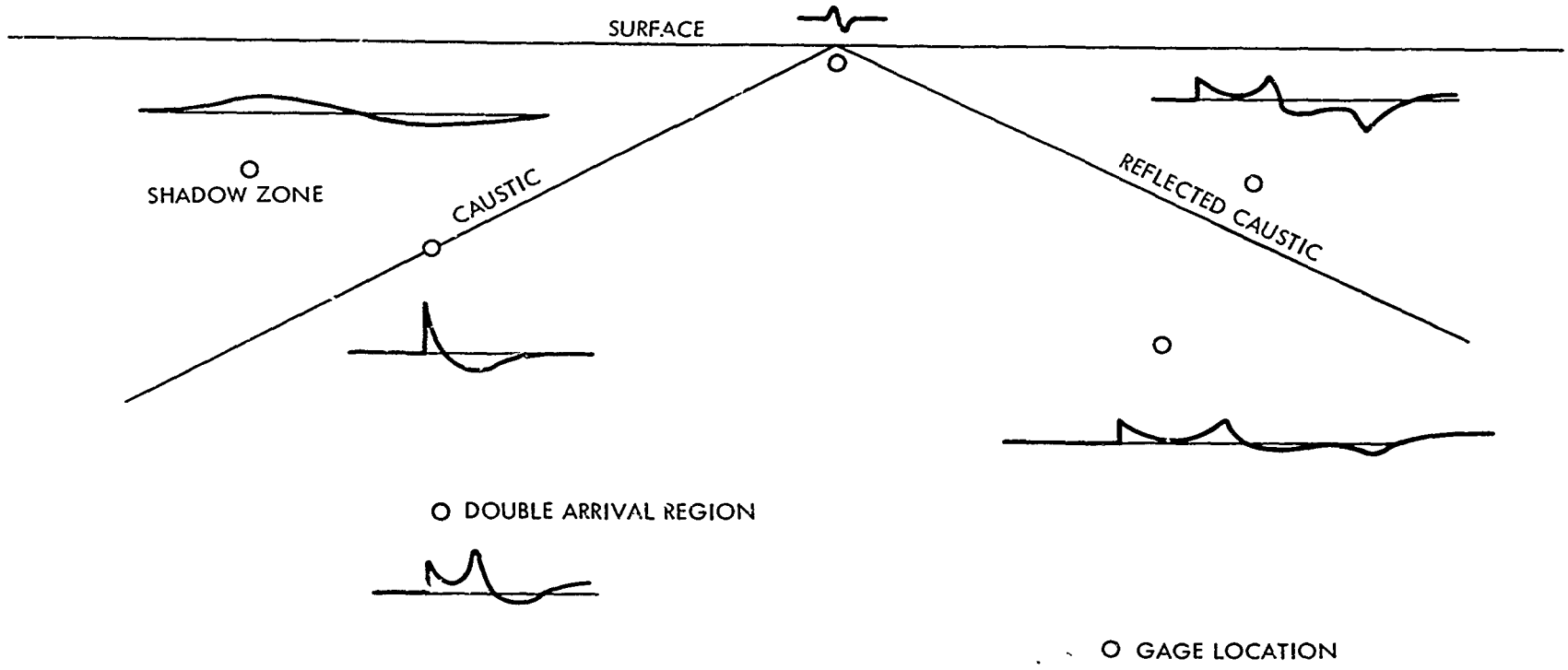

FIG. 7 TYPICAL WAVEFORMS AT CONVERGENCE ZONE

deep velocity gradient and focused near the surface at the convergence zone where the gage array recorded the shock wave pulse. The rays that start upward are bent downward by the sound velocity gradient of the surface thermocline and focused at a range of a few miles. The upward-starting rays eventually return to a shallow depth at the first convergence zone where they again form a caustic, but at a range miles beyond the recording ship.

4.3 The general pattern of shock wave arrivals at the convergence zone is shown in Figure 7. There is a single high amplitude arrival very near the caustic, a single arrival in the shadow zone that gets weaker with distance from the caustic, and a pair of arrivals on the other side of the caustic. The time separation of the two arrivals increases with distance from the caustic. The shock wave pressures reflected from the surface are the negative of the direct arrivals. If the gages are near the surface it is possible to locate them so that they receive both the direct arrivals in the vicinity of the direct caustic and the reflected arrivals in the vicinity of the reflected caustic, and this was accomplished on two shots, 119 and 120.

4.4 In addition to the convergence zone arrivals, there were surface channel arrivals. The sharp negative sound velocity gradient at the surface and the slight positive gradient extending to a depth of 1200 feet formed a sound channel that confined the nearly horizontal rays. The many turning points of the surface channel rays and their greater dependence on local inhomogeneities makes them harder to predict than the convergence zone rays. In general, the surface channel arrivals were rather weak, but on one shot they were strong enough to trigger the recording system.

5. CONVERGENCE ZONE SHOCK WAVE DATA

As indicated by the previous discussion, the main purpose of the operation was to measure shock waves, and the bulk of the measurements were of shock waves. Other measurements were incidental to shock wave measurements or were measurements of environmental factors that might affect shock waves.

5.1 ARRIVAL TIME DIFFERENCES

5.1.1 The easiest data to reduce was that for arrival time difference. This was done at sea for operational purposes and later, more precisely, in the laboratory. The arrival time difference, Δt, was taken to be the time from the middle of the first sharp rise in pressure (the point normally regarded as the beginning of a shock wave) to the second pressure peak.

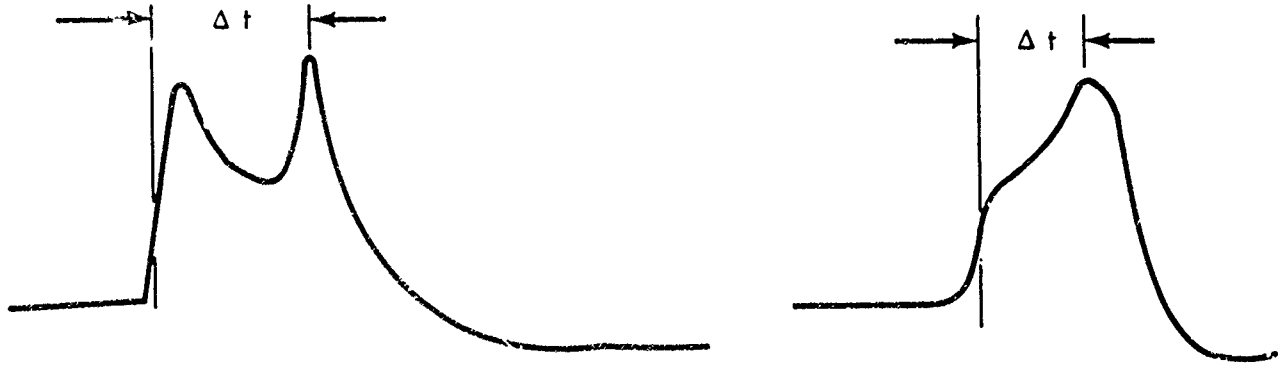

FIG. 8

By ray theory, $\Delta t = 0$ only on the caustic surface. Recent theoretical work (reference 7) indicates that there is a region of finite thickness where $\Delta t = 0$. However, when we extrapolated the curve of arrival time difference vs depth to find a depth where $\Delta t = 0$, we very nearly located the depth of highest peak pressure. Figures 9 and 10 show the various caustic positions. The range to each point was measured by the DECCA system. The depth of the caustic was determined by extrapolation of the arrival time differences from the gage string to $\Delta t = 0$. To show the quality of the data used in getting caustic locations, two of the arrival time vs depth curves are reproduced as Figures 11 and 12. Shot 26 is one of the worst for scatter. A shift of 60 feet in the inferred depth of the reflected caustic could be effected by choosing a different line through the points. Shot 67 is about average in the amount of scatter.

5.1.2 Generally, the arrival time difference increased linearly with distance from the caustic. The deviation from linearity very close to the caustic, as shown in the Shot 67 data, is common.

5.2 PEAK PRESSURE

5.2.1 Shock wave peak pressures were measured for all shots that were recorded. This data is presented graphically in Appendix E. The peak pressure of a single arrival and the first and second peaks of a double arrival are distinguished by different symbols. Since pressure histories in the double-arrival region can be predicted reasonably well, measurements were concentrated near the caustic. Some detailed pressure-time curves are shown in Appendix F.

5.2.2 Several things should be noted about the peak pressure readings. Most were derived from the analog playouts of the magnetic tape recordings. Since the amplitudes were small and difficult to read, comparison with oscilloscope recordings and digital playouts were made whenever possible.

5.2.3 The scope records generally showed slightly lower pressures than the tape playouts. This may be explained by the nature of the pressure pulses and the methods of recording. There was a slow, small rise in pressure just before the shock front. The oscilloscopes were triggered by the sharp shock front. The slow rise was not observed on the scopes. The short baseline that preceded the shock front on the scope records was at the end of the slow rise and was not at ambient pressure. The baseline for the tape records was drawn through the record just before the slow pressure rise. The digital playouts produced essentially the same peak pressure as the analog playouts, indicating that the analog playouts were correctly read in spite of difficulties.

5.2.4 On some graphs of peak pressures vs depth, a double arrival above the caustic is indicated. Most of these are probably not real. On the visicorder playouts what may be another peak can be seen. On all the shadow zone records that were digitized and plotted at high resolution, the other peak turned out to be an insignificant wiggle lost in the general noise level. These measurements were corrected on the graphs, but the others remain as originally read.

5.2.5 The measured peak pressures were compared with those predicted for isovelocity water by similitude equations (Appendix D). The pressure amplitude factors at caustics were often ∿8. On Shot 82, and that shot only, we observed an amplitude factor of 12.

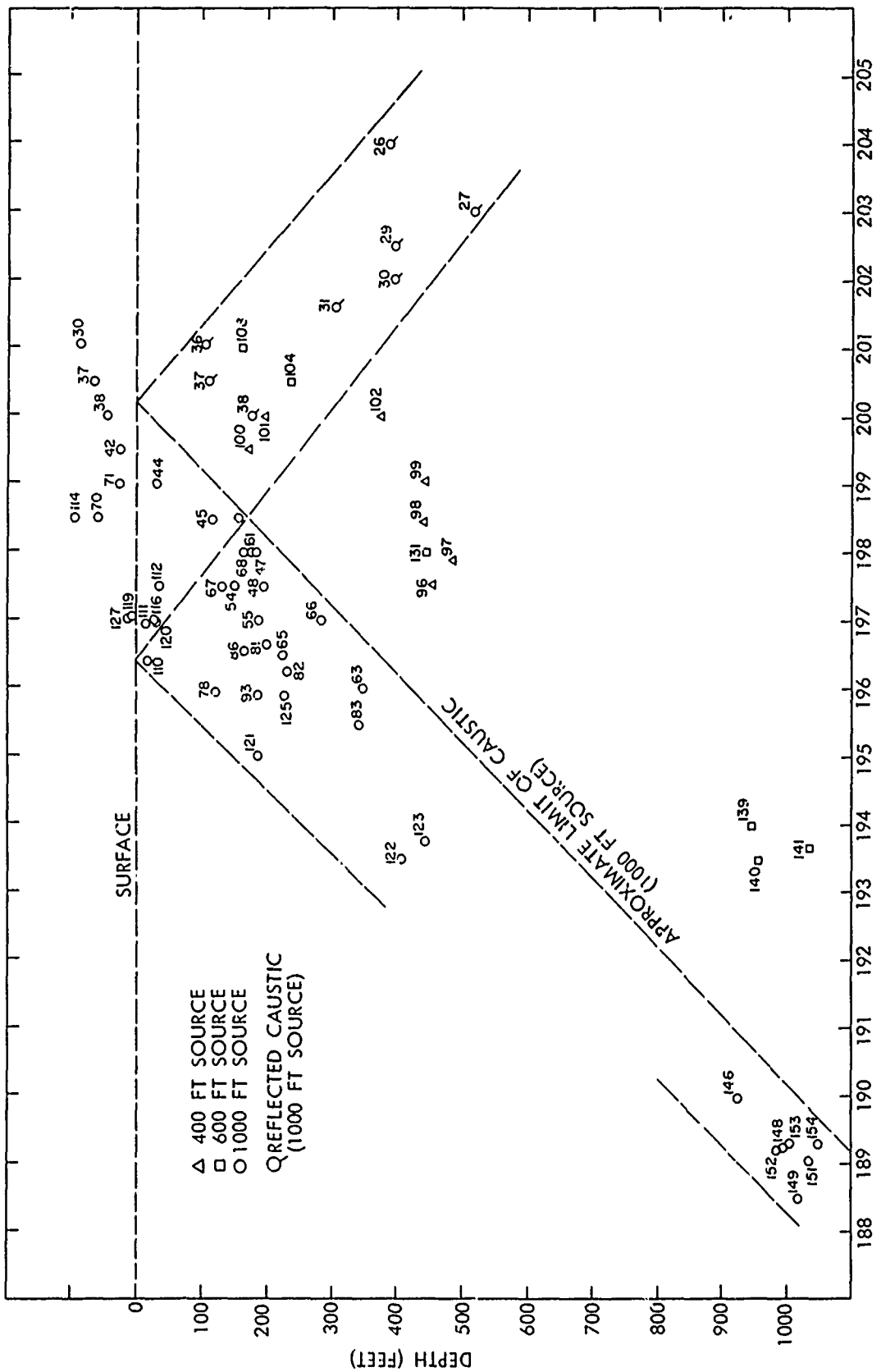

FIG. 9 LOCATION OF POINTS ON CONVERGENCE ZONE CAUSTIC

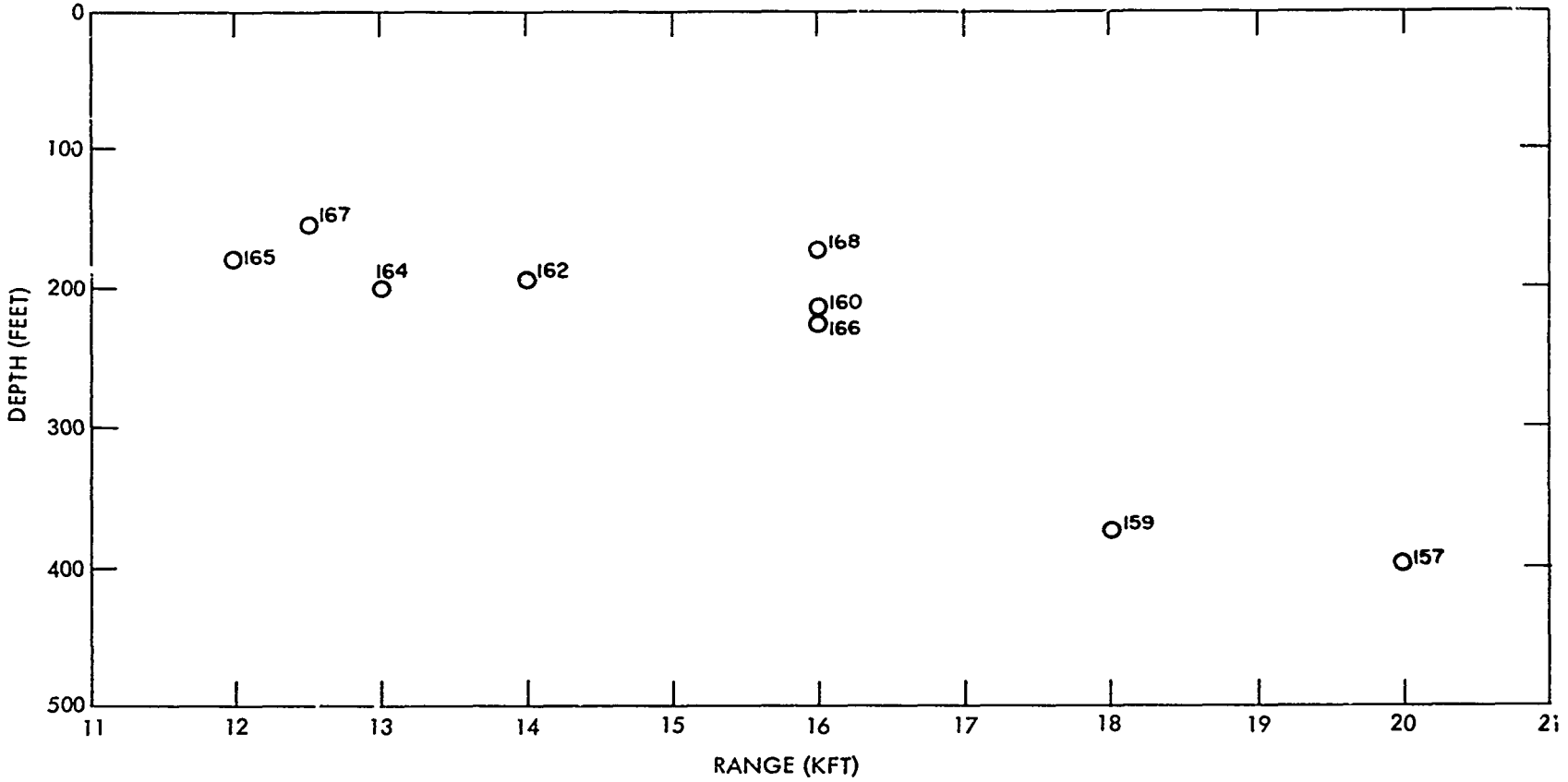

FIG. 10 LOCATION OF POINTS ON CLOSE-IN CAUSTIC FROM 1000 FT SOURCE

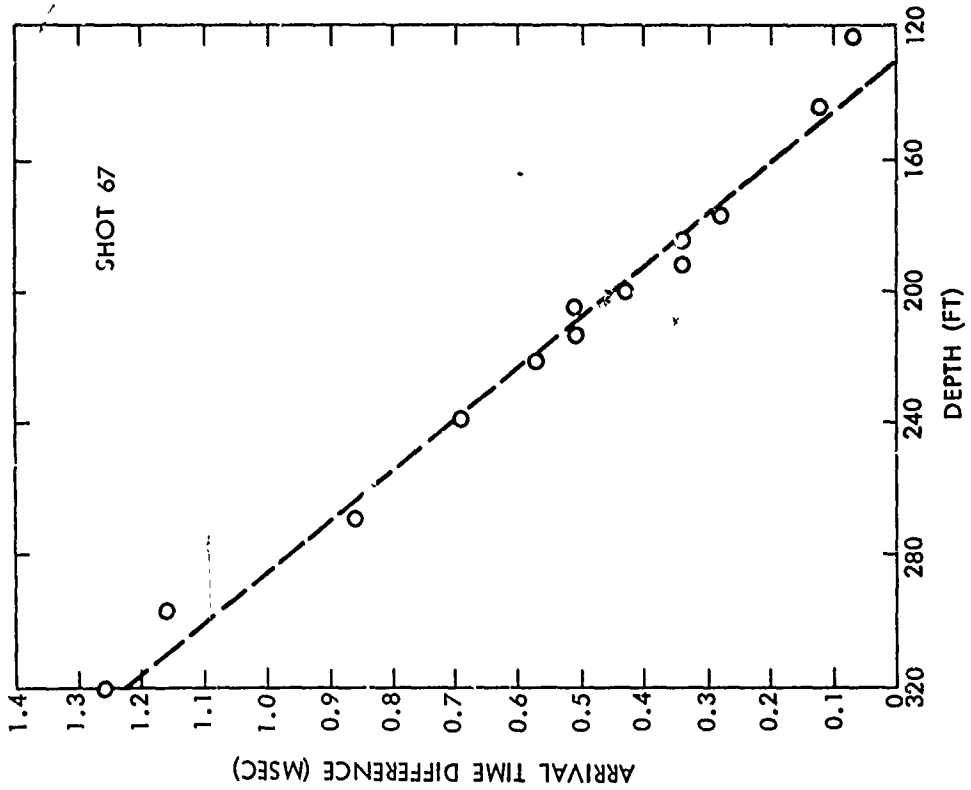

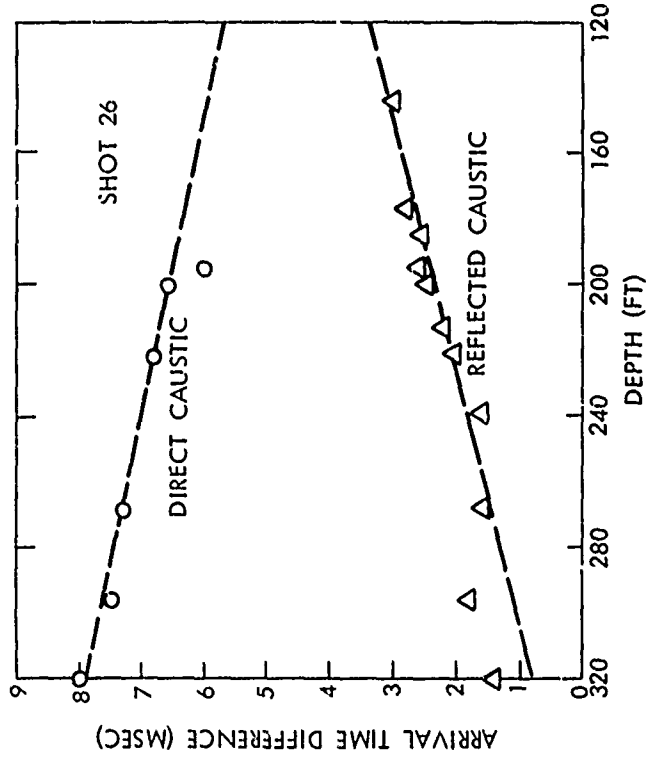

FIGS. 11-12 ARRIVAL TIME DIFFERENCE VS DEPTH

5.2.6 Digitization of the analog records and computer processing were performed on the shots we thought most useful or informative. These were Shots 82, 119, 120, 151, and 154. On three shots, 82, 151, and 154, we measured a continuous region, from the shadow zone, through the caustic and into the double-arrival region. On Shots 119 and 120, the reflections from the surface of pulses that would otherwise have passed above the gage string, enabled the gages to cover an effective vertical extent of 400 feet instead of the normal 200 feet. The immediate surface reflection on 119 and 120 cut off the pulses on the upper gages and reduced peak pressure, impulse, and energy. This effectively created a gap near the surface in the region covered by the gage string. These shots, however, were able to provide simultaneous measurements far into the shadow zone and double-arrival region.

5.3 ENERGY AND IMPULSE

5.3.1 The shock wave impulse and energy were calculated for all the digitized records. Comparisons with isovelocity values are presented in Appendices G and H.

5.3.2 The shock wave impulse is defined as the integral of pressure with respect to time. The integration is done from the beginning of the pulse to an arbitrary limit, which is, for unrefracted shock waves that exhibit a nearly exponential decay, customarily 5 or 6.7 times the initial decay constant, θ. Because of the irregular pulse shapes that were observed in this experiment and the difficulty of defining a time constant, a different limit criterion must be used. Barash and Goertner (reference 4) used the time at which the pressure fell to .07 of the initial peak value. For an unrefracted pulse this corresponds to 5θ. However, the pulses they examined exhibited, like an unrefracted shock wave, an asymptotic decay to zero pressure, while the pulses examined here quickly drop below zero pressure and stay below zero pressure for a relatively long time. The only clearly distinguishable and reproducible limit for our integrations is the crossing of the zero pressure level and this is the time limit that is used here. The magnitude of the impulse of the negative portion of the shock wave exceeds that of the positive portion of the shock wave. If the integration of impulse were carried to the point where later pressures were very low, the total impulse on all records would be negative.

5.3.3 The impulse obtained by integrating to the time of the crossing of zero pressure varied only slightly, ranging from .7 to 1.5 of that predicted by the similitude equations. The variation was less on any one shot. There was a trend for the impulse to increase steadily with depth, similar to the trend noted by Barash and Goertner (reference 4).

5.3.4 The shock wave energy flux density, commonly referred to simply as energy, is proportional to the integral of the square of the pressure with respect to time. The selection of a time limit is not as critical for energy as it is for impulse because the pressure squared dependence causes the energy integral to converge more rapidly to a limiting value. However, it is customary to use the same time limit for both energy and impulse, and this was done here. The energy peaked very strongly at the caustic. Energy amplifications of 15 to 25 (compared with similitude equations for isovelocity water) were recorded. The curves of energy amplification factors are similar in shape to the pressure amplification curves, but the range of variation is greater for energy amplification.

5.4 SPECTRAL ANALYSIS

5.4.1 Power spectra for Shots 82 and 154, both of which were 900-pound charges, are presented in Appendix I. The pressure-time curves for Shot 82 are presented in Appendix I along with the spectra. The pressure-time curves that correspond to the spectra presented in Appendix I for Shot 154 are in Appendix F along with other pressure-time records for Shot 154. The spectra demonstrate that refraction is a high-frequency phenomenon. The pulses in the shadow zone consist of low frequencies that are not sharply focused. The caustic arrival contains a maximum of high frequency content. The spectra for the double arrival zone have a large high frequency content, and show peaks at frequencies corresponding to periods that are multiples of the time spacing between the two arrivals. Many of the spectra also show a peak in the 5000 Hz to 9000 Hz region. This is due to ringing of the gage-amplifier combination, which was probably a mechanical effect of the amplifier case.

5.4.2 Shot 82 exhibited higher pressures than other shots. It appeared that this might be due to ringing. The gage at 239 feet, which recorded the highest pressure, showed particularly strong ringing. It was hoped that the ringing might be such as to cause a peak in the Fourier transform that could be removed by digital filtering. Unfortunately, no outstanding peaks were found in the power density spectrum on that gage. This was in spite of the fact that the oscillations were clearly visible in the pressure-time record. Because the ringing was so obvious and its frequency could be roughly measured, attempts were made to filter it out. The filtering had little effect, and the results are not shown.

6. CLOSE-IN CAUSTICS

6.1 The close-in caustics presented a different pattern. On two of the shots there was so much scatter that no curve could be fitted to the peak pressure vs depth data. On two other shots the highest pressures were not observed at the caustic. Instead, the peak pressures were highest in the double arrival region. The extreme amounts of scatter might be accounted for by horizontal variations in sound velocity and inhomogeneities in the water. The increase in pressures in the double arrival region has not been accounted for.

6.2 Pressure amplifications of 1 to 4 were obtained for the close-in caustic. This was considerably less amplification than at the convergence zone.

7. SURFACE CHANNEL ARRIVALS

7.1 Shock wave energy also propagated through a sound channel near the surface. The surface channel arrivals reached the gages about 600 milliseconds before the convergence zone arrivals. They were usually weak, but on one shot, Shot 152, they triggered the recorders prematurely. There are many paths possible in the sound channel. The recorded pulses are very complex because the shock waves traveled through many different paths. Two of the shock wave pressure records are shown in Figure 13 to illustrate their complexity. The maximum positive and negative pressures are shown in Figure 14. The pressure amplification was about 1.

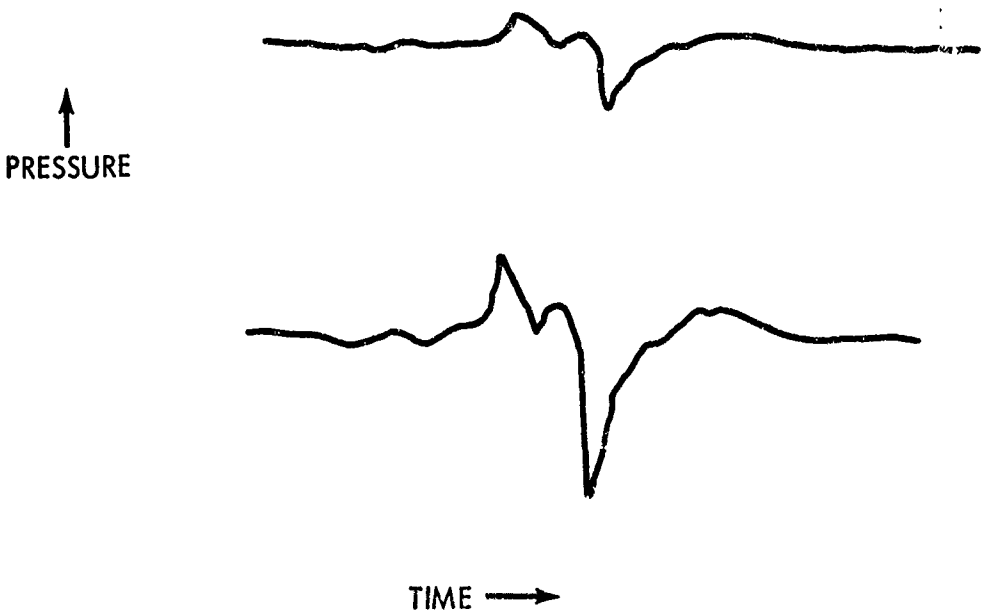

FIG. 13 SURFACE CHANNEL WAVEFORMS FROM SHOT 152

8. SUMMARY AND CONCLUSIONS

8.1 Sound velocity gradients in the ocean and their effects on the propagation of underwater shock waves from 8-pound and 900-pound charges were measured. The shock wave measurements were concentrated near caustics, where the effects of refraction are the greatest. The shock wave peak pressures, impulses, and energies were compared with what might be expected in isovelocity water, as given by the similitude equations. Pressure histories and a few shock wave spectra were presented.

8.2 At the convergence zone caustic, pressure amplifications of about 8 were generally observed and, on one shot, an amplification of 12 was observed. The maximum energy amplifications were from 15 to 25. The shock wave impulse was about the same as would be expected for isovelocity water. At the close-in caustic, the pressure amplification was less, from 1 to 4.

8.3 The experiment combined precise measurements of oceanic sound velocity profiles with precise measurements of the effects the sound velocity profiles had upon the propagation of underwater shock waves. Although the sound velocity profile was relatively constant throughout the experiment, variations in experimental conditions were produced by varying the charge weight, burst depth, and gage depth. The experiment provides a means for judging the validity of theoretical models (such as that in references 7 and 8), which may then be used to predict effects under more general oceanic conditions.

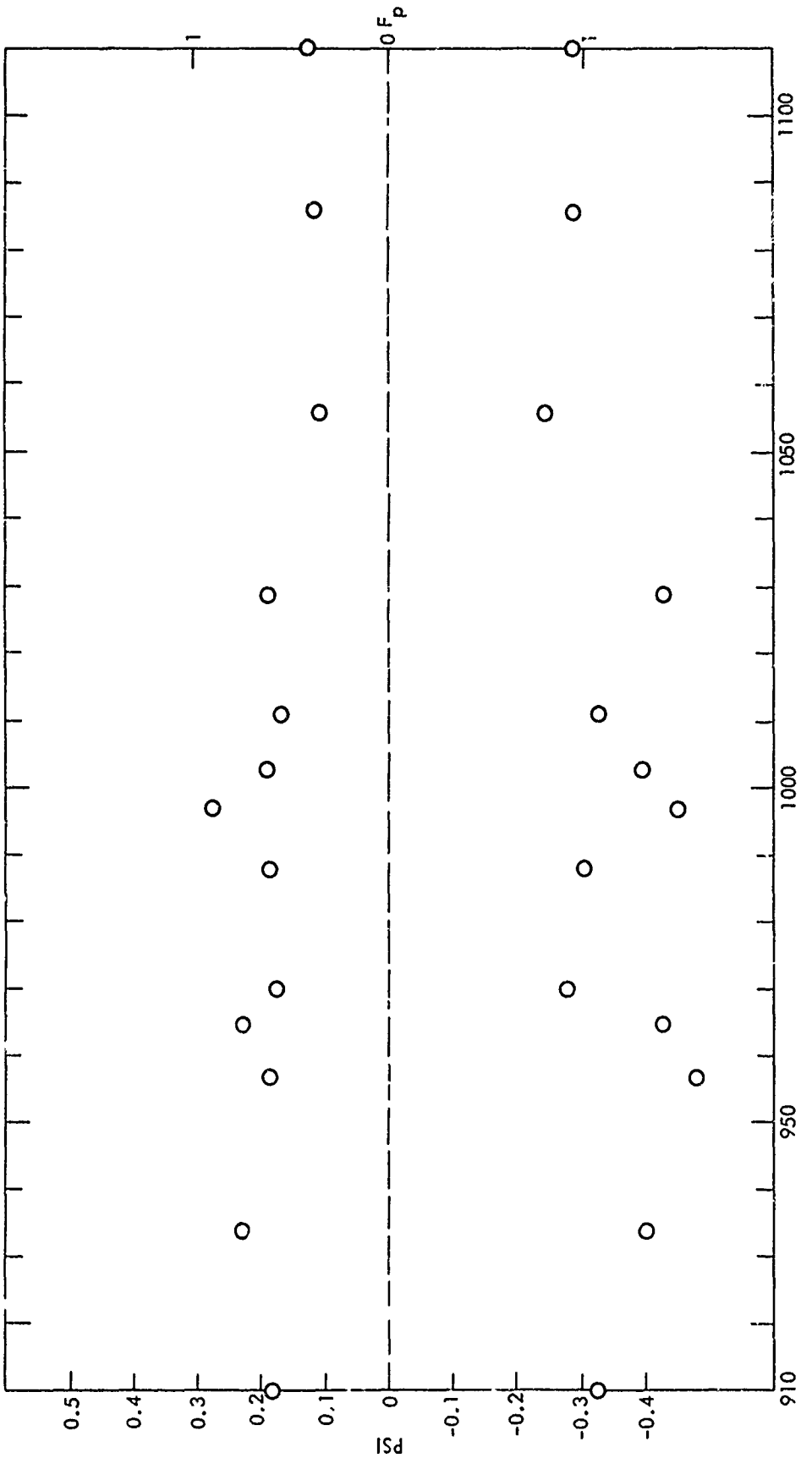

FIG. 14 POSITIVE AND NEGATIVE PEAK PRESSURES OF SURFACE CHANNEL ARRIVALS ON SHOT 152

REFERENCES

1. R. Brockhurst, J. Bruce, and A. Arons, "Refraction and Diffraction of Explosion Pressure Pulses by Gradients in the Propagation Velocity; I. Observations with 56-lb TNT Charges in a Late Summer Thermocline in a Flooded Quarry," Woods Hole Oceanographic Institution Reference No. 57-10, Jan 1957

2. H. H. Hall, and D. G. Clark, "Small Scale Studies of Refraction of Underwater Shock Waves," University of New Hampshire, Ref. no. 41, 1961

3. H. H. Hall, D. G. Clark, and R. M. Barash, Supplement to "Small Scale Studies of Refraction of Underwater Shock Waves," University of New Hampshire, Ref. no. 41, 1961

4. R. M. Barash and J. A. Goertner, "Refraction of Underwater Explosion Shock Waves: Pressure Histories Measured at Caustics in a Flooded Quarry," Naval Ordnance Laboratory, NOLTR 67-9, Apr 1967

5. R. S. Price, "Refraction of Underwater Explosion Shock Waves: Pelagic Operations in Measuring Convergence Zone Pressures," Naval Ordnance Laboratory, NOLTR 66-220, Jan 1967

6. "Calibration of Massa HY 15 Hydrophones, Serials 145, 153, 160, 165, and 171," Underwater Sound Reference Division, Naval Research Laboratory, USRD Calibration Report No. 2531, Sep 1966

7. I. M. Blatstein, "Refraction of Underwater Explosion Shock Waves: Calculations of Pressure Histories in a Convergence Zone," Naval Ordnance Laboratory, NOLTR 71-93, June 1971, p. 10

8. I. M. Blatstein, "Calculations of Underwater Explosion Pulses at Caustics," Journal of the Acoustical Society of America, Vol. 49, No. 5 (Part 2), 1568-1579, May 1971

APPENDIX A

TEST CONDITIONS

The following table, based on a table in reference 5, gives test conditions for the shots analyzed in this report. Shots that misfired or were not recorded are not included here. The shot numbers are the shot identification numbers that were put on the shock wave records at the time of recording and were consistently used as the identification while working with the records. Note that reference 5 uses a system of line numbers that do not always match the shot numbers. The ranges given are the horizontal ranges between the explosions and the gage array. The ranges are based on the ranges given by the Decca ranging system with corrections made for the positions of the drop point and the gage array relative to the antennas of the Decca system. The times are drop times, which are the times at which the charges were dropped into the water. The actual explosion times were not determined.

APPENDIX A

SHOT DATA

Shot No.	Drop Time Day Z	Drop Time Time Z	Charge Wt lb-oz	Firing Depth (ft)	OCEANIC Lat °N	OCEANIC Long °W	LYNCH Range (ft)	LYNCH Lat °N	LYNCH Long °W	Depth of Top Gage (ft)
26	116 26 Apr	1320	7-15	1000			203,495	30-14	65-13	120
27		1400	8-1	1000			202,995	30-14.5	65-12.5	120
48	117 27 Apr	0015	8	1000			197,510	30-18	65-10	120
54		1515	8-1	1000			197,505	30-17	65-17	120
55		1605	7-15	1000			197,000	30-15	65-15	120
65		2050	8	1000			196,525	30-29	65-11	120
75	119 29 Apr	1410.5	8-	1000			196,970	30-37	65-06	120
78		1951	923.5	1000	30-26	65-36	195,908	30-39	65-04	120
81	120 30 Apr	1410.5	8-1	1000			196,620	30-44	65-08.5	120
82		1431	887.8	1000	30-24	65-40	196,467	30-44	65-08.5	120
86		2010.5	7-14	1000			196,535	30-44.5	65-06	120
93	122 2 May	1430.5	7-15	1000			195,920	30-38	65-11.5	120
96		1650.5	8-	600			197,560	30-38	65-11	120
100		1811	7-15	600			199,502	30-41	65-9.5	120
101		1831	8-	600			199,994	30-41	65-9.5	120
102		1851	8-1	600			200,015	30-41	65-9.5	120
106		1932	8-	400			200,506	30-41	65-9.5	120
111	123 3 May	1510	7-15	1000			196,990	30-36.5	65-01	2
112		1530	8	1000			197,503	30-36.5	65-01	2
114		2250	7-15	1000			197,040	30-39.5	64-54.5	2
120		2331	890.3	1000	30-51	65-29	196,516	30-38.5	64-51	2

APPENDIX A (continued)

Shot No.	Drop Time Day Z	Drop Time Time Z	Charge Wt lb-oz	Firing Depth (ft)	OCEANIC Lat °N	OCEANIC Long °W	LYNCH Range (ft)	LYNCH Lat °N	LYNCH Long °W	Depth of Top Gage (ft)
122	124 4 May	1510	8	1000			193,514	30-35	64-55	310
123		1630	8	1000			193,800	30-38	64-54	310
131	125 5 May	0116.5	8	400			198,005	30-39	64-48	310
139	126 6 May	1500	8	400			194,000	30-45.5	64-51	910
140		1512	8	400			193,500	30-45.5	64-51	910
141		1534.5	8-1	400			193,700	30-47	64-50	910
151		1956.5	8	1000			189,100	30-50	64-45	910
153	127 7 May	2105	870.3	1000	30-23	65-10	189,275	30-48	64-46	910
154		2320	911.8	1000			189,300	30-49.5	64-47	910
160	128 8 May	1246	8	400			16,003	---	---	160
166		1420	7-14	400			16,018	---	---	160
167		1450	7-15	400			12,520	---	---	160
168		1758	896.5	400	30-55	64-51	15,947	30-56	64.49.5	160

APPENDIX B

VELOCIMETER CAST INFORMATION
M/V OCEANIC

Cast No.	Direction (Down/Up)	Date	Data at Start				Data at Stop			
			Time (local)	Water Depth (ft)	N. Lat.	W. Long.	Time (local)	Water Depth (ft)	N. Lat.	W. Long.
1	Down	4/12/66	1605				1913		29°43'	65°01'
	Up	4/12/66	2002				2302		29°42'	65°02'
2	Down	4/13/66	0623	15,900	29°10'	64°58'	0927			
	Up	4/13/66	0951				1252		29°06'	65°05'
3	Down	4/14/66	0333				0700	14,850*	28°30'	64°50'
	Up	4/14/66	0701				1140	14,850*	28°35'	64°50'
4	Down	4/15/66	0319				0612		28°00'	65°00'
	Up	4/15/66	0612				0916	15,900		
5	Down	4/15/66	2355	16,000	29°42'	64°00'	0250	16,080		
	Up	4/16/66	0250	16,080			0552			
6	Down	4/16/66	1310		30°20'	64°00'	1522	13,842		
	Up	4/16/66	1524	13,842			17??		30°11'	64°11'
7	Down	4/16/66	2305	13,980	30°20'	64°30'	2355	(Unit Failed)		
	Up									
8	Down	4/18/66	1048		30°17'	65°10'	1646	14,950		
	Up	4/18/66	1647				2035		25°12'	65°00'
9	Down	4/21/66	1547							
	Up	4/21/66					1850	15,330	30°11'	65°13'
10	Down	4/24/66	2221	15,850	29°42'	65°04'	0112			
	Up	4/25/66	0137				0435	15,990	29°48'	65°00'

* Corrected for non-constant sound velocity.

APPENDIX B (continued)

VELOCIMETER CAST INFORMATION

Cast No.	Direction (Down/Up)	Date	Data at Start: Time (local)	Water Depth (ft)	N. Lat.	W. Long.	Data at Stop: Time (local)	Water Depth (ft)	N. Lat.	W. Long.
11	Down	4/26/66	2145	(Cast to 2500 ft, held for several hours to check for internal waves)						
	Up	4/27/66					0445	16,020	29°47'	65°25'
12	Down	4/28/66	0215	15,078	30°19'	65°12'	0510			
	Up	4/28/66	0510				0805	~15,000	30°13'	65°14'
13	Down	4/28/66	2146	15,000	30°27'	65°39'	2244			
	Up	4/28/66	2244				2340			
14	Down	4/29/66	1152	15,883*	30°22'	65°38'	1211			
	Up	4/29/66	1211				1230			
15	Down	4/30/66	1216	15,806*	30°24'	65°41.5'	1235			
	Up	4/30/66	1235				1253			
16	Down	4/30/66	2116	16,117*	30°30'	65°38'	2230			
	Up	4/30/66	2230				2340			
17	Down	5/2/66	0015				0315			
	Up	5/2/66	0315				0615	15,845*	30°31'	65°41.5'
18	Down	5/3/66	0015	14,615*	30°29'	65°32'	0301			
	Up	5/3/66	0301				0535	15,490*		
19	Down	5/3/66	1528				1547			
	Up	5/3/66	1547		30°48'	65°36'	1607	15,775*		
20	Down	5/4/66	0015				~0315			
	Up	5/4/66	~0315				0613	16,084	30°43½'	65°25'

* Corrected for non-constant sound velocity.

VELOCIMETER CAST INFORMATION

Cast No.	Direction (Down/Up)	Date	Data at Start				Data at Stop			
			Time (local)	Water Depth(ft)	N. Lat.	W. Long.	Time (local)	Water Depth(ft)	N. Lat.	W. Long.
21	Down	5/4/66	2245	>15,000	30°59'	65°16'	0205			
	Up	5/5/66	0205				0525	>15,000		
22	Down	5/6/66	2013							
	Up	5/6/66			30°31'	65°09'	2025	15,670*		
23	Down	5/7/66	0600				0305			
	Up	5/7/66	0305				0625	15,430*	30°34'	65°09'
24	Down	5/7/66	~0900						30°53'	64°47'
	Up	5/7/66	(lying to about 0.7 miles from LYNCH)				~0930	14,385		
25	Down	5/7/66	1420				1431	15,740*	30°25'	65°12'
	Up	5/7/66	1431				1443			
26	Down	5/7/66	2025				2047	16,068*	30°23'	65°10'
	Up	5/7/66	2047				2105			
27	Down	5/8/66	0045				0340			
	Up	5/8/66	0340				0605	14,461*	30°45'	64°49'
28	Down	5/8/66	1202	(approx. midway between				14,660*	30°56'	64°51'
	Up	5/8/66		LYNCH and site of shot #168)			1245			

* Corrected for non-constant sound velocity.

APPENDIX C

SOUND VELOCITY PROFILES

The sound velocity profiles were based on the raw output from the velocimeter. The velocimeter was temperature compensated and the response of the pressure transducer was sufficiently linear so that no corrections had to be made for these effects. The pressures were converted to depths on the assumption of constant density of seawater. The correction for change of density with pressure would be roughly proportional to the depth squared and would change the depth of the bottom of the deepest profiles by about 100 feet. The profiles have been smoothed slightly in the drafting process.

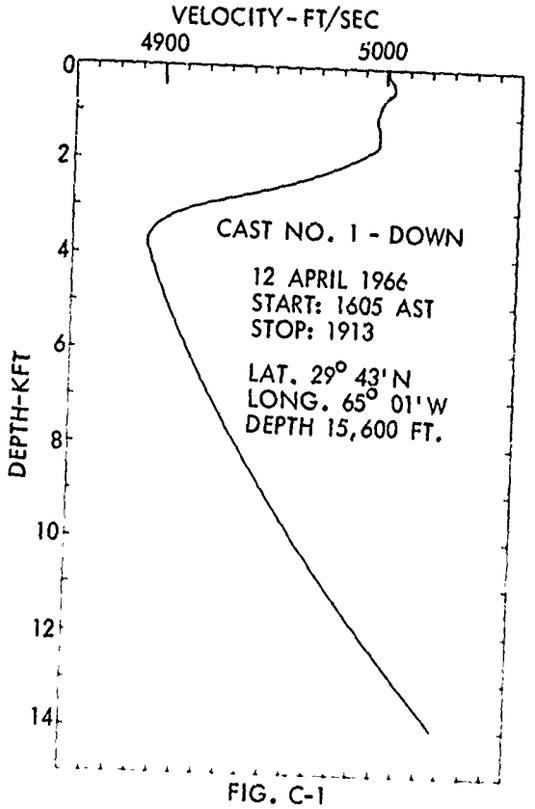

FIG. C-1

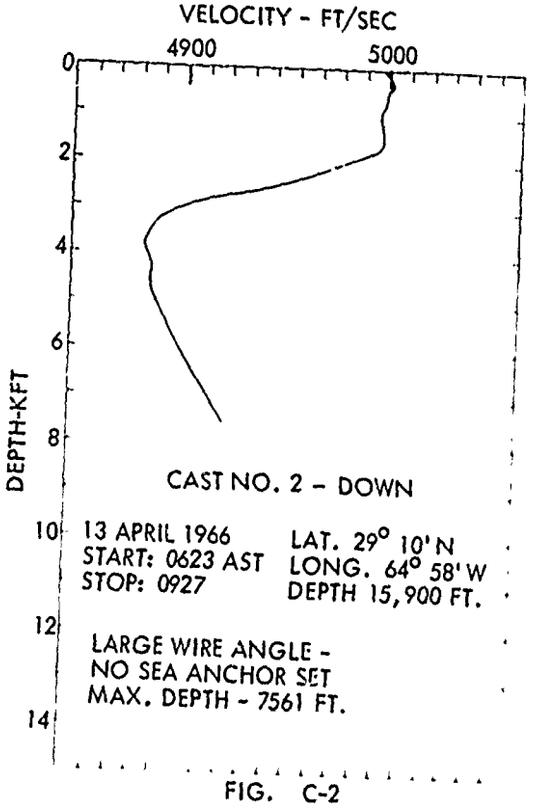

FIG. C-2

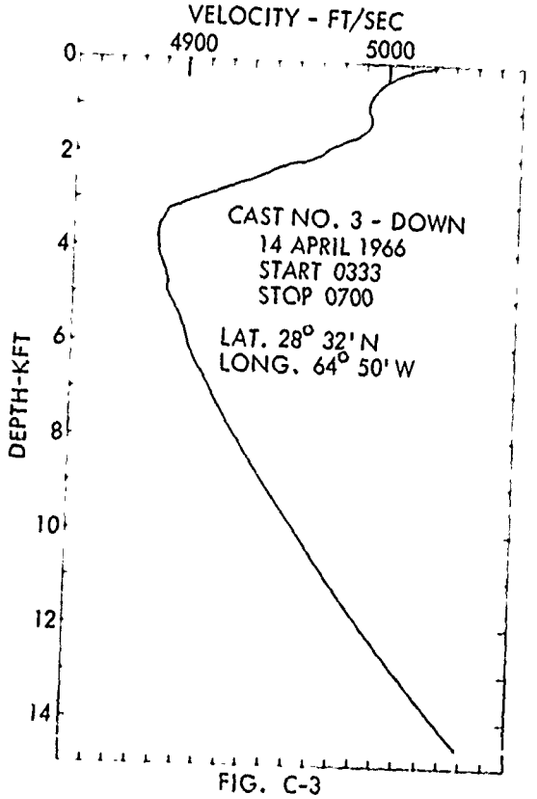

FIG. C-3

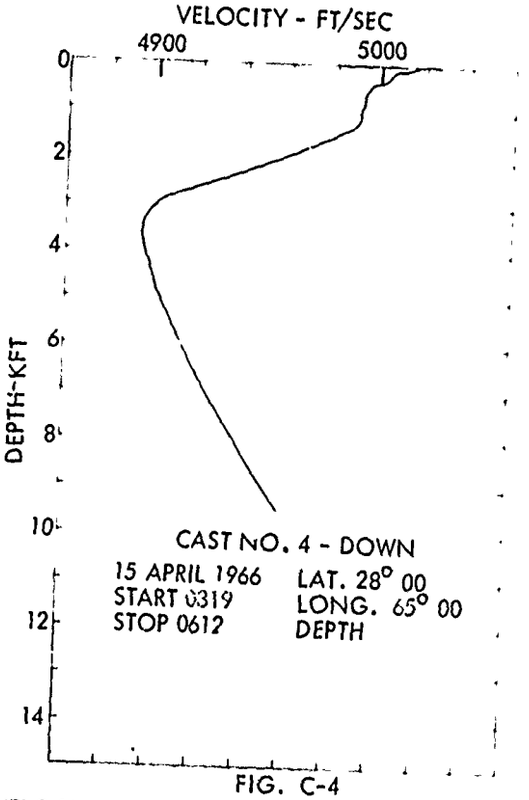

FIG. C-4

FIGS. C1-C4 SOUND VELOCITY PROFILES

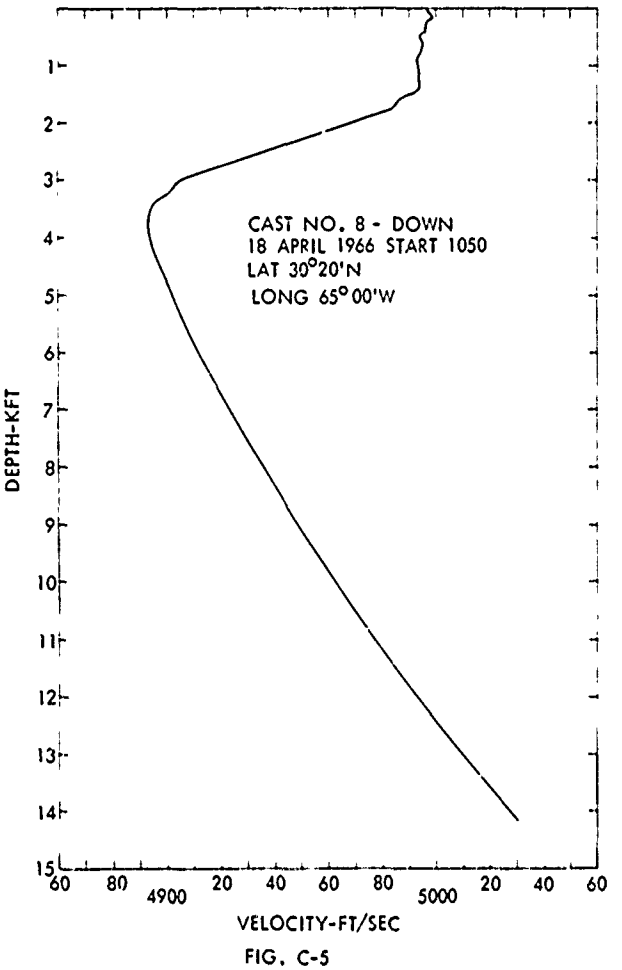

FIG. C-5

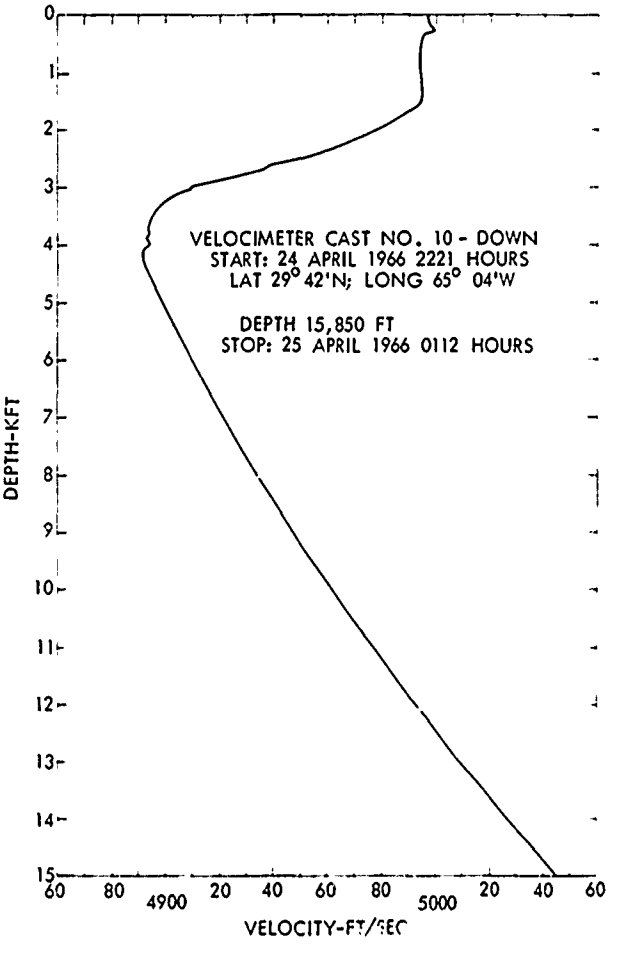

FIG. C-6

FIGS. C5-C6 SOUND VELOCITY PROFILES

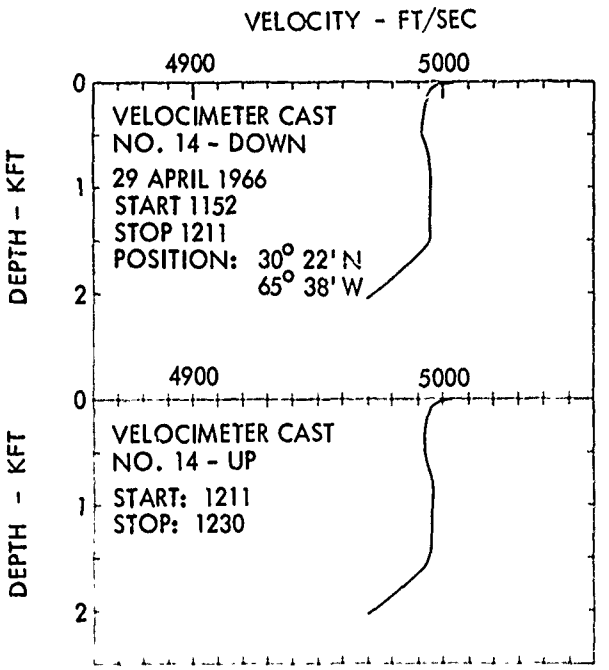

FIG. C7

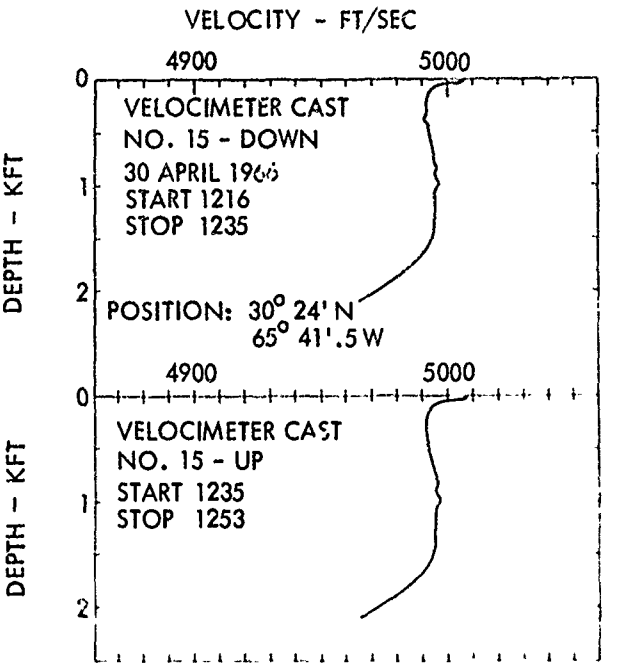

FIG. C8

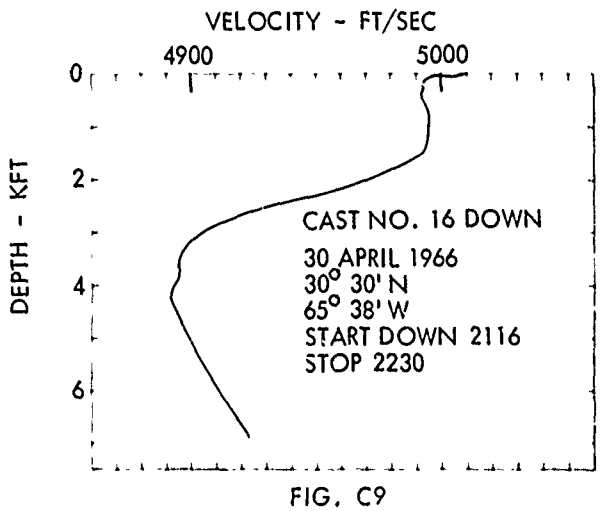

FIG. C9

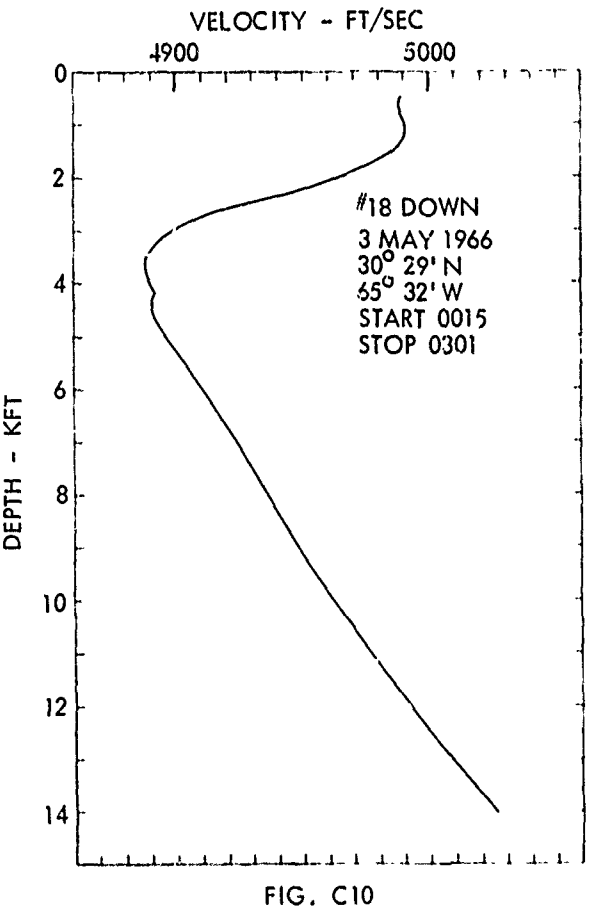

FIG. C10

FIGS. C7-C10 SOUND VELOCITY PROFILES

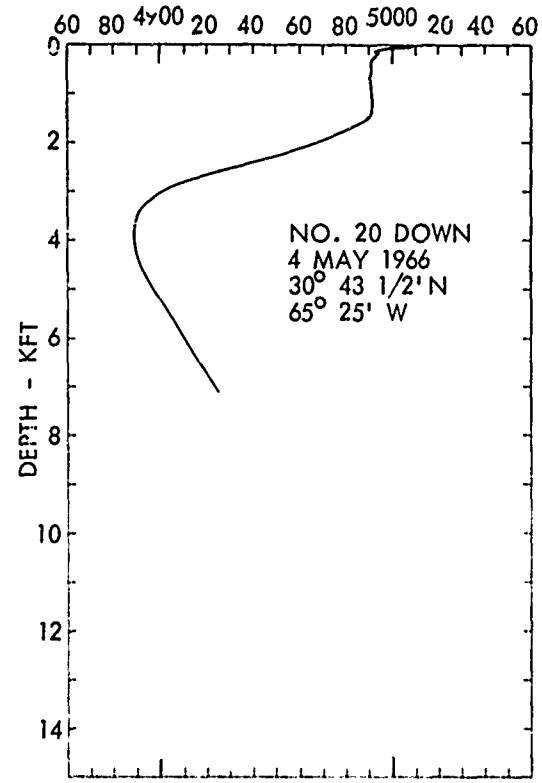

FIG. C-11

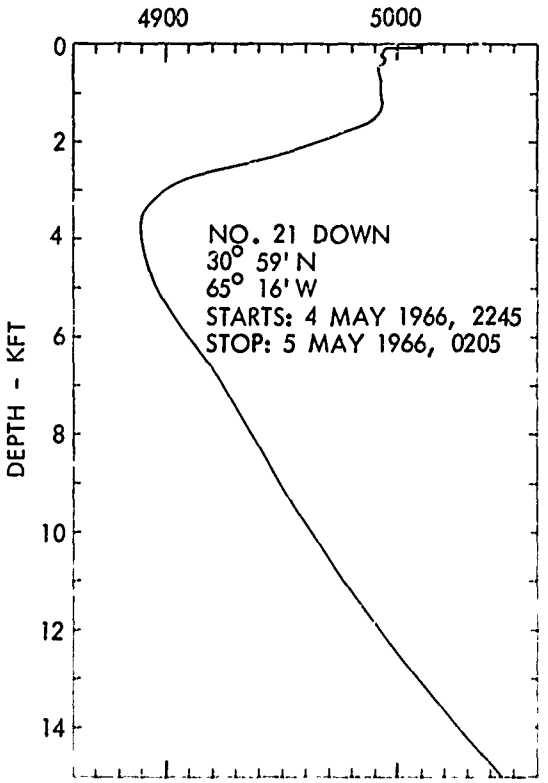

FIG. C-12

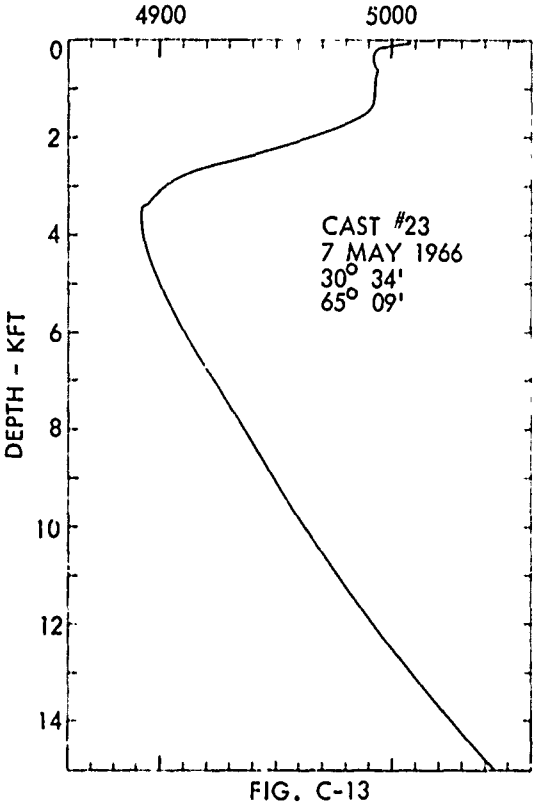

FIG. C-13

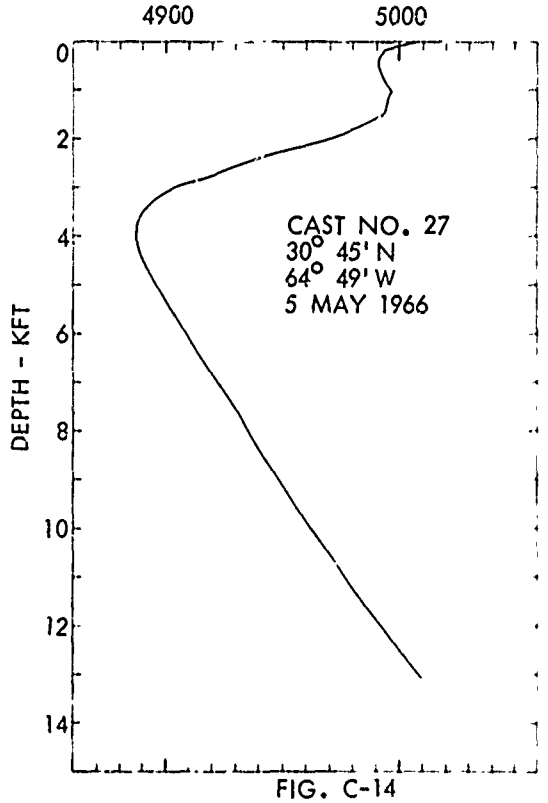

FIG. C-14

FIGS. C11-C14 SOUND VELOCITY PROFILES

APPENDIX D

COMPARISON FACTORS

The pressure factor, impulse factor, and energy factor are all defined in an analogous manner. They are the ratio of the quantity under refracting conditions to the quantity under isovelocity conditions. The similitude equations were used to get the isovelocity quantities even though they have not been experimentally verified (in isovelocity water) to convergence zone ranges.

Pressure factor

$$F_P = \frac{\text{peak pressure (refracting)}}{\text{peak pressure (isovelocity)}}$$

Impulse factor

$$F_I = \frac{\text{impulse (refracting)}}{\text{impulse (isovelocity)}}$$

Energy factor

$$F_E = \frac{\text{energy (refracting)}}{\text{energy (isovelocity)}}$$

The similitude equations used to get the isovelocity quantities for comparison were:

Peak pressure

$$p = 2.16 \cdot 10^4 \, (W^{1/3}/R)^{1.13} \, \frac{lb}{in^2}$$

Impulse (to 6.7θ)

$$I = 1.46 \, W^{1/3} (W^{1/3}/R)^{.89} \, \frac{lb\text{-}sec}{in^2}$$

Energy (to 6.7θ)

$$E = 2.44 \cdot 10^3 \, W^{1/3} (W^{1/3}/R)^{2.04} \, \frac{in\text{-}lb}{in^2}$$

where:

W = charge weight (pounds)
R = range (feet)

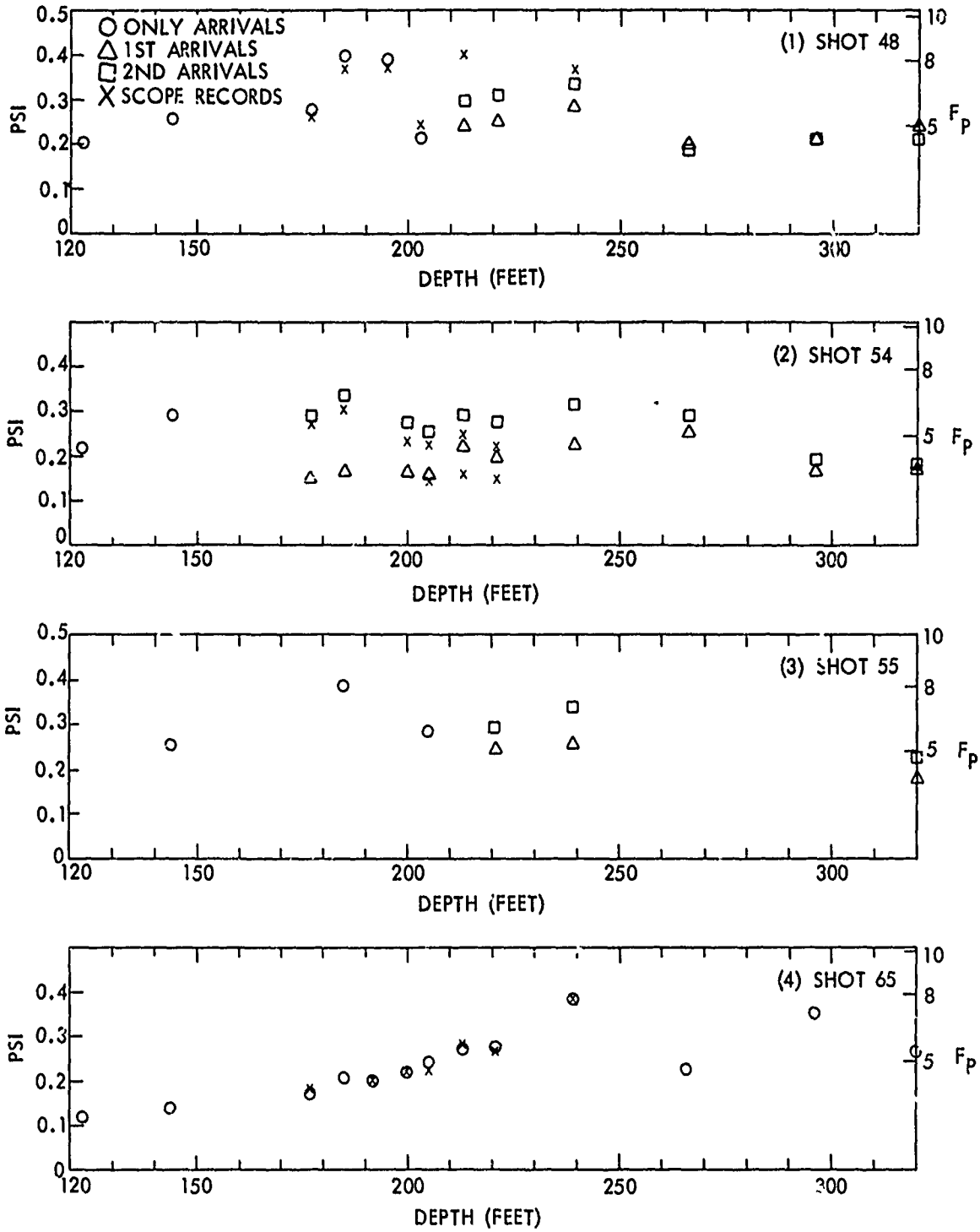

FIGS. E1-E4 PEAK PRESSURES AND PRESSURE FACTORS

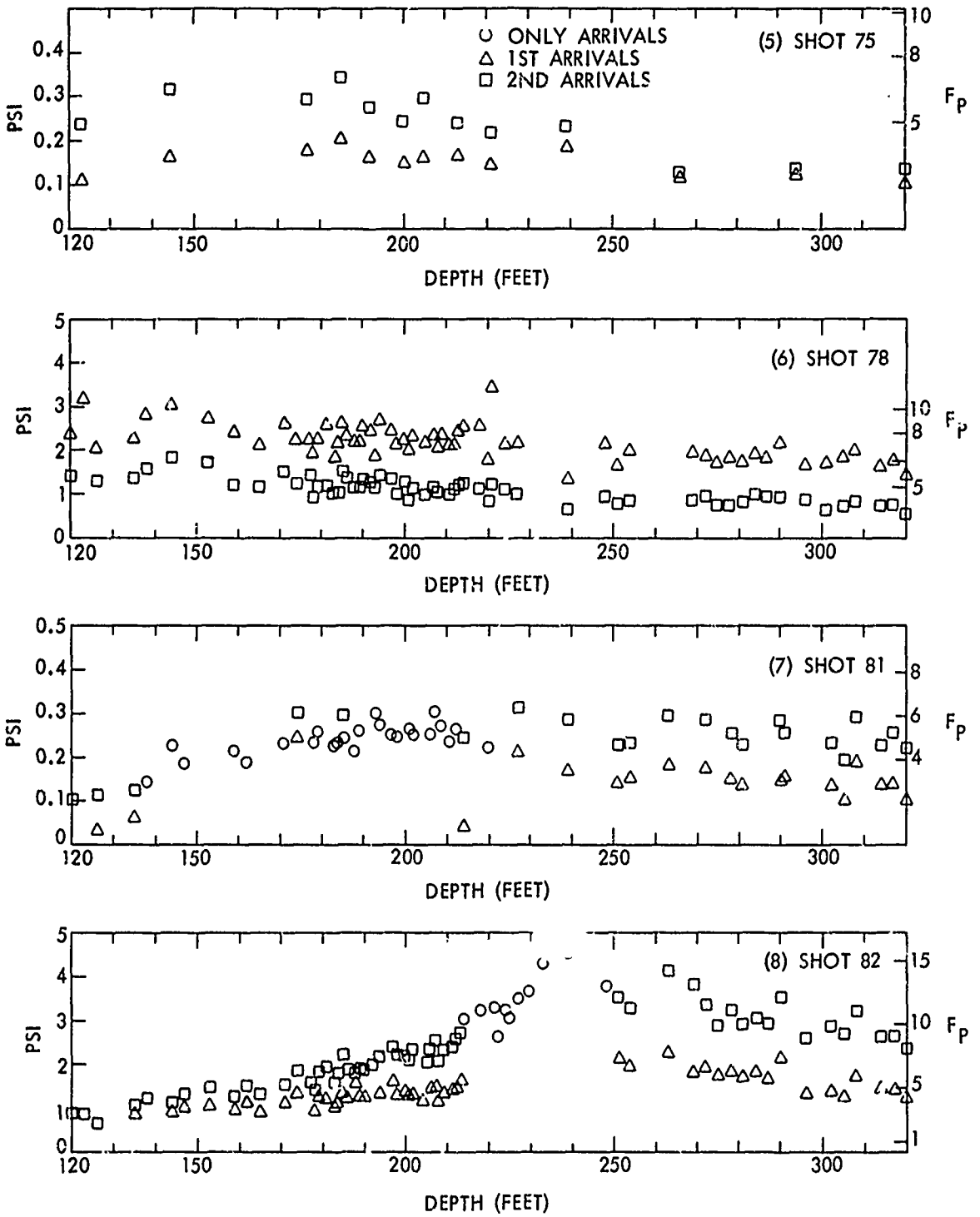

FIGS. E5-E8 PEAK PRESSURES AND PRESSURE FACTORS

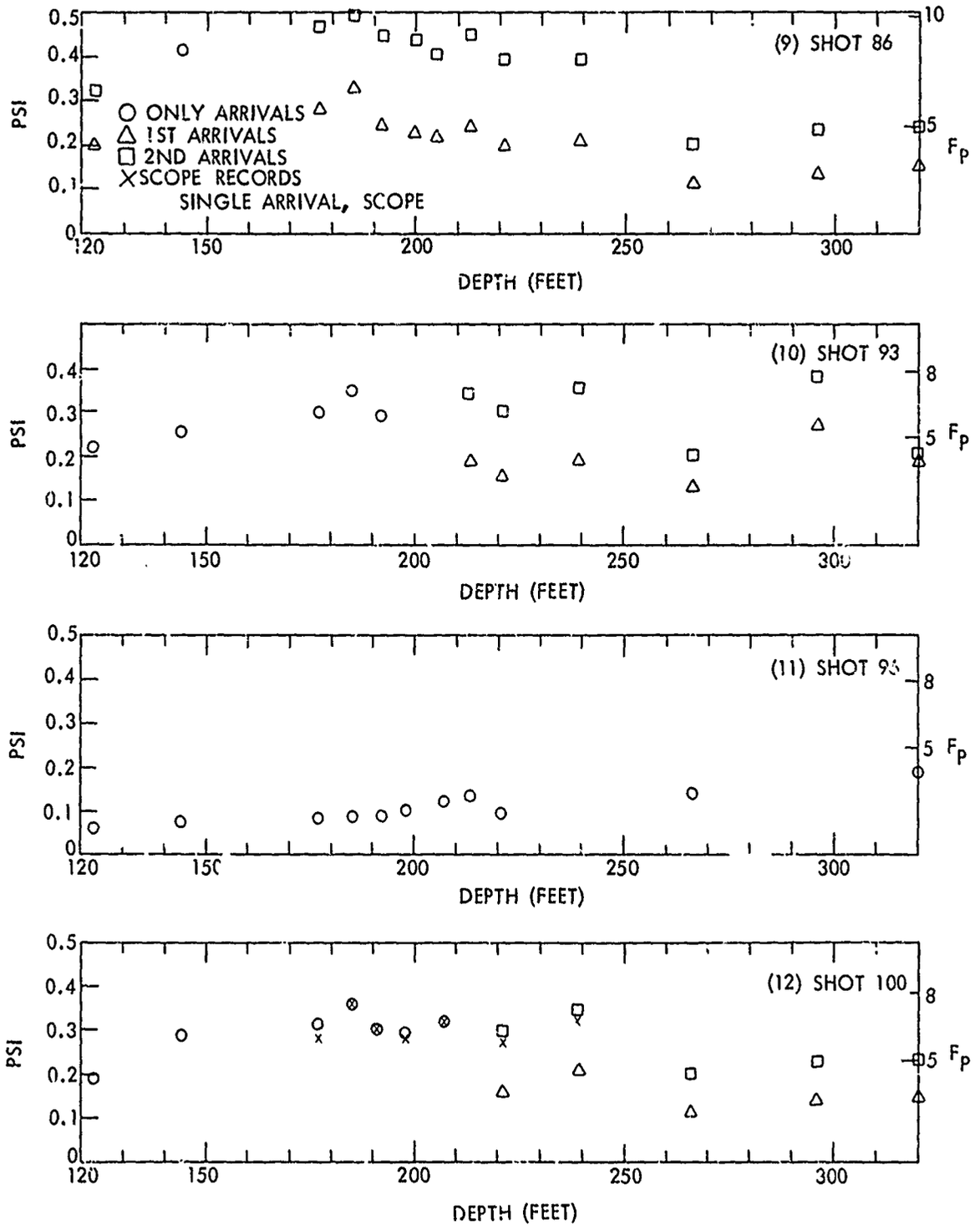

FIGS. E9-E12 PEAK PRESSURES AND PRESSURE FACTORS

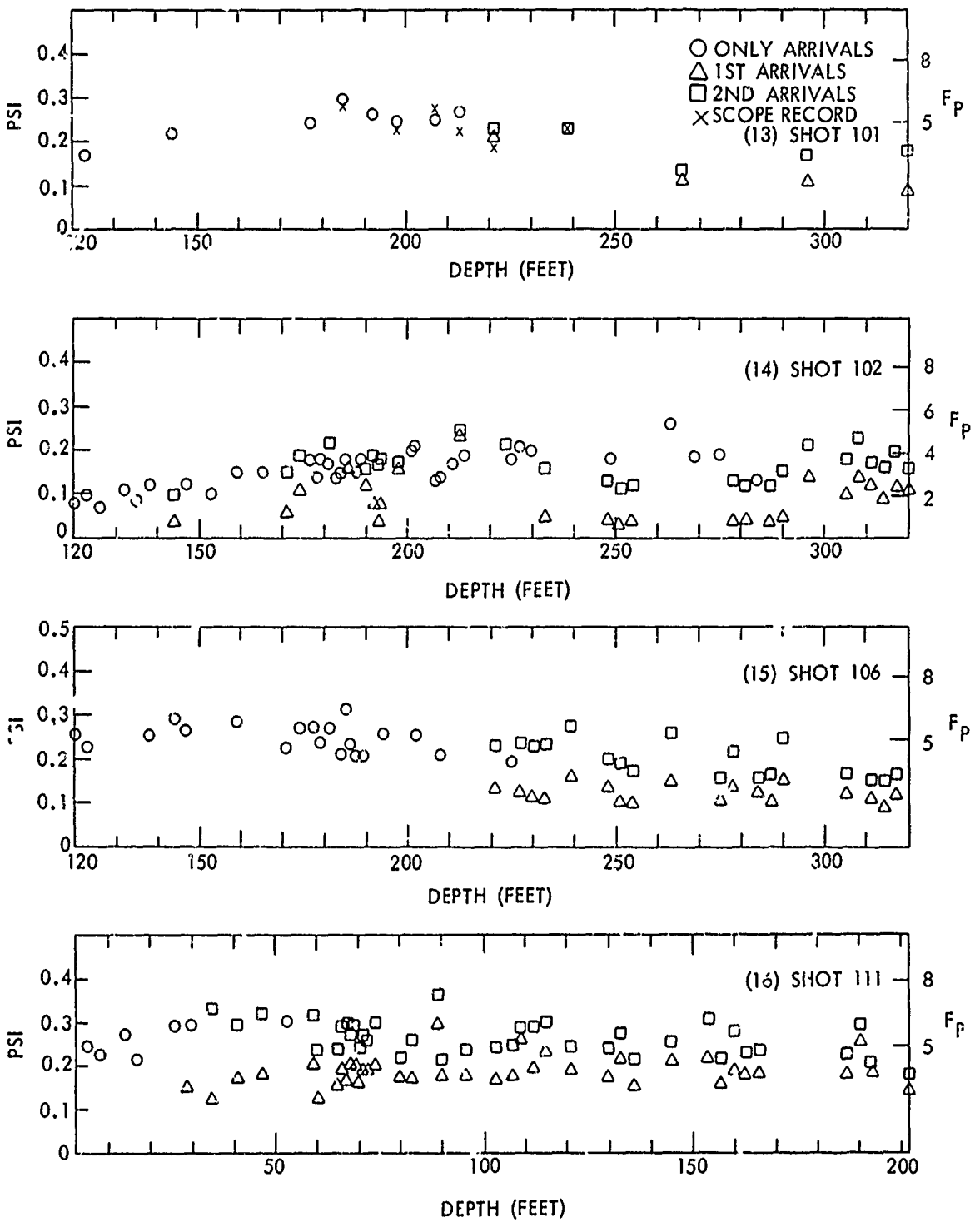

FIGS. E13-E16 PEAK PRESSURES AND PRESSURE FACTORS

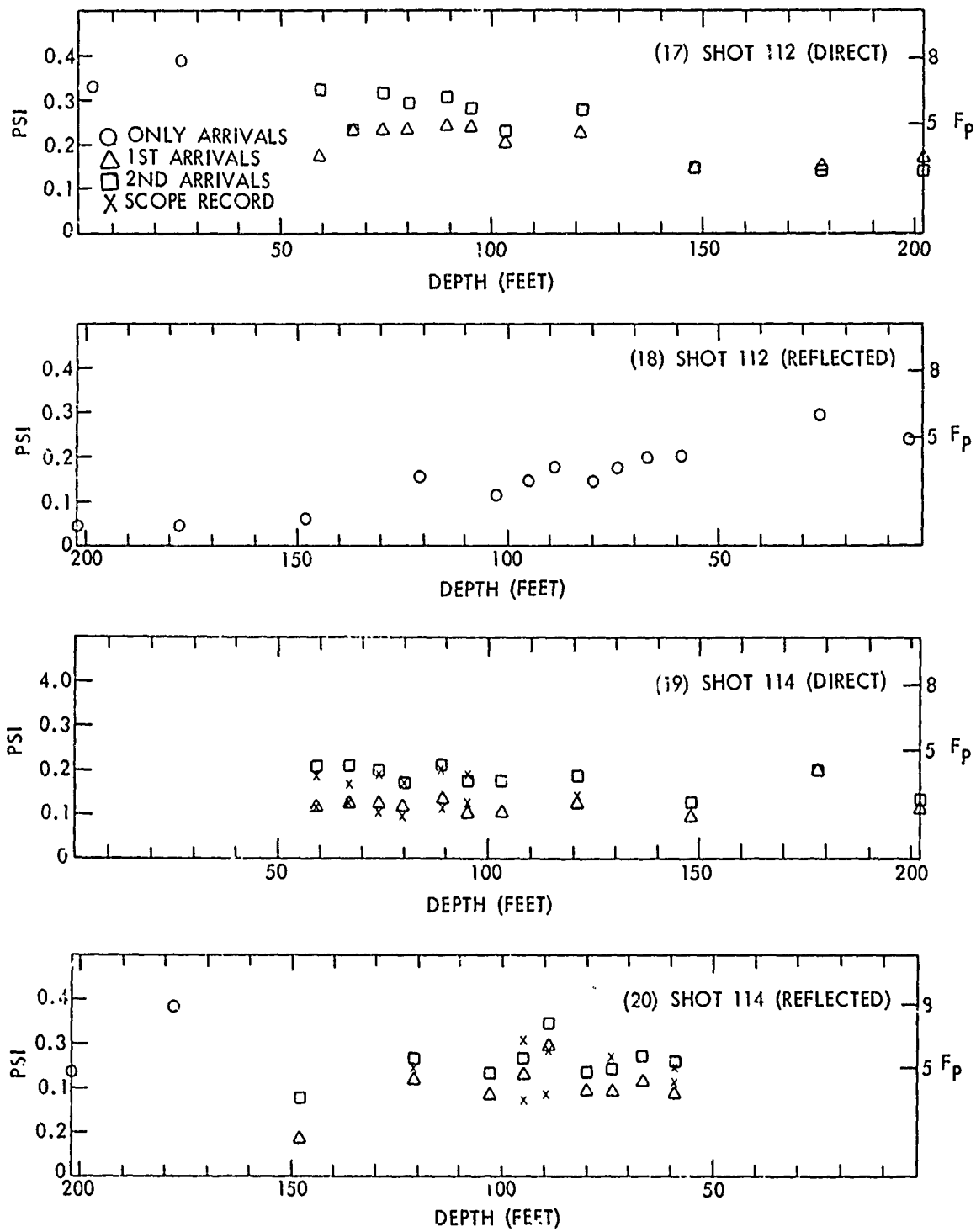

FIGS. E17-E20 PEAK PRESSURES AND PRESSURE FACTORS

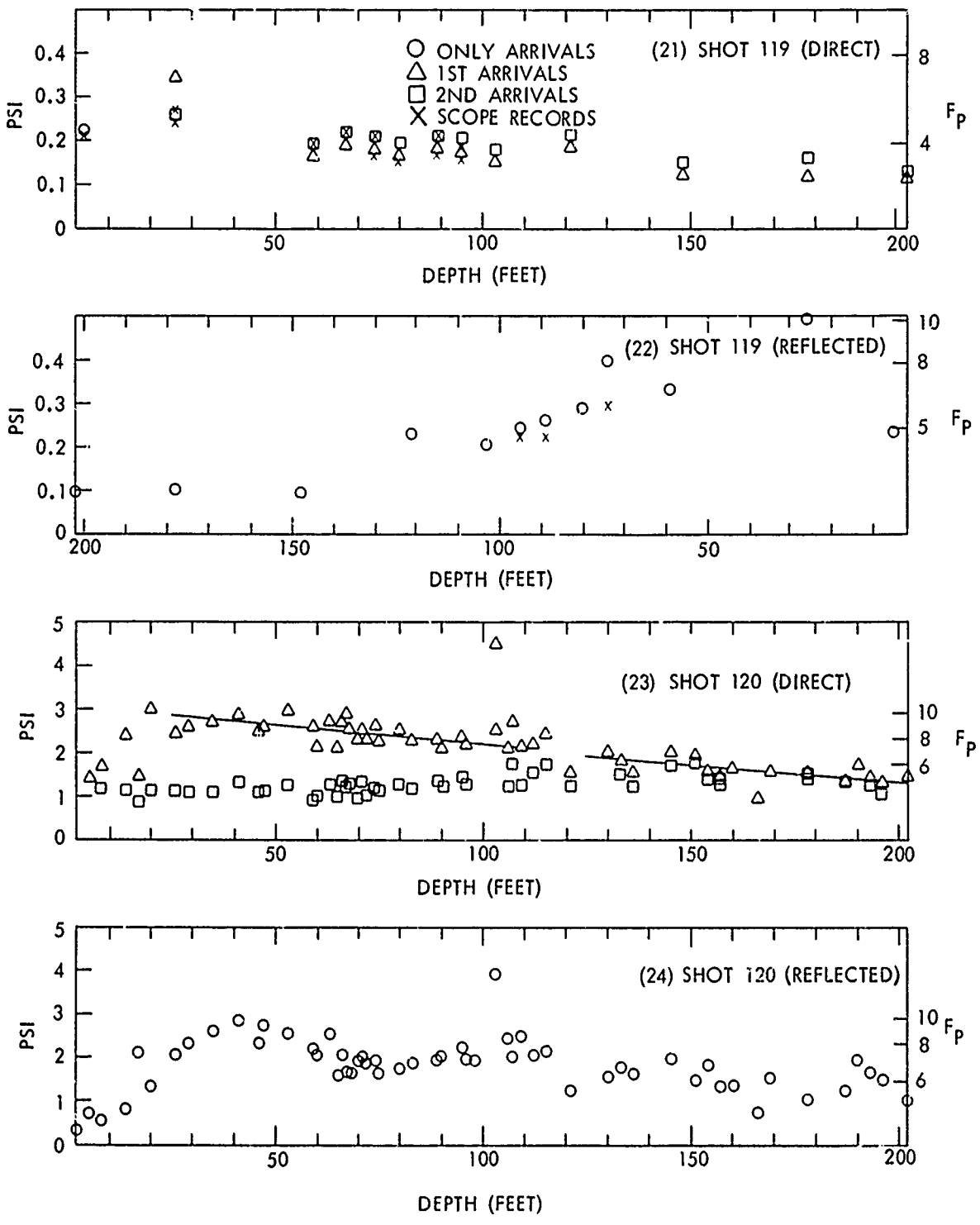

FIGS. E21-E24 PEAK PRESSURES AND PRESSURE FACTORS

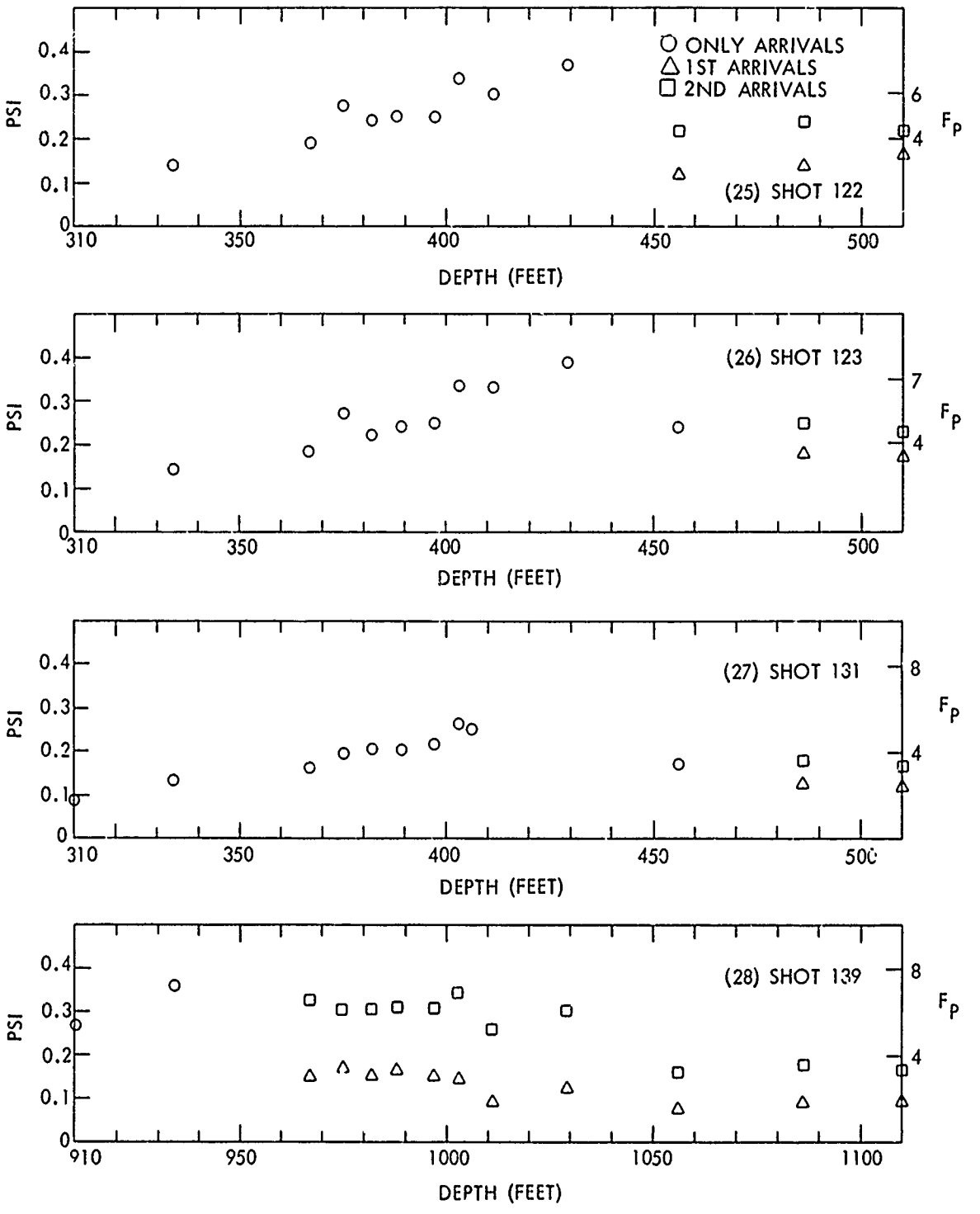

FIGS. E25-E28 PEAK PRESSURES AND PRESSURE FACTORS

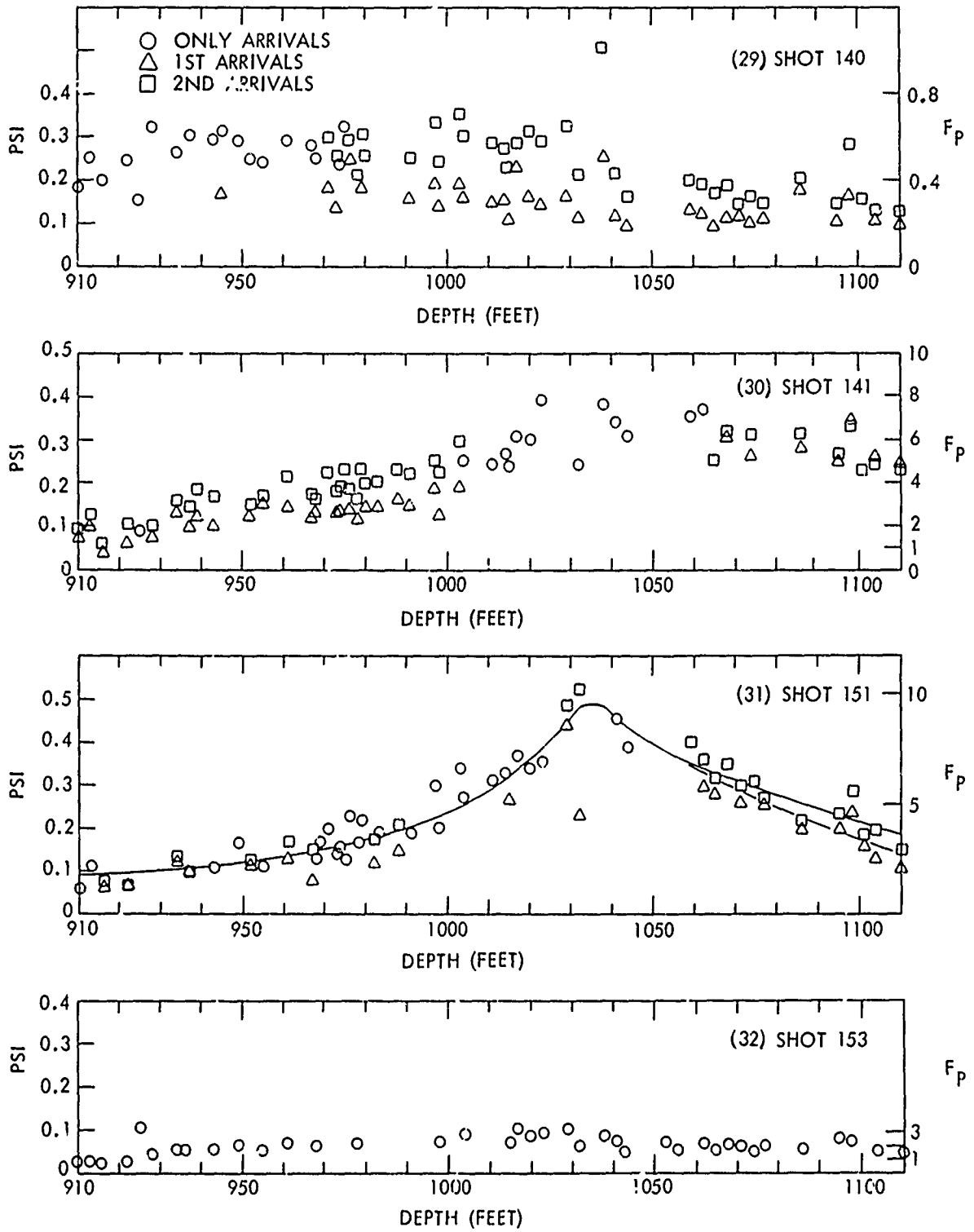

FIGS. E29-E32 PEAK PRESSURES AND PRESSURE FACTORS

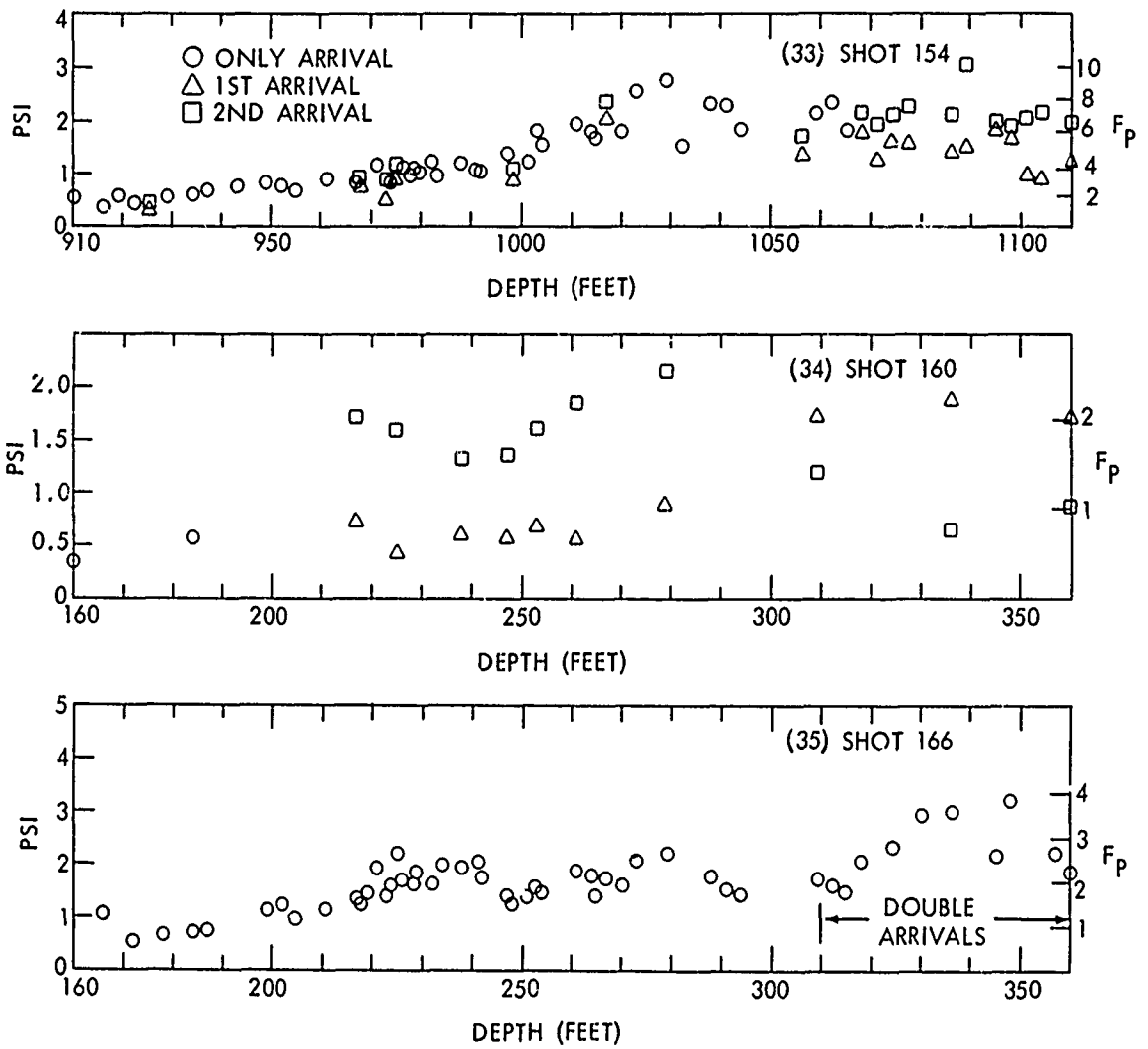

FIGS. E33-E35 PEAK PRESSURES AND PRESSURE FACTORS

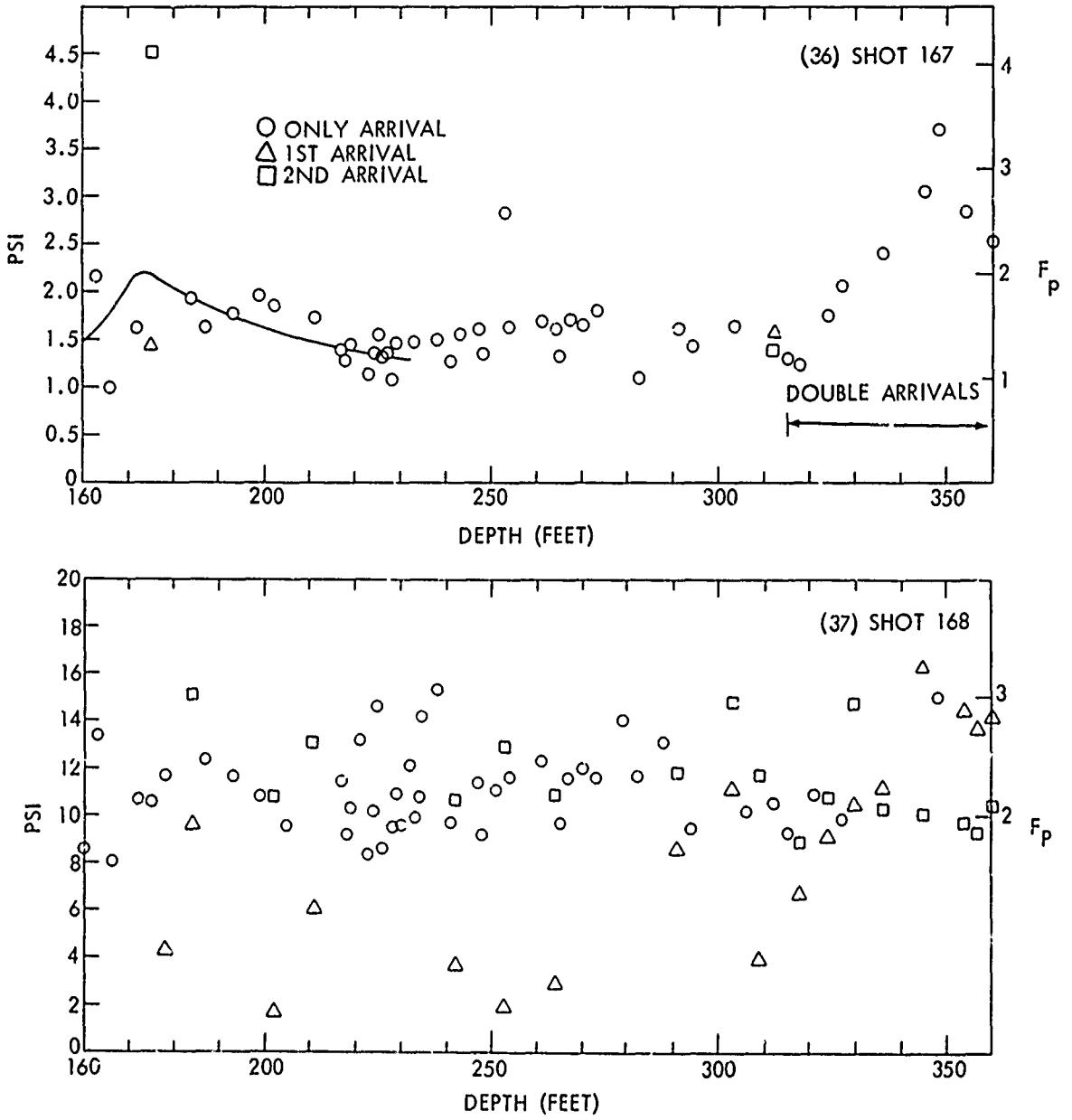

FIGS. E36-E37 PEAK PRESSURES AND PRESSURE FACTORS

APPENDIX F

PRESSURE HISTORIES

The pressure-time curves in this appendix were derived from the analog magnetic tape recordings. They were played back, digitized, and converted to standard scales. Because the digitizing equipment had to be started manually, a long portion of the record was digitized to insure that the shock wave was included. A computer program searched through the digital data to find the beginning of the shock wave. The zero time for each channel is at the first perceptible rise of the signal above the noise level inherent in the baseline. Because the noise levels and signals were different among the channels, there is no common time base for the pressure as presented here.

The pressure histories for each shot are identified by the depth, in feet, of the gage for each pressure history.

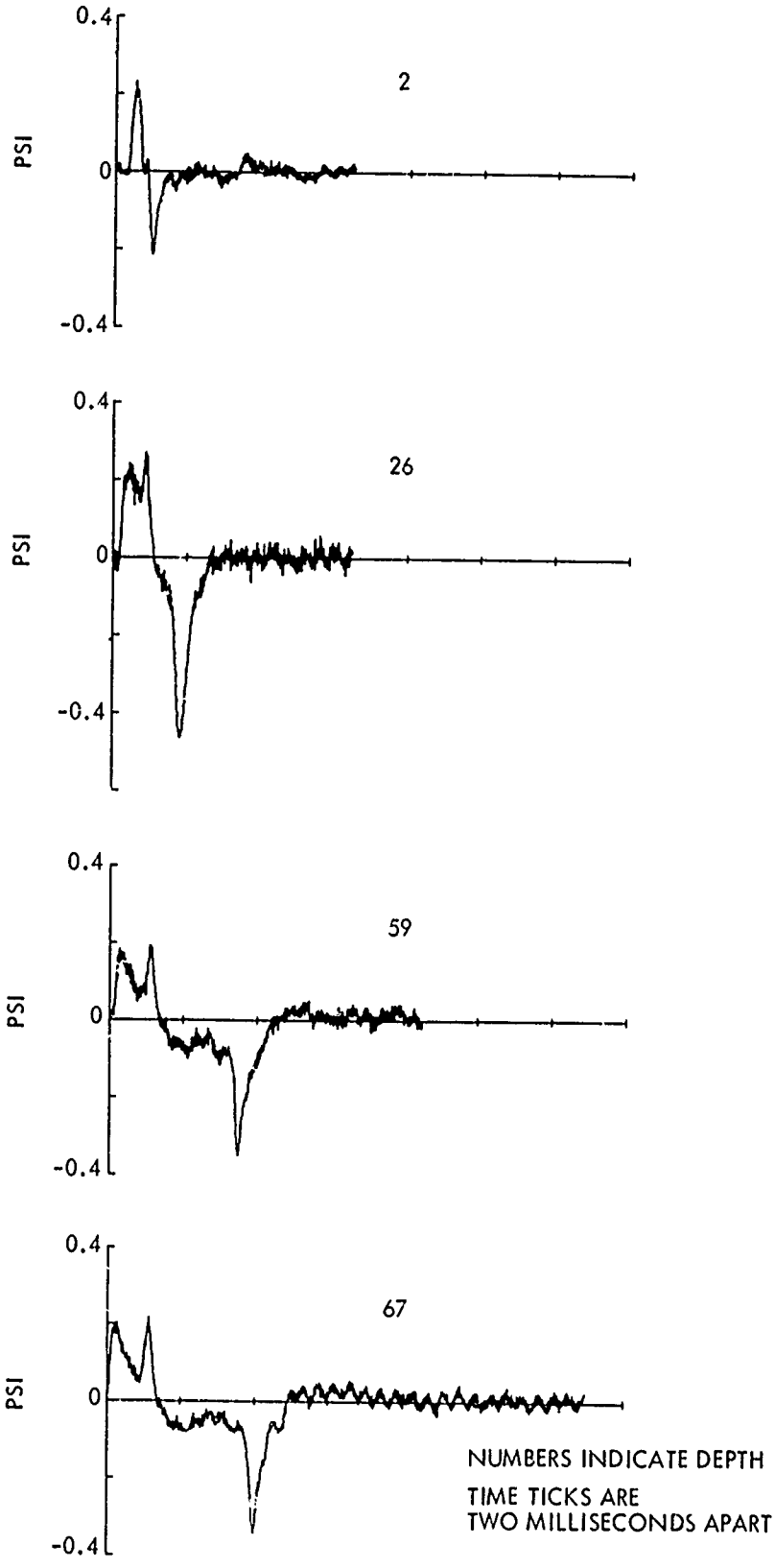

FIGS. F1 - F4 PRESSURE VS. TIME - SHOT 119

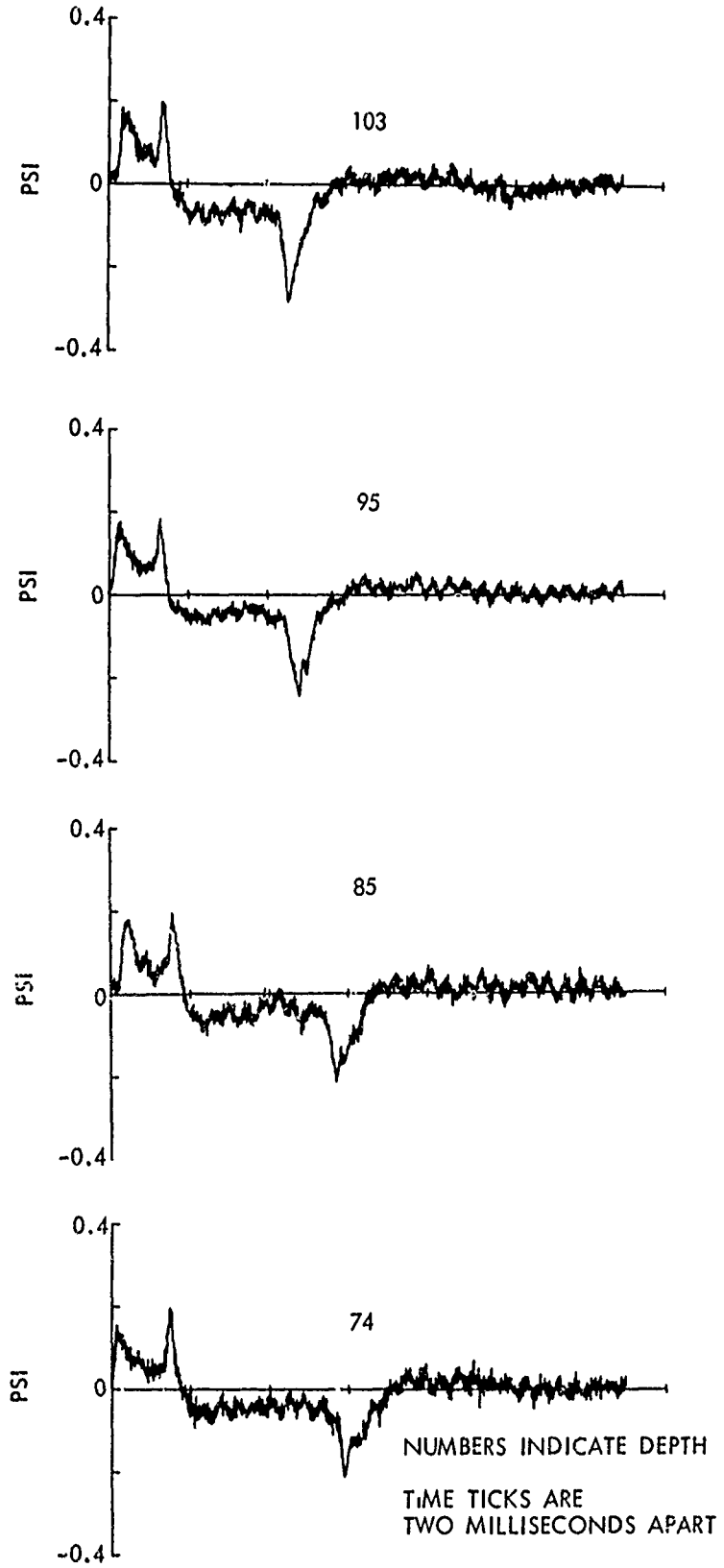

FIGS. F5-F8 PRESSURE VS TIME-SHOT 119

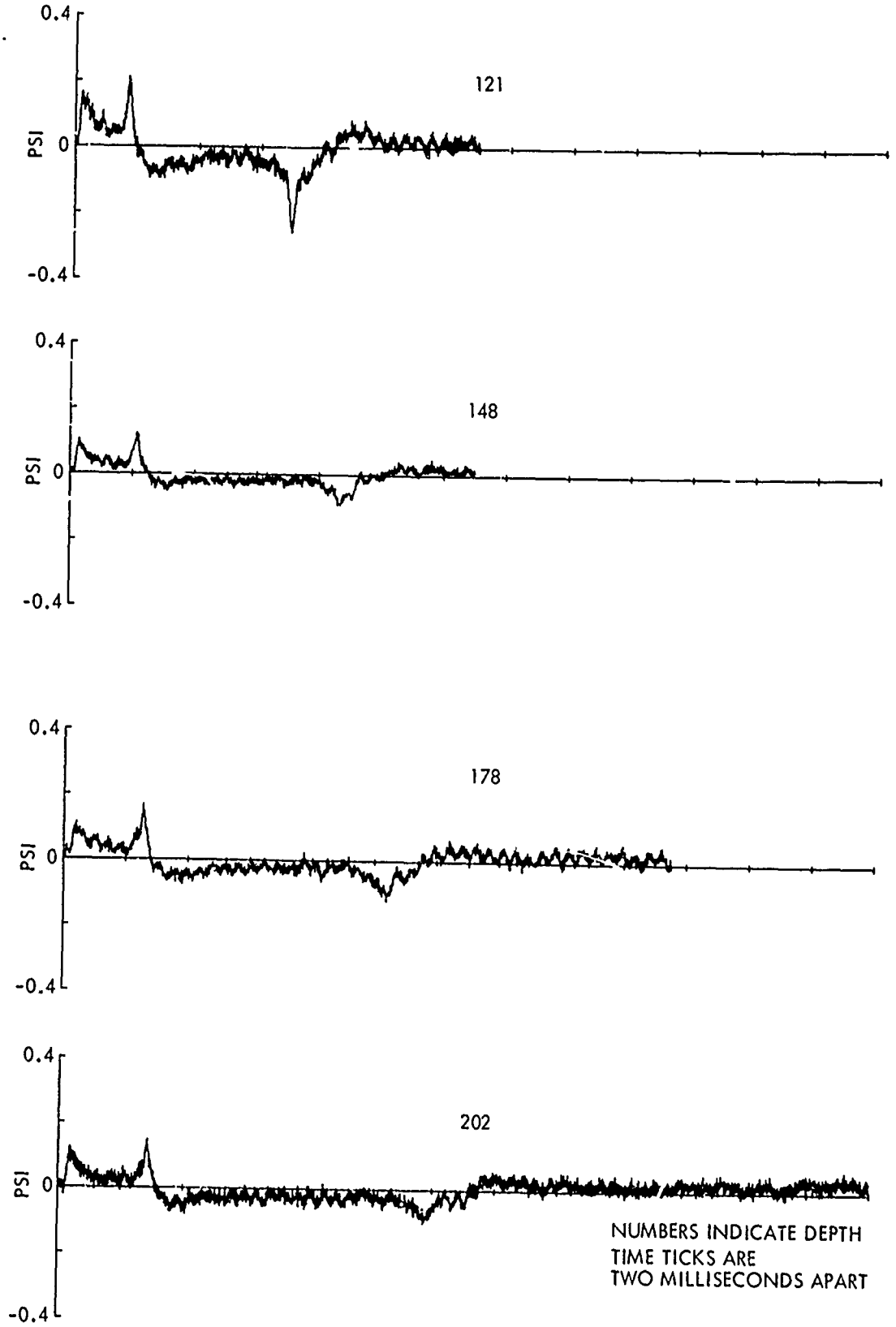

FIGS. F9 - F12 PRESSURE VS. TIME - SHOT 119

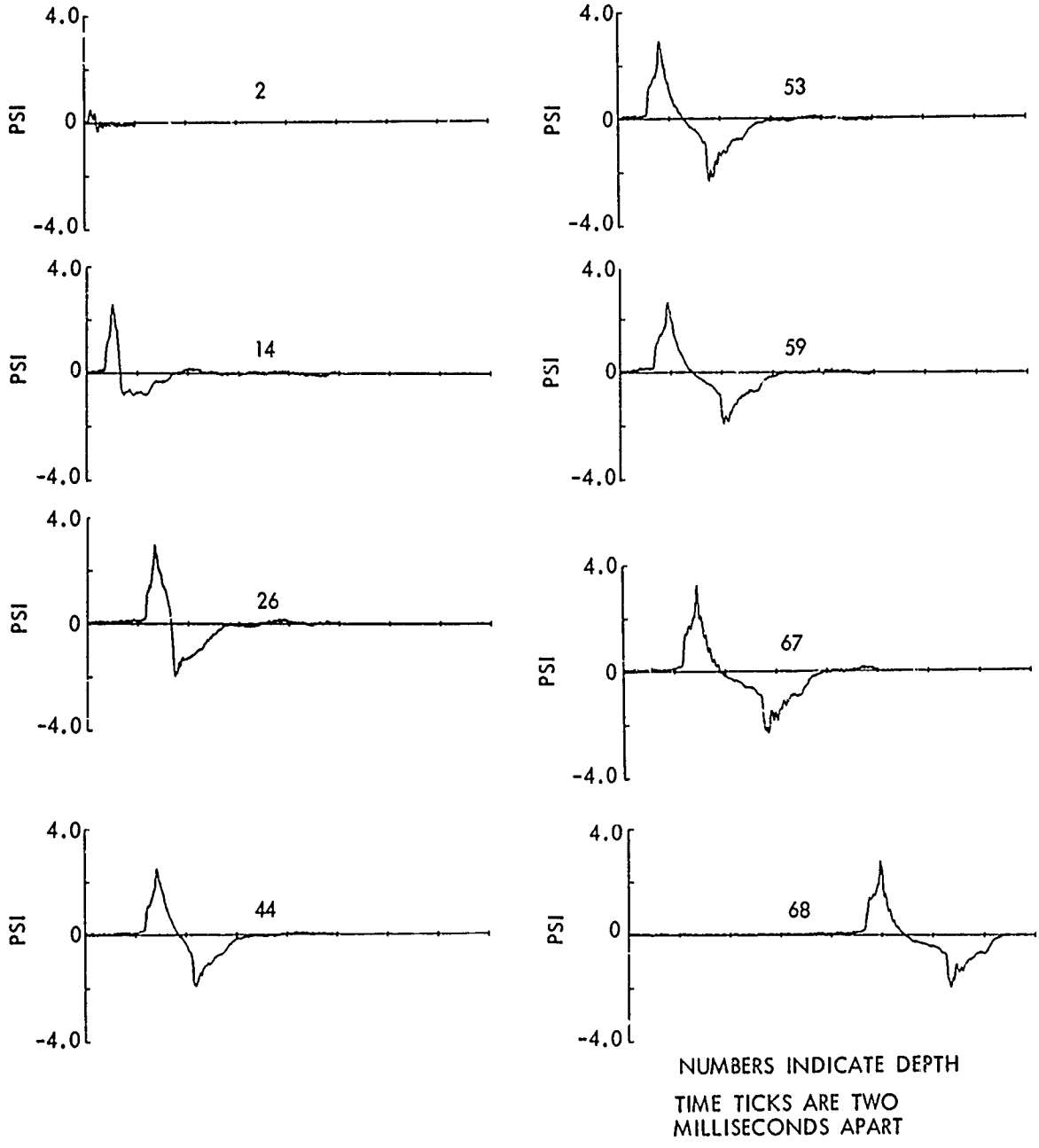

FIGS. F13-F2C PRESSURE VS TIME-SHOT 120

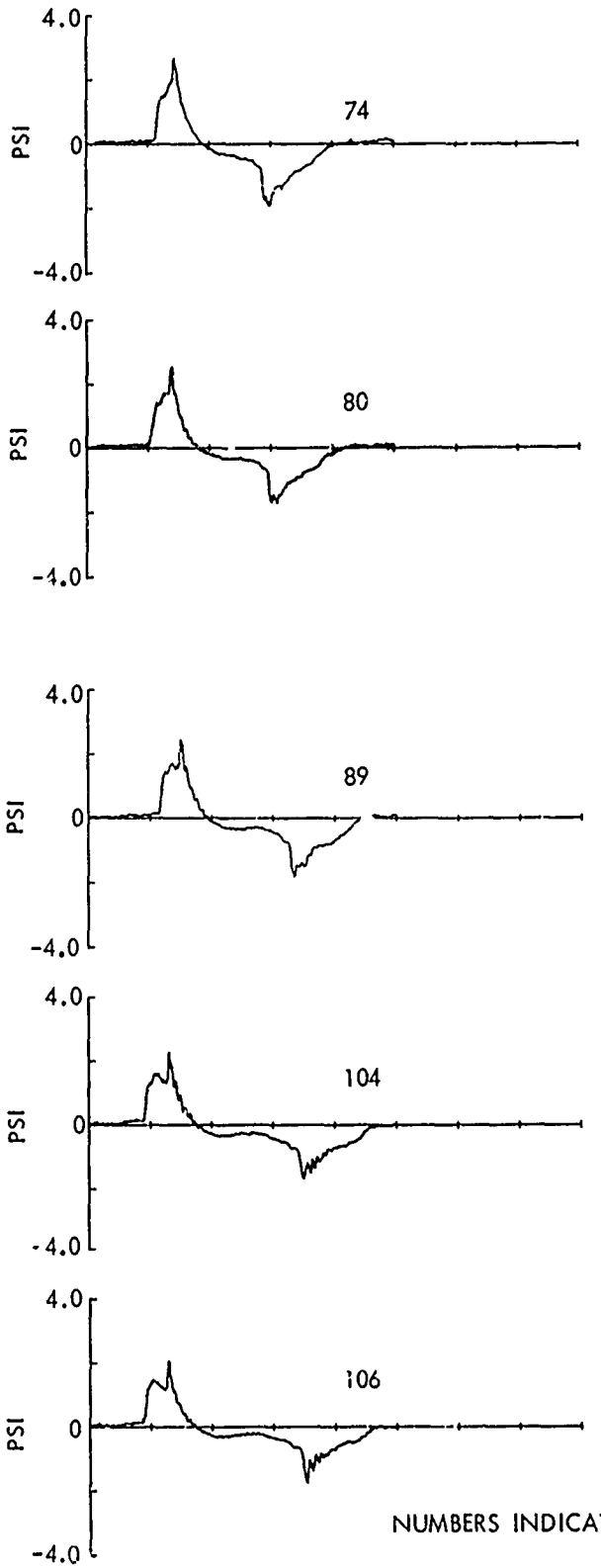

FIGS. F21-F25 PRESSURE VS TIME-SHOT 120

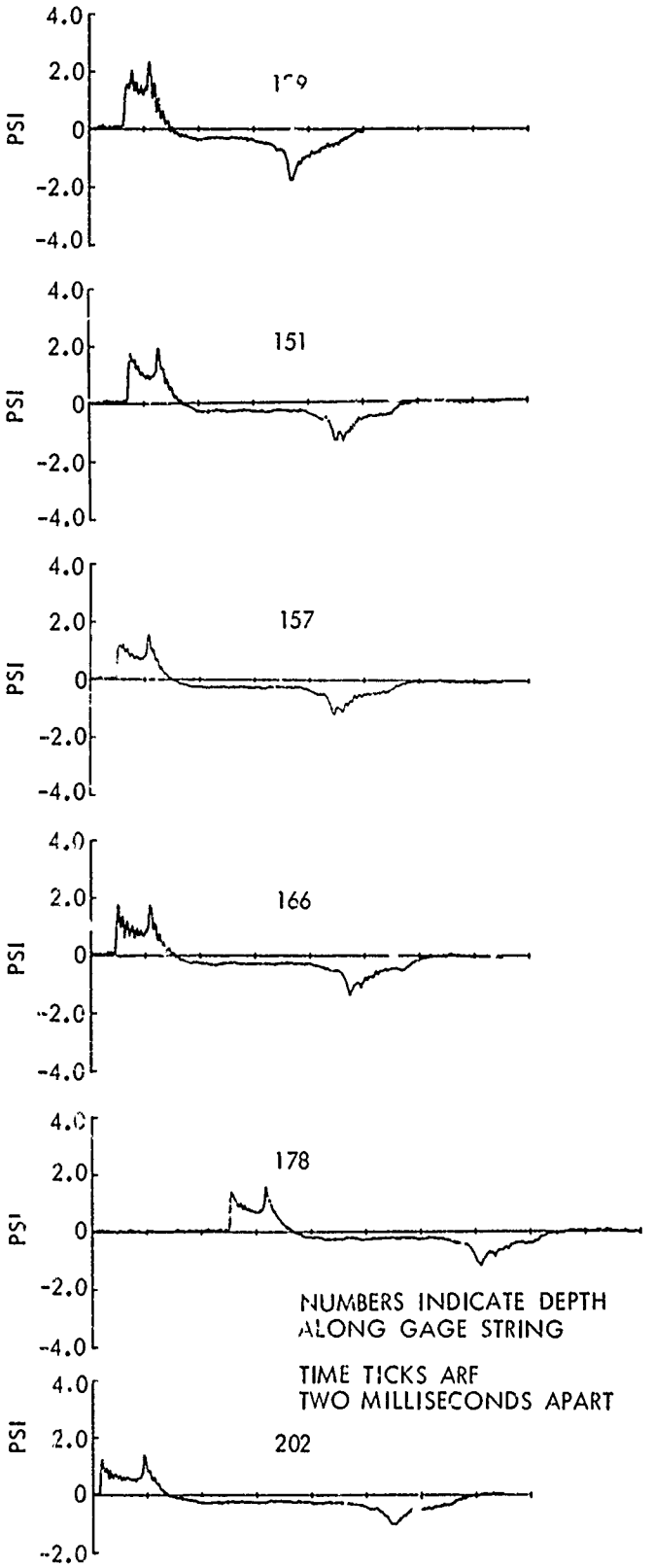

FIGS. F26-F31 PRESSURE VS TIME -SHOT 120

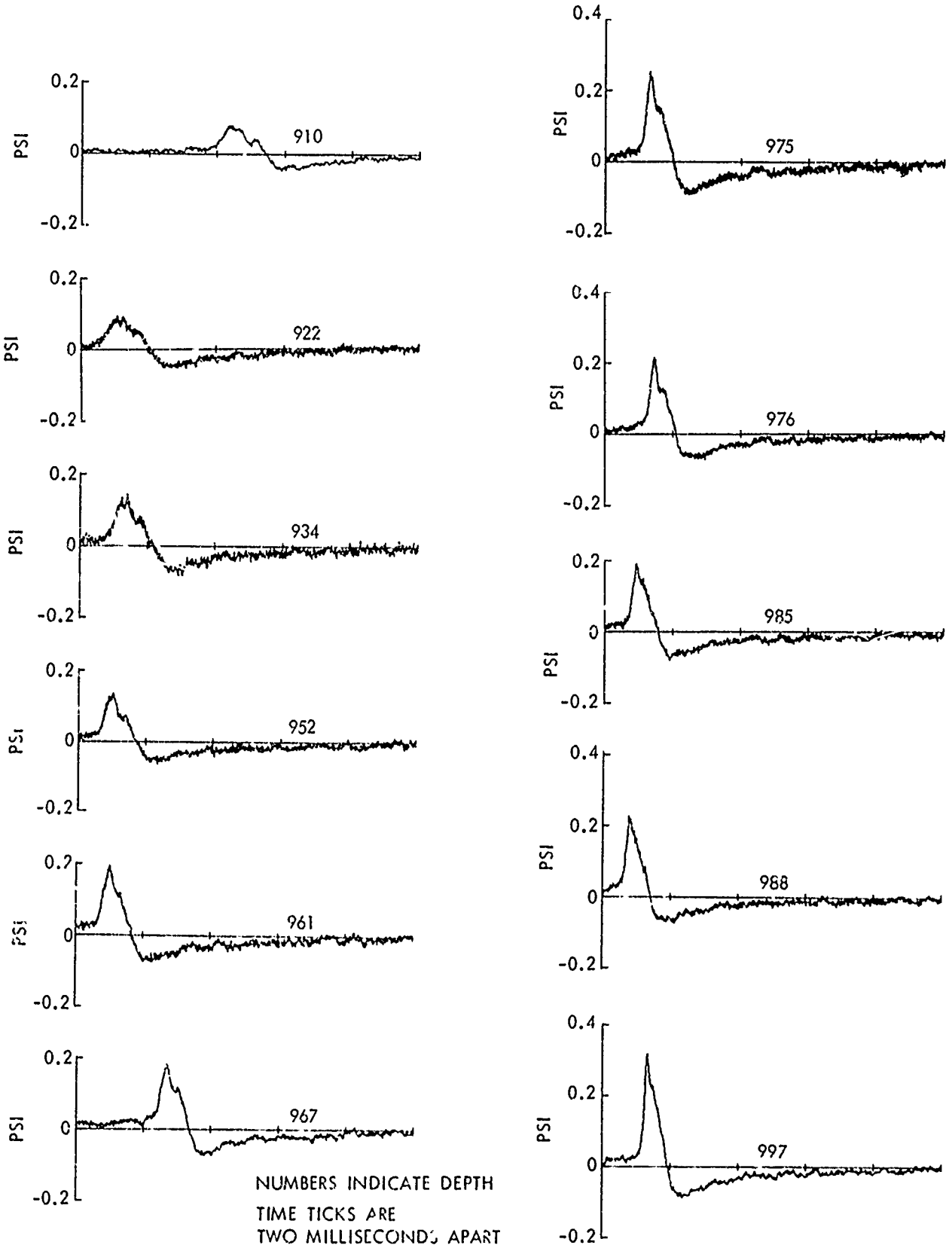

FIGS. F32-F42 PRESSURE VS TIME - SHOT 151

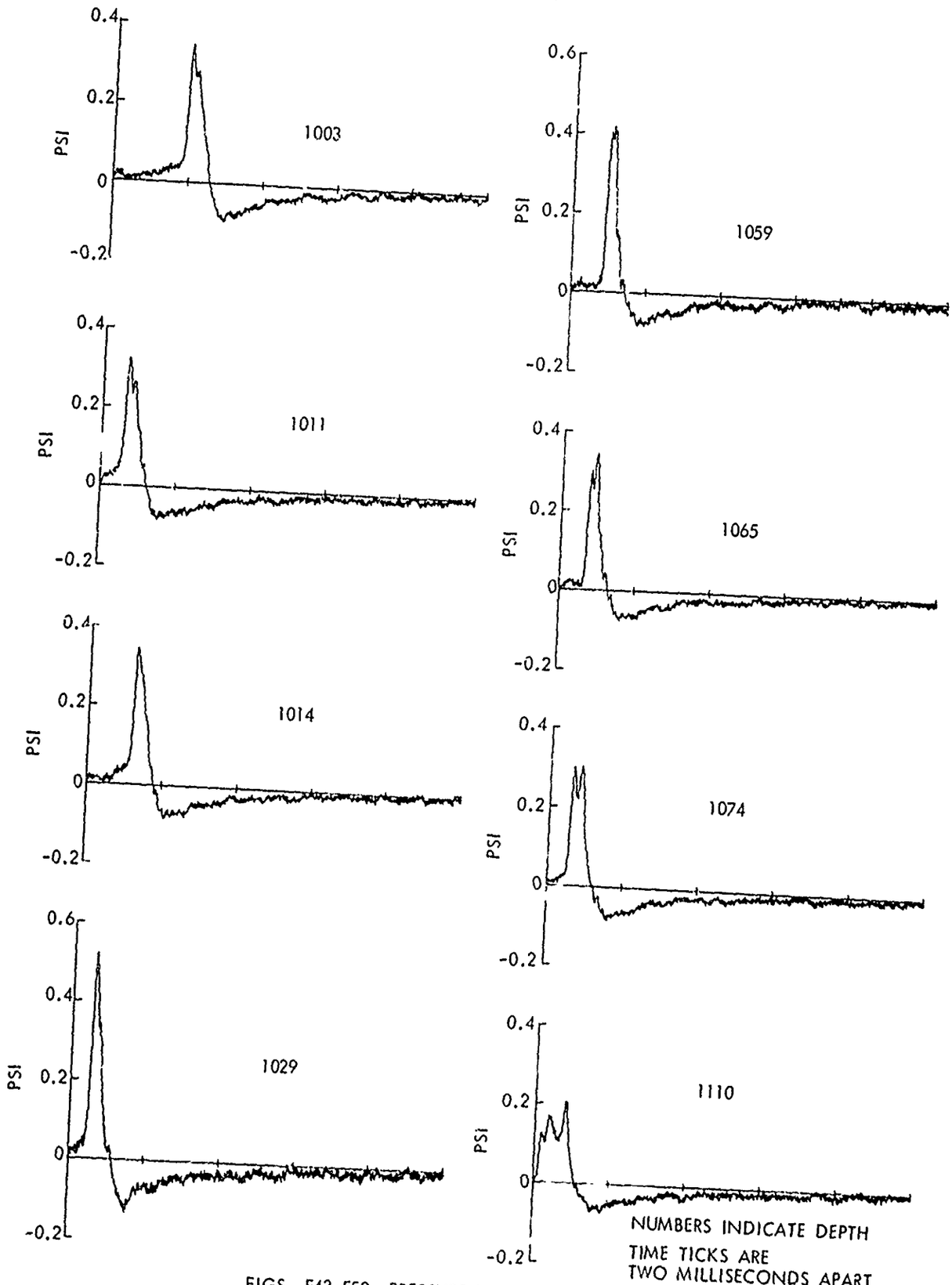

FIGS. F43-F50 PRESSURE VS TIME-SHOT 151

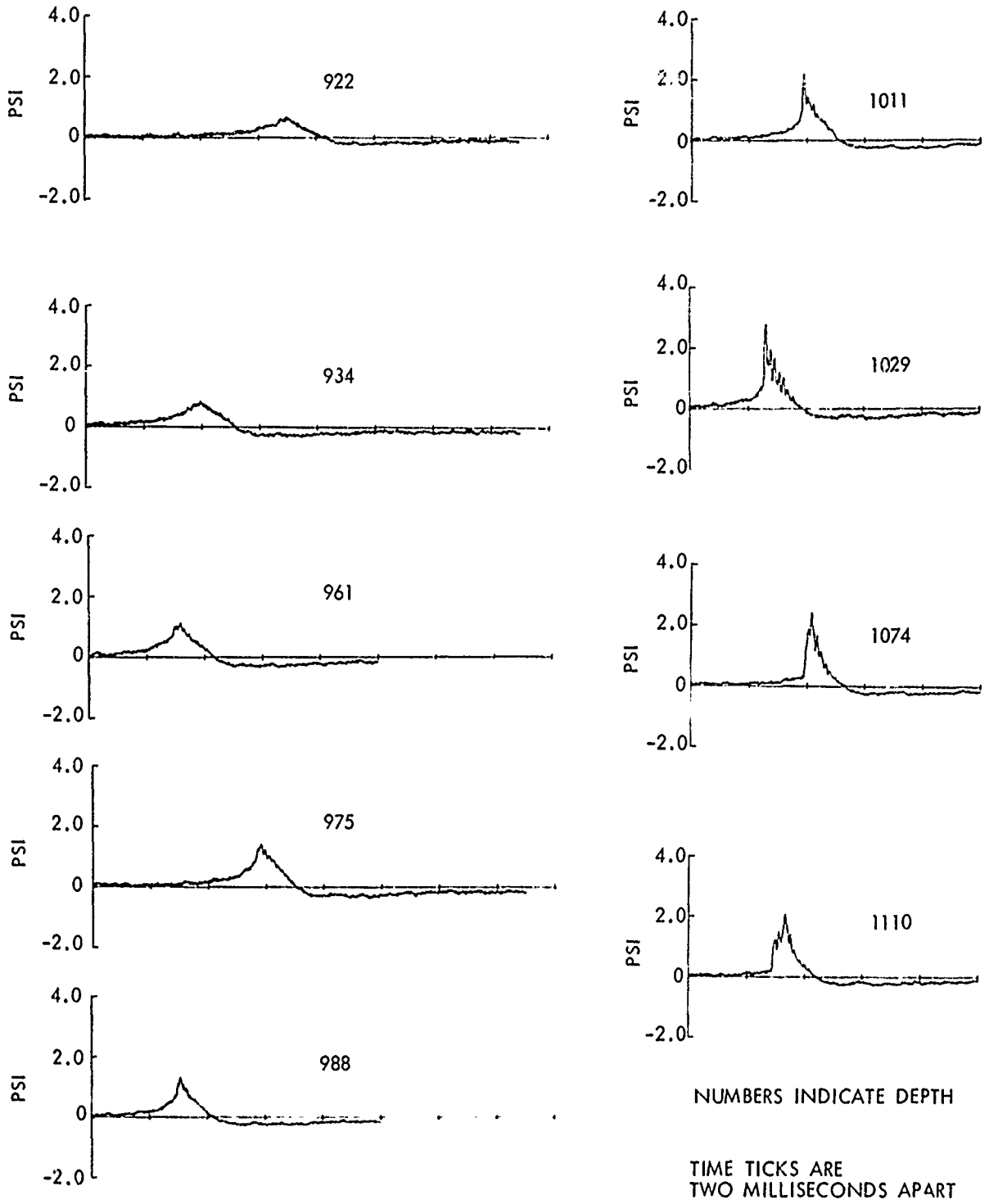

FIGS. F51-F59 PRESSURE VS TIME - SHOT 154

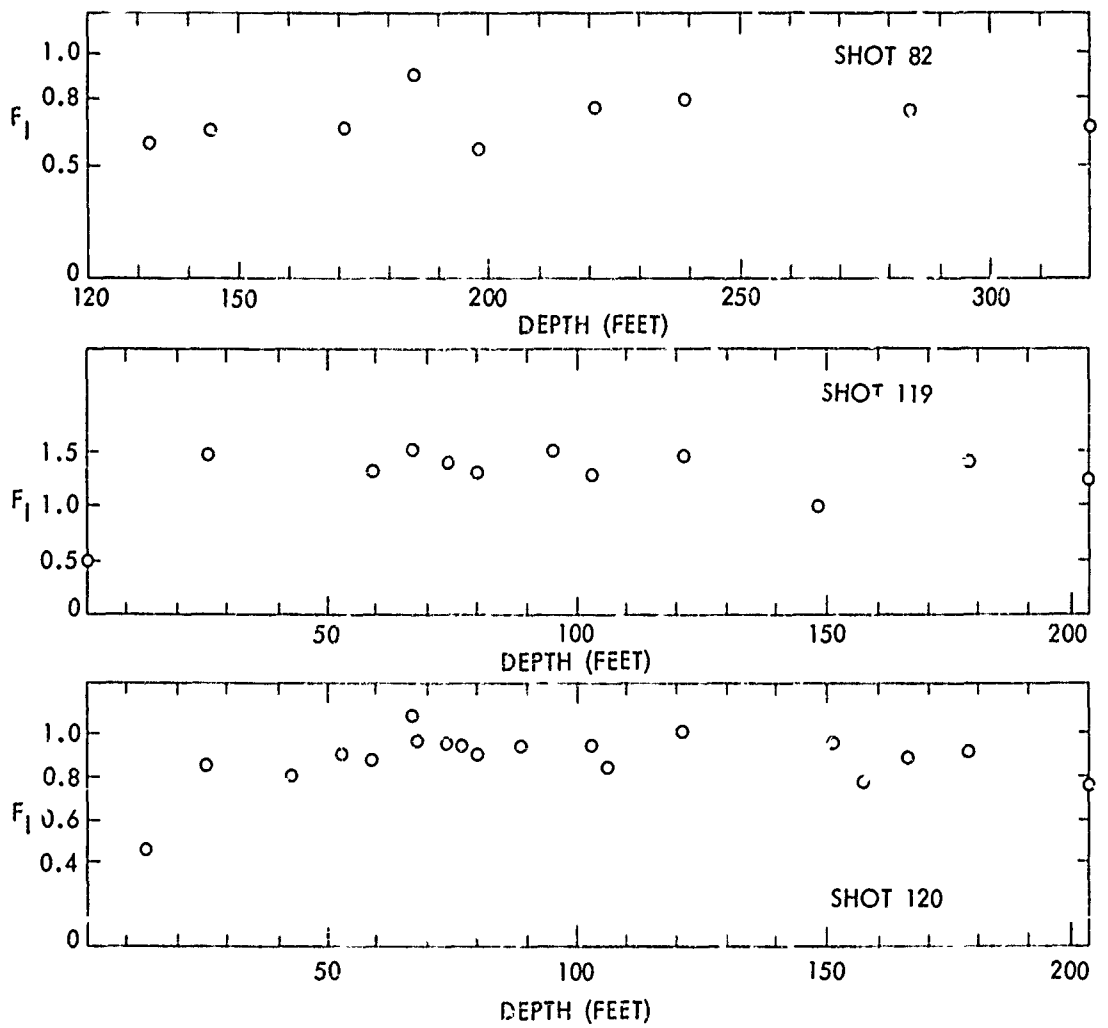

FIGS. G1-G3 IMPULSE FACTOR VS DEPTH

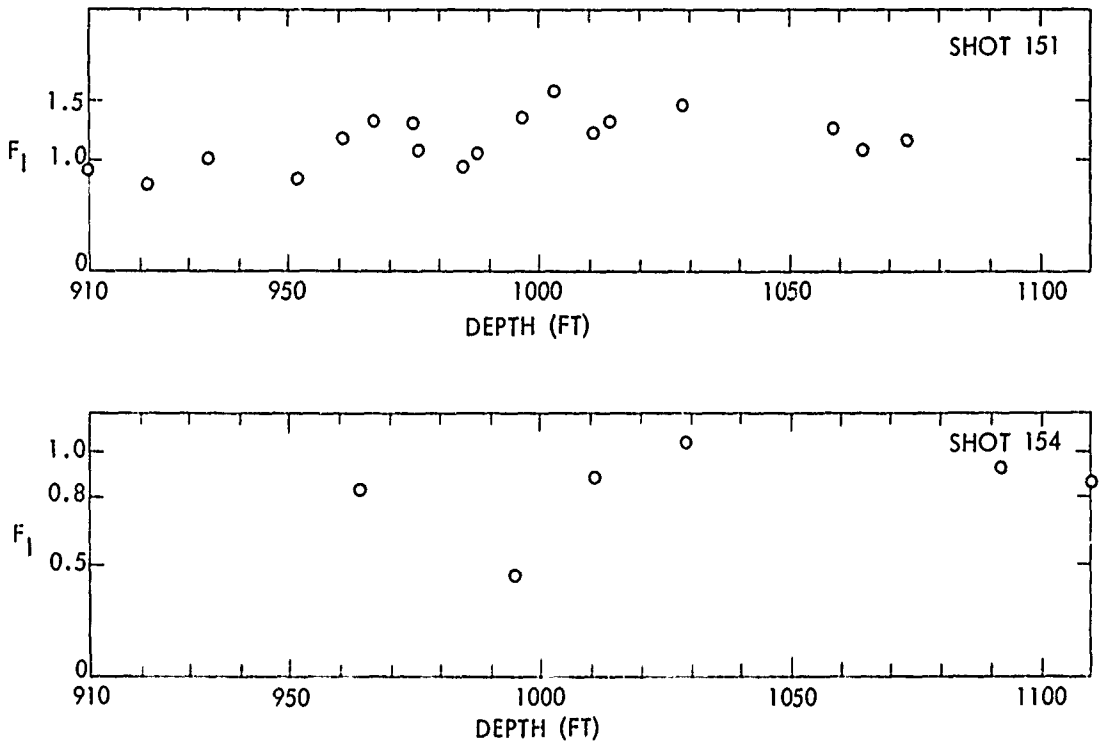

FIGS. G4 - G5 IMPULSE FACTOR VS DEPTH

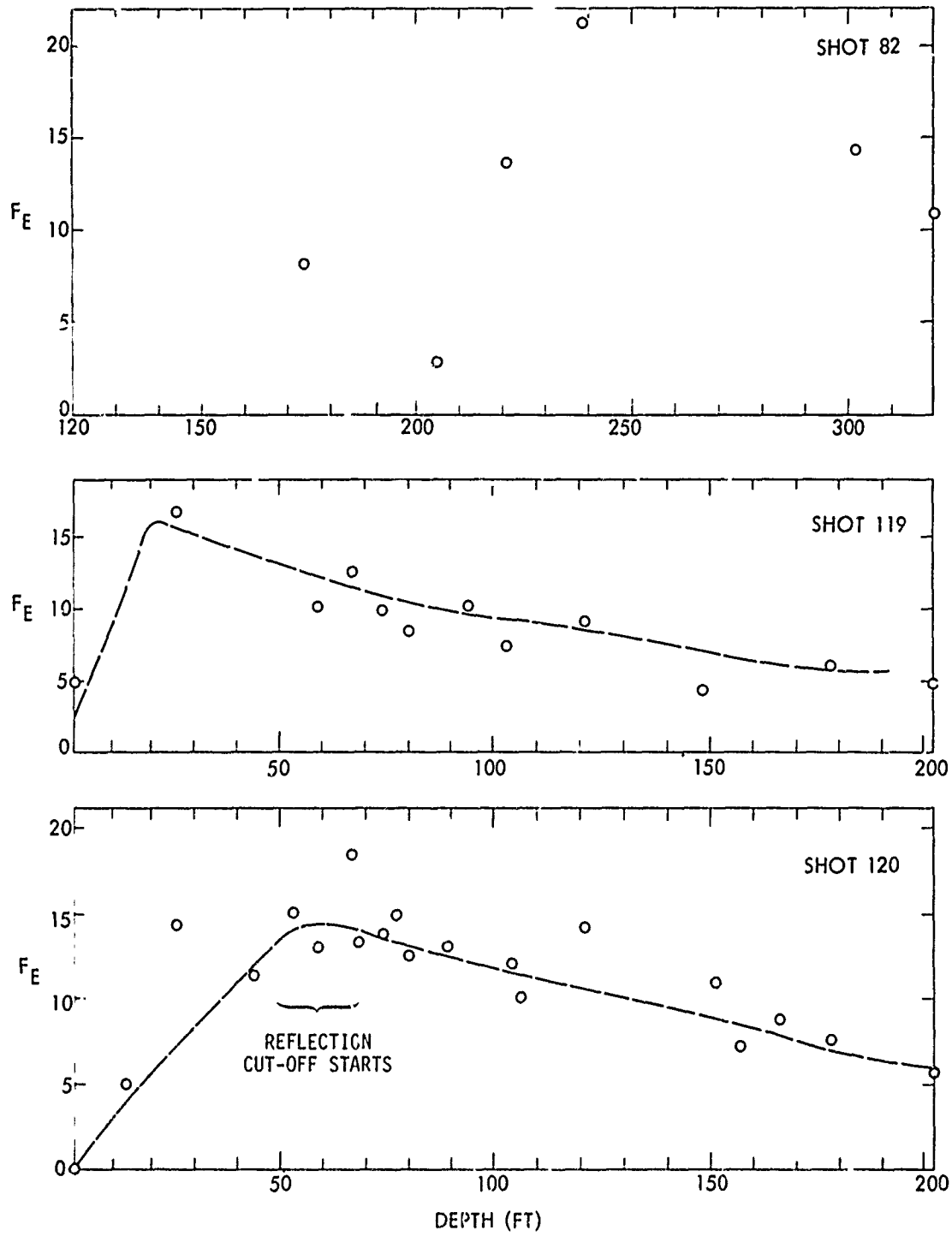

FIGS. H1-H3 ENERGY FACTOR VS DEPTH

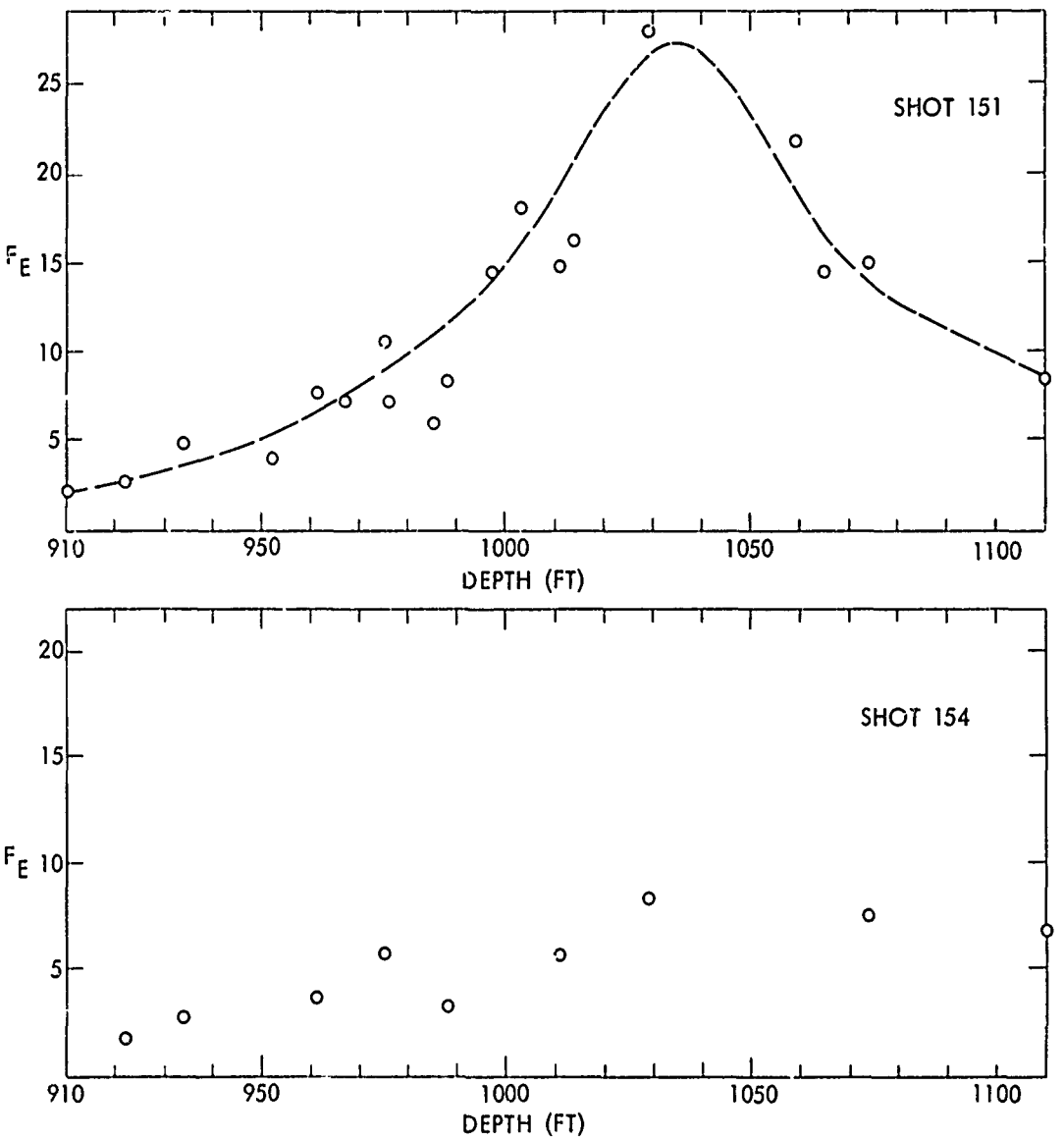

FIGS. H4 - H5 ENERGY FACTOR VS DEPTH

APPENDIX I

FREQUENCY SPECTRA

The frequency spectra were derived from the digitized pressure-time histories. A computer program in wide use at NOL, MR WISARD, was used to obtain the one-sided power spectrum density from the pressure-time data, using a Fast Fourier Transform method. The resolution bandwidth was 127 Hz for all the records that were analyzed.

The pressure-time records and their spectra are shown together for Shot 82. For Shot 154, the pressure-time records are in Appendix F. The decibel scale was arbitrarily chosen. However, the decibel scale shown may be converted to decibels relative to 1 erg/cm^2/Hz by subtracting 35 dB from the existing scale.

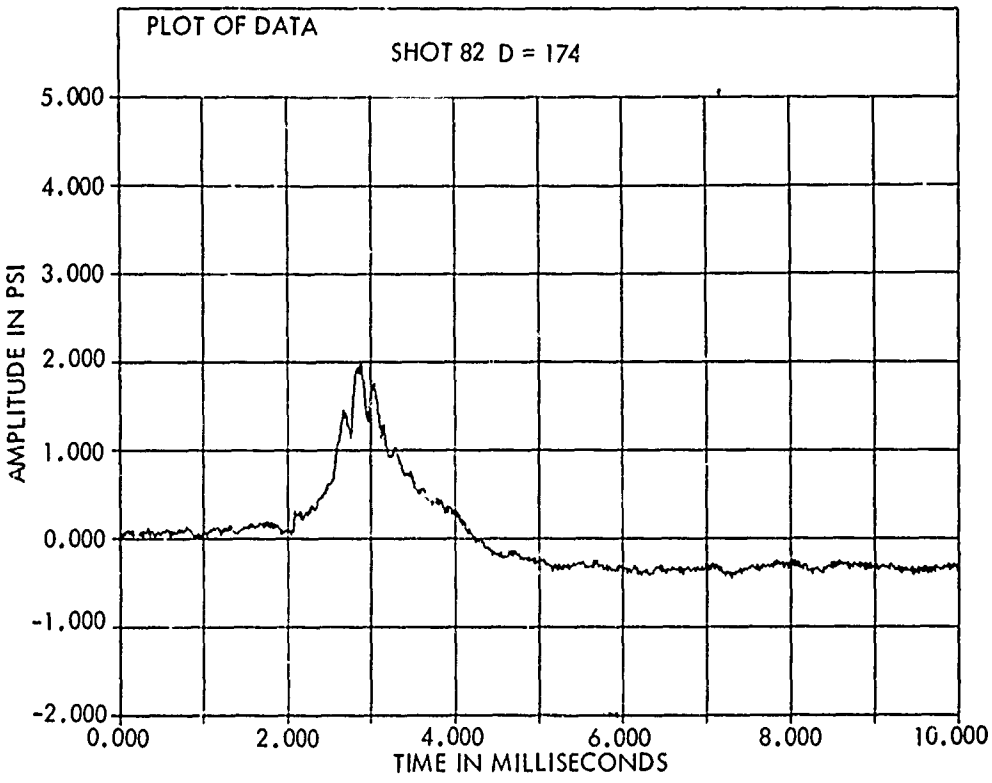

FIG. 11

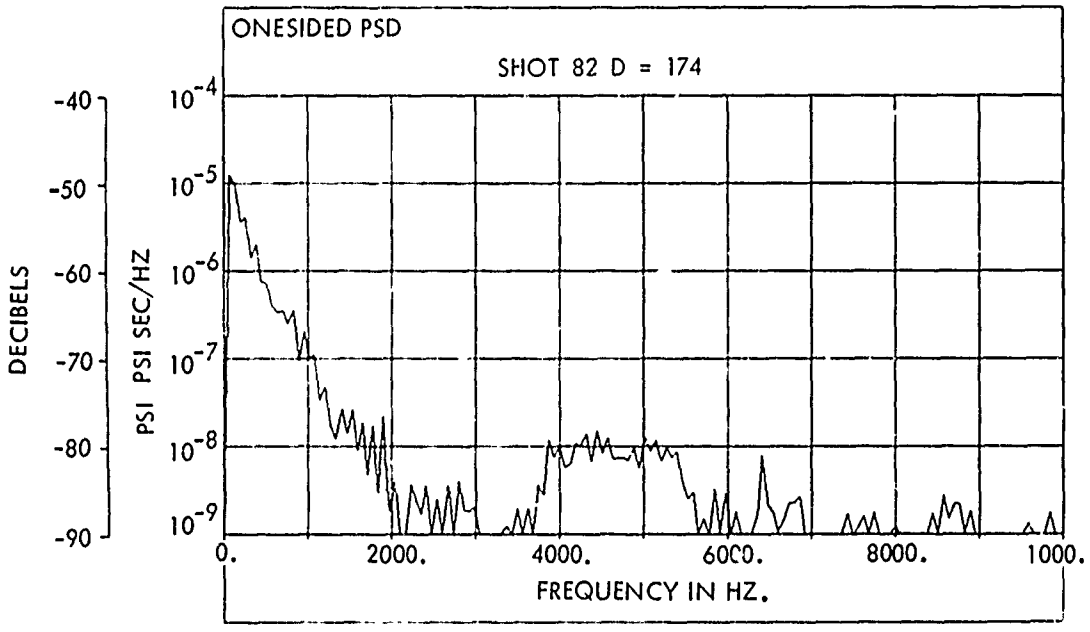

FIG. 12
POWER SPECTRAL DENSITY

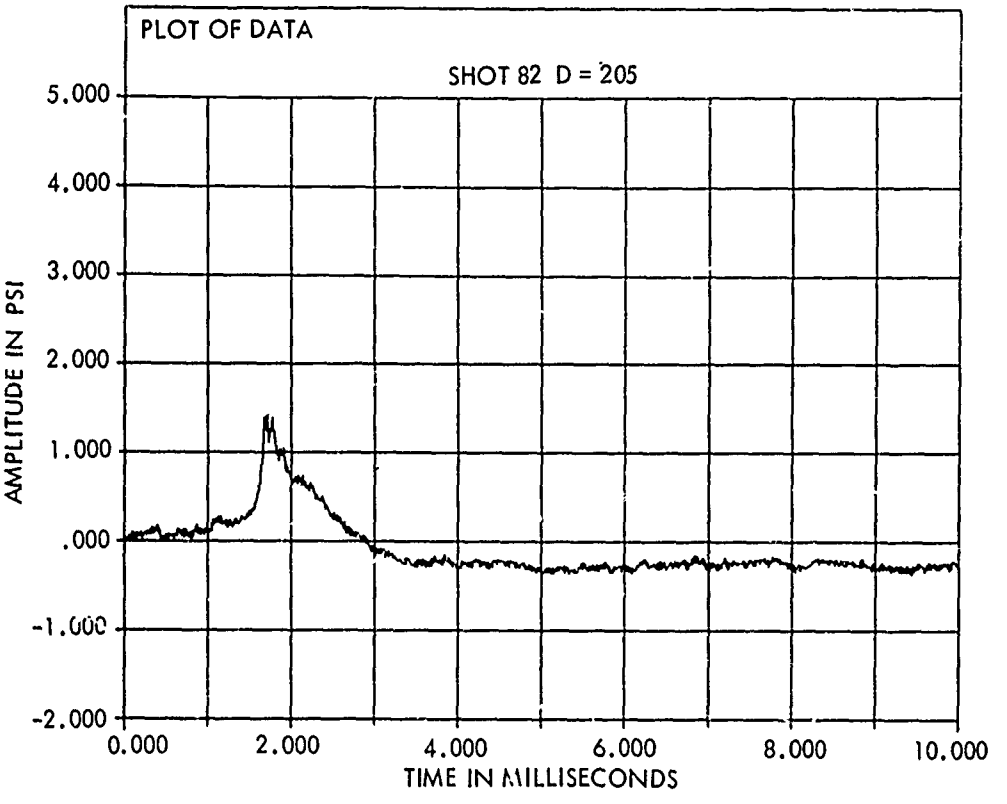

FIG. 13

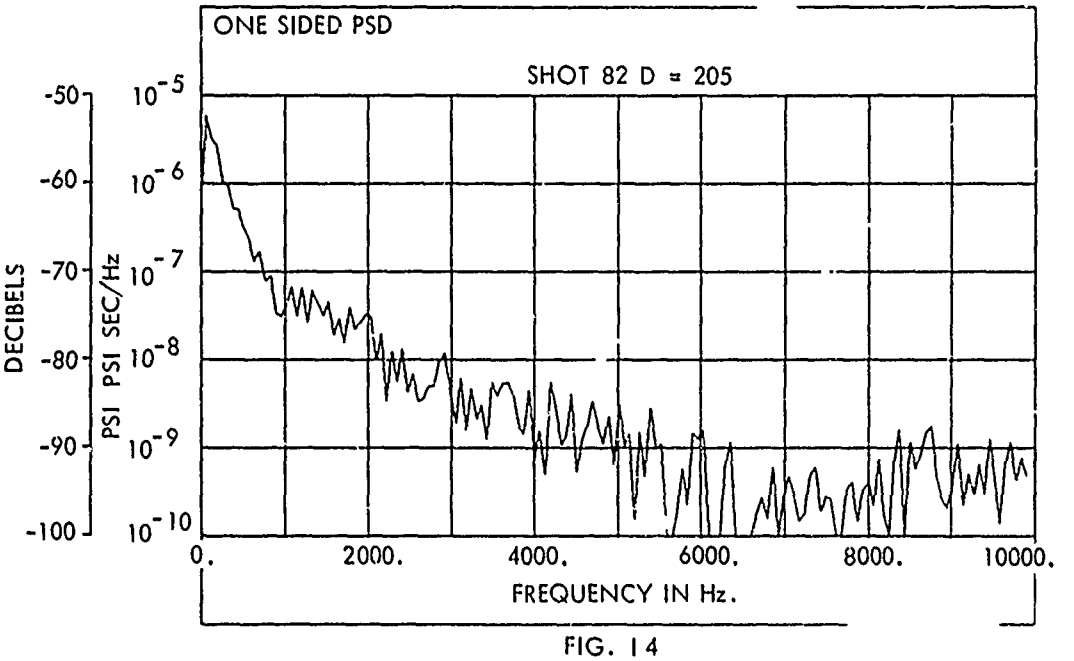

FIG. 14
POWER SPECTRAL DENSITY

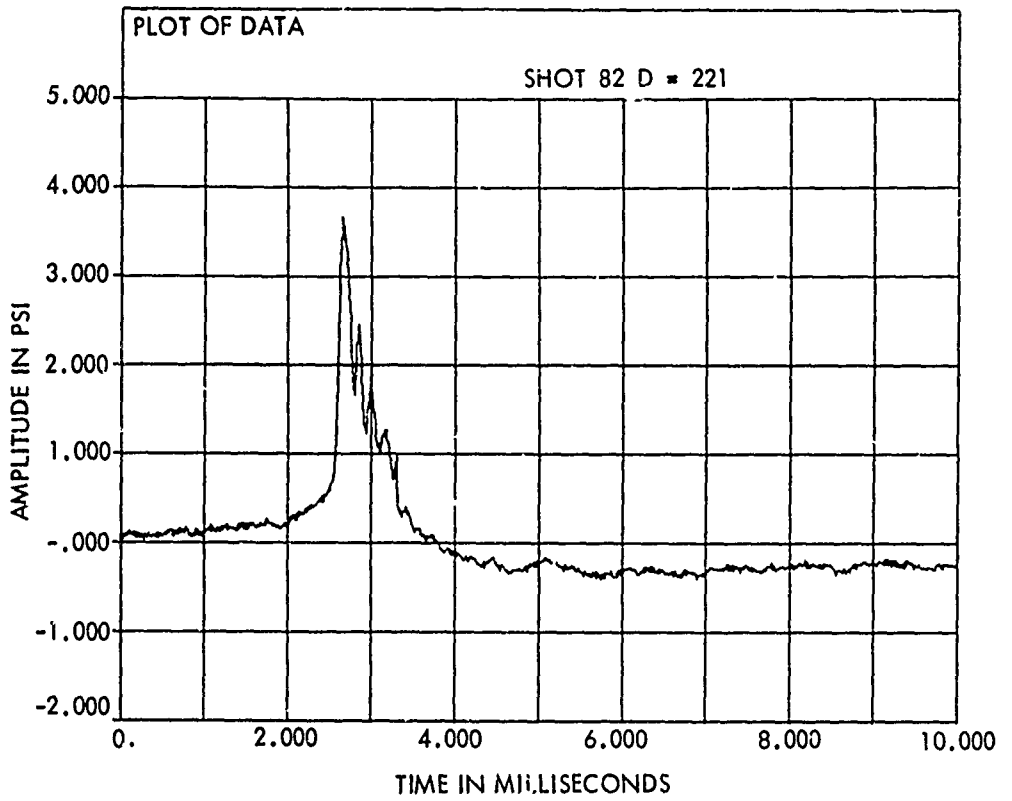

FIG. I 5

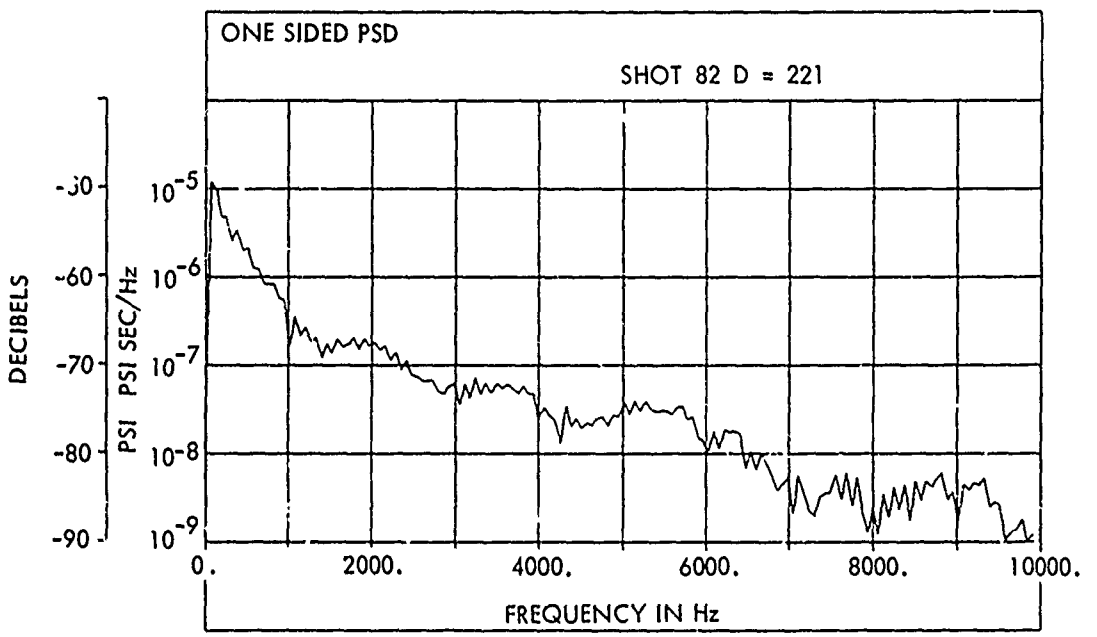

FIG. I 6
POWER SPECTRAL DENSITY

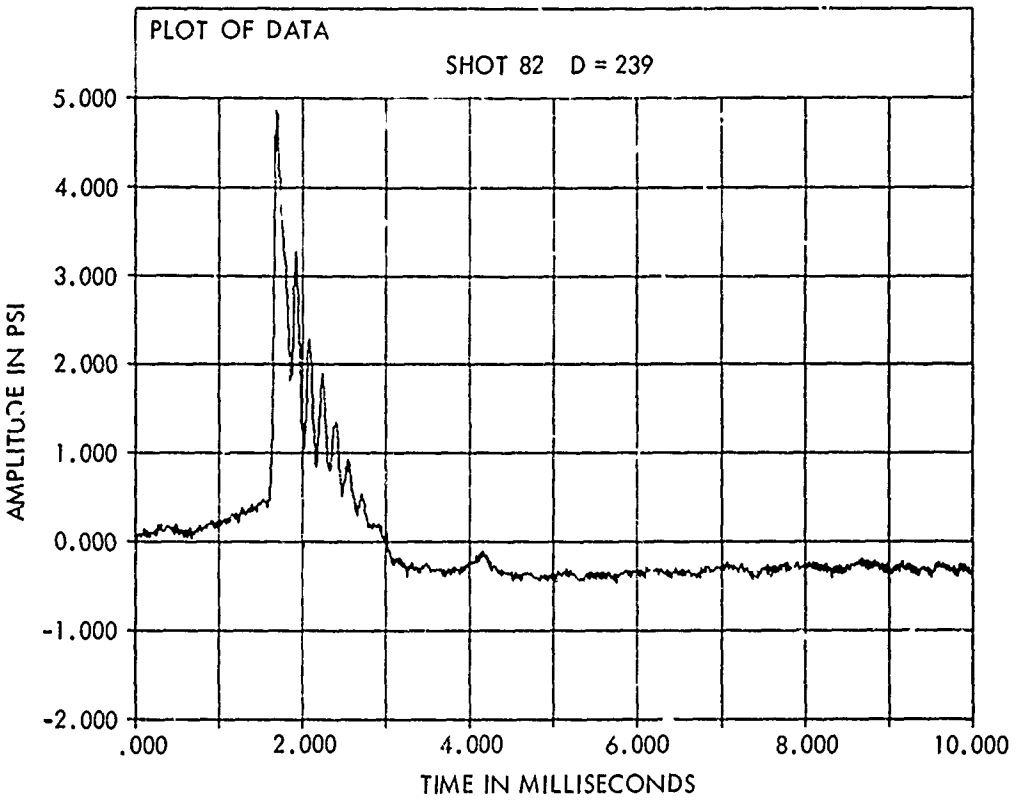

FIG. I 7

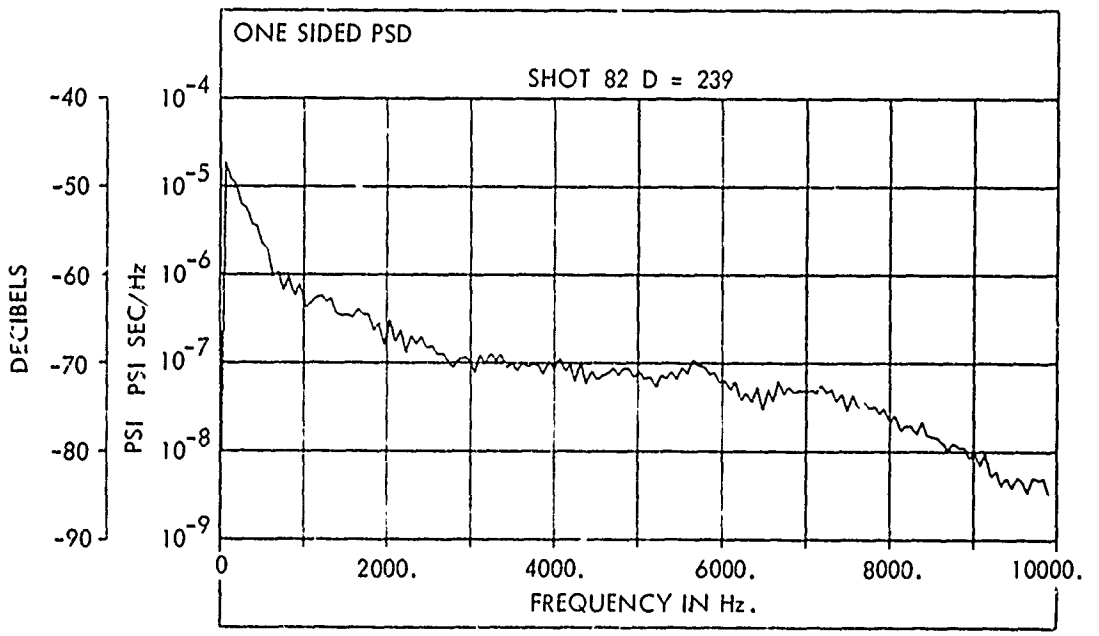

FIG. I 8
POWER SPECTRAL DENSITY

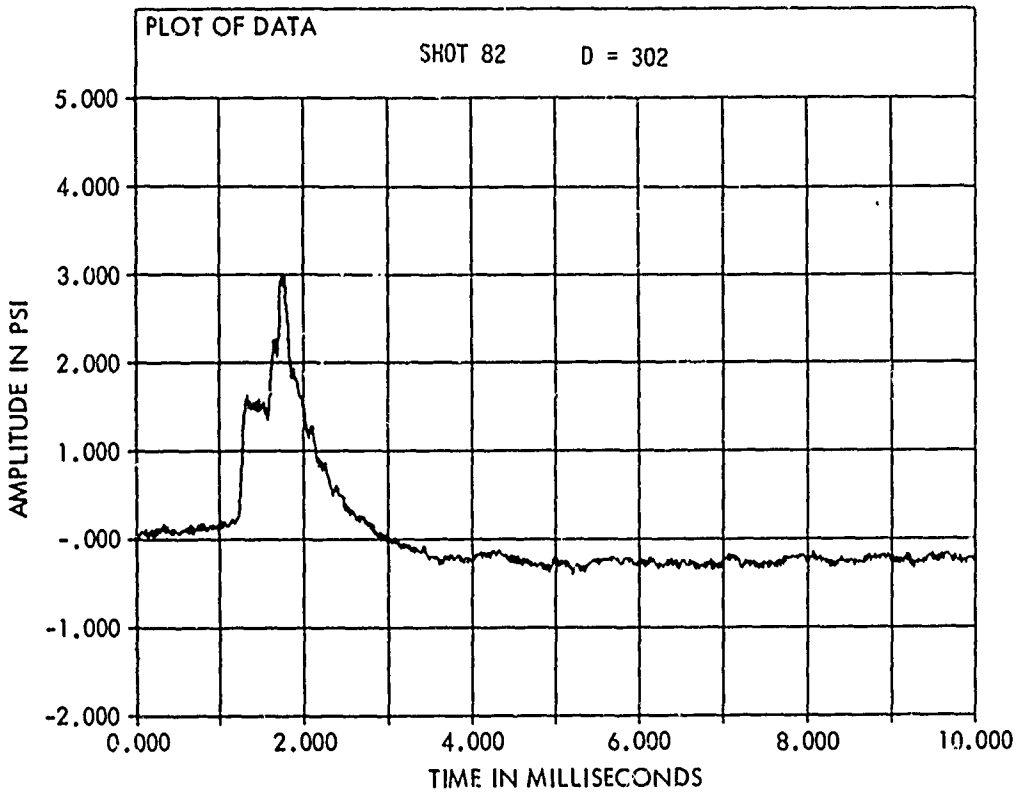

FIG. I 9

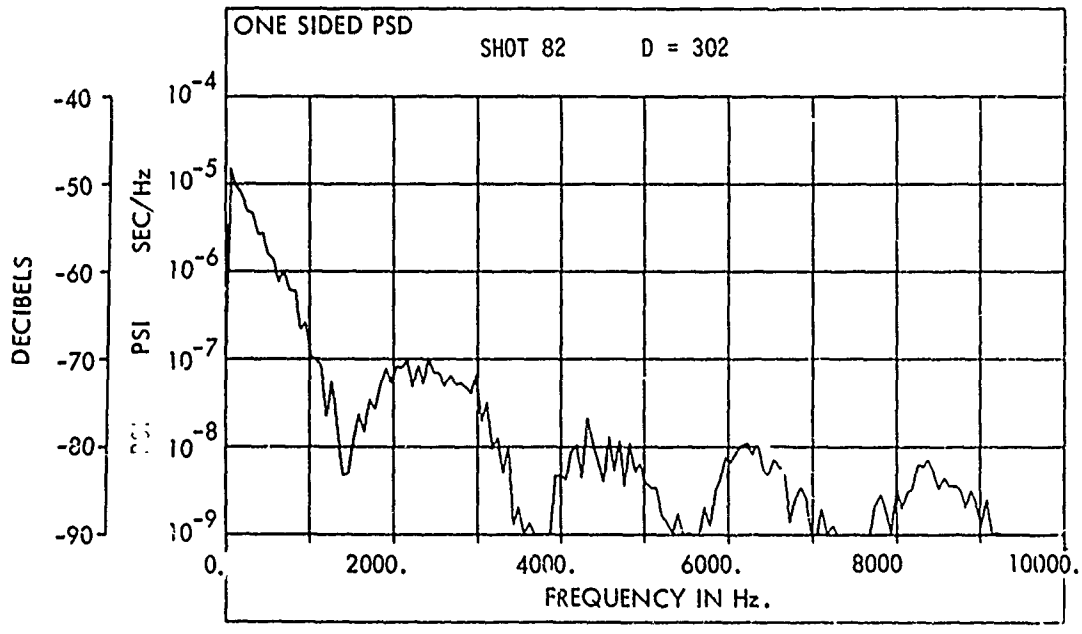

FIG. I 10
POWER SPECTRAL DENSITY

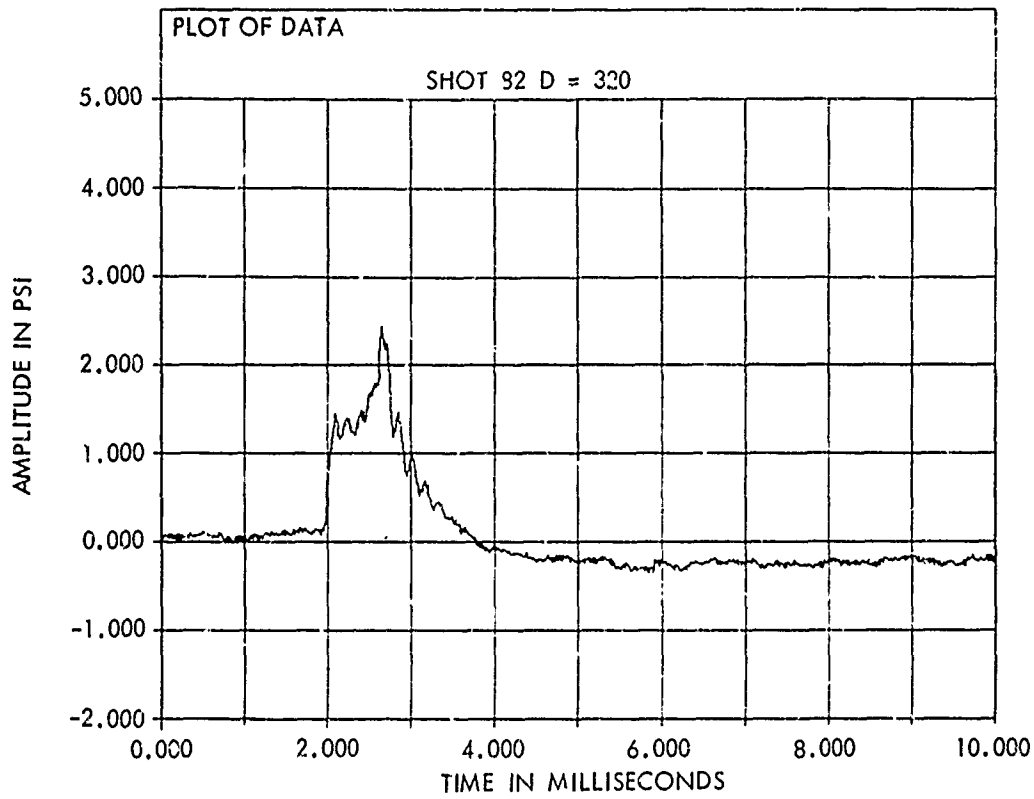

FIG. I 11

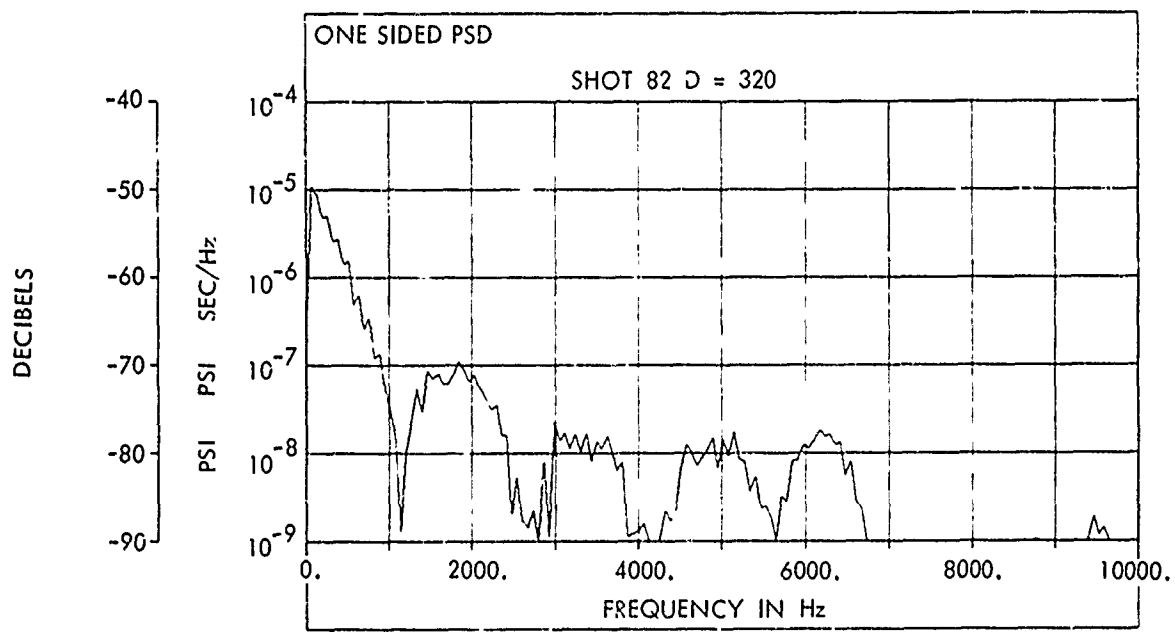

FIG. I 12 POWER SPECTRAL DENSITY

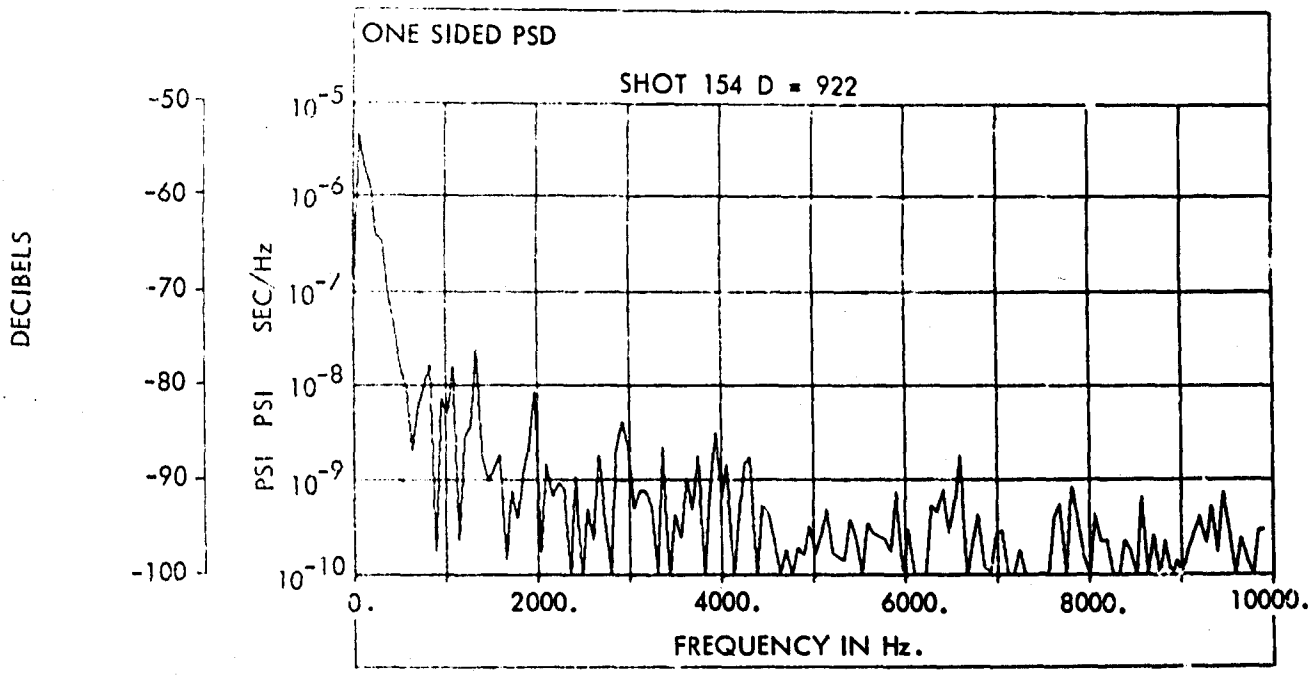

FIG. I 13

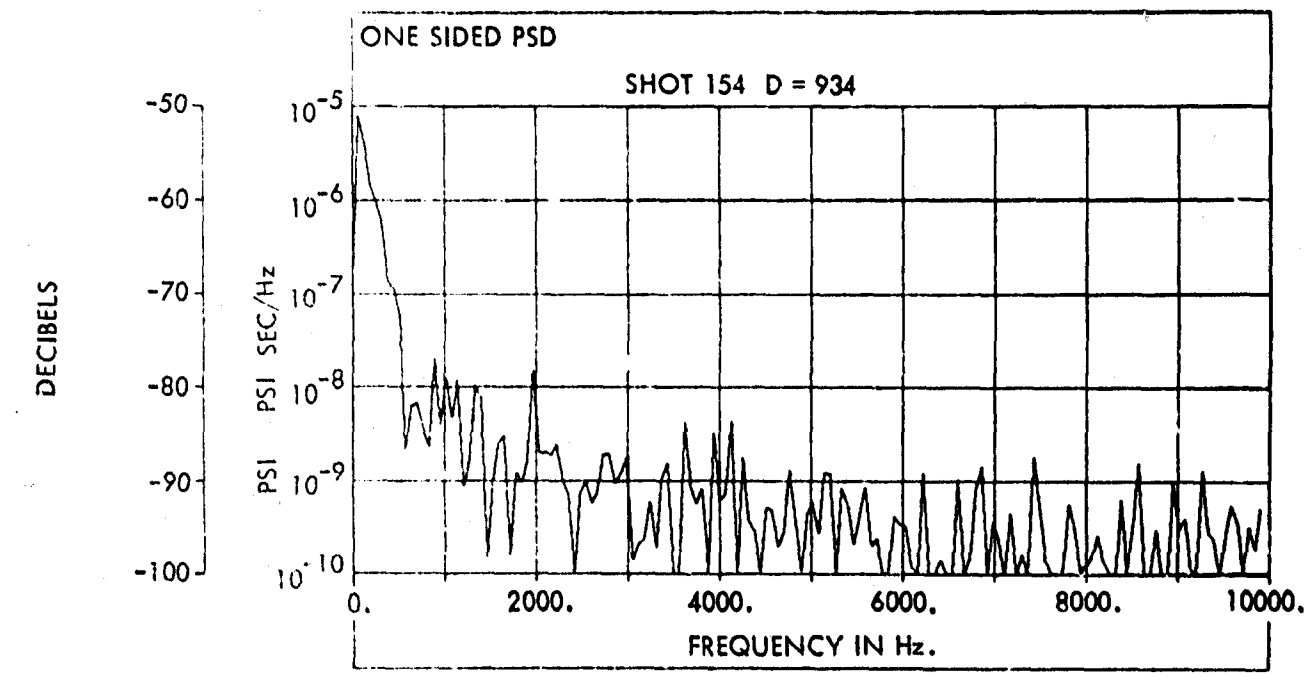

FIG. I 14

POWER SPECTRAL DENSITY

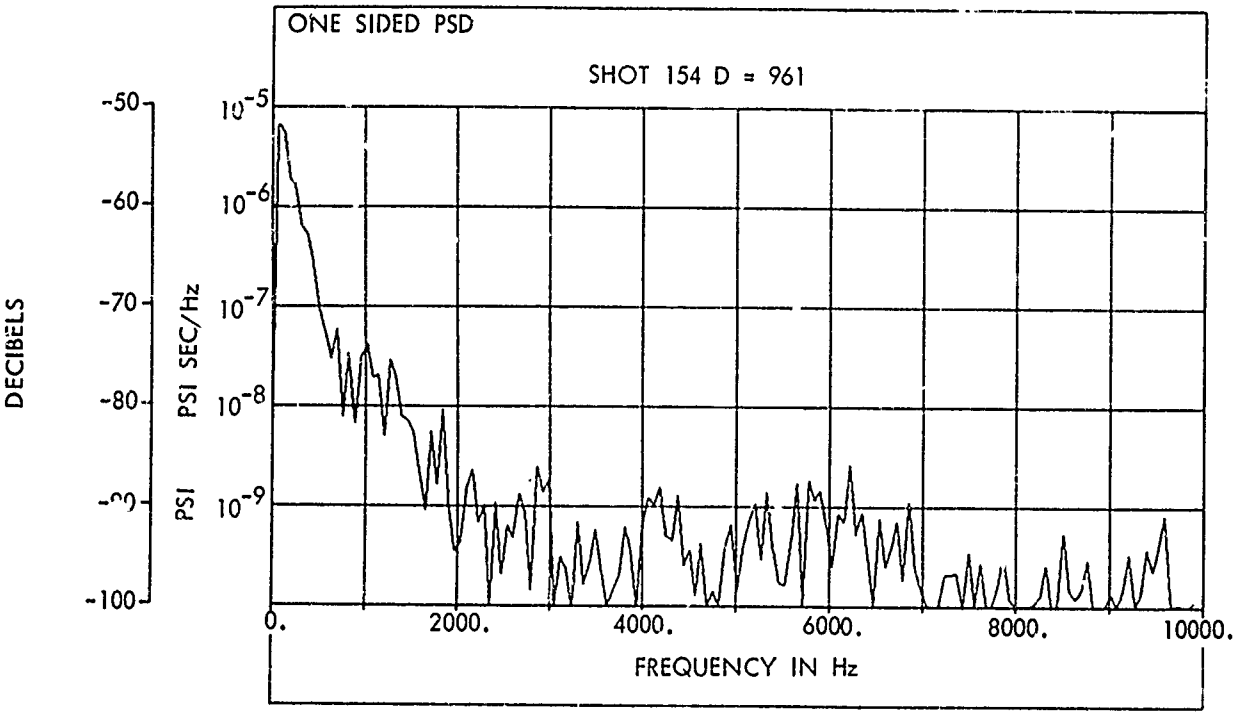

FIG. I 15

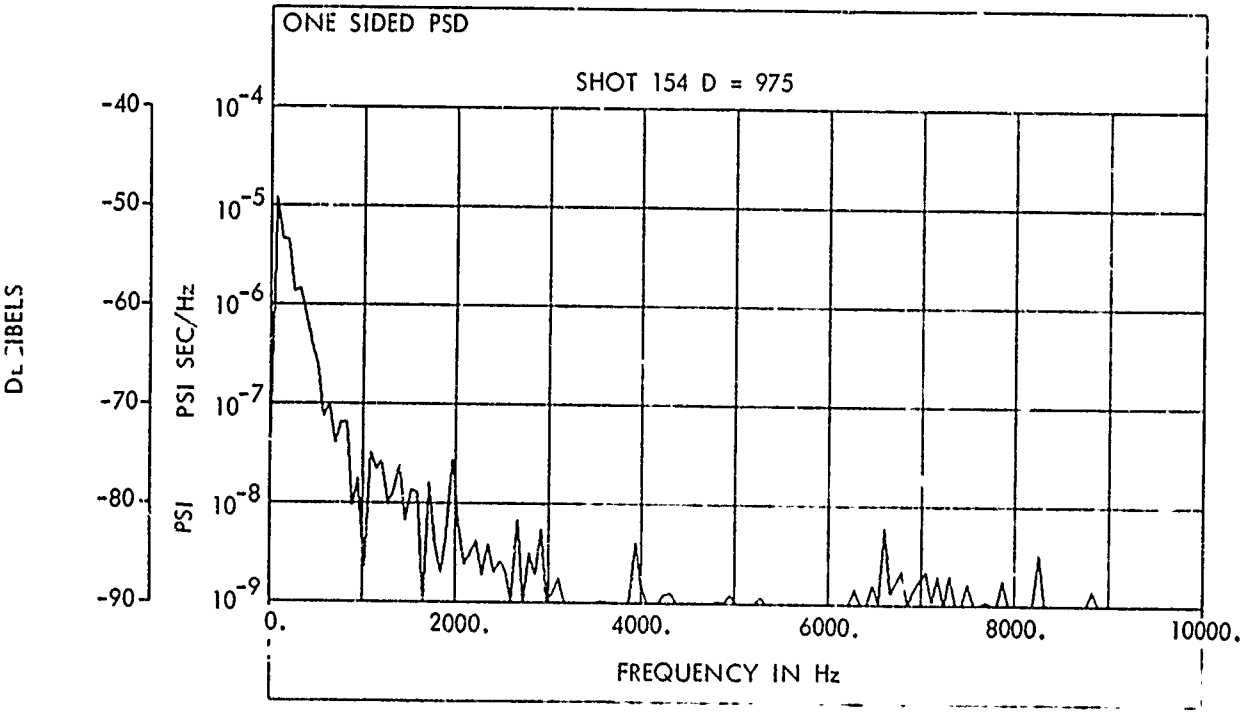

FIG. I 16
POWER SPECTRAL DENSITY.

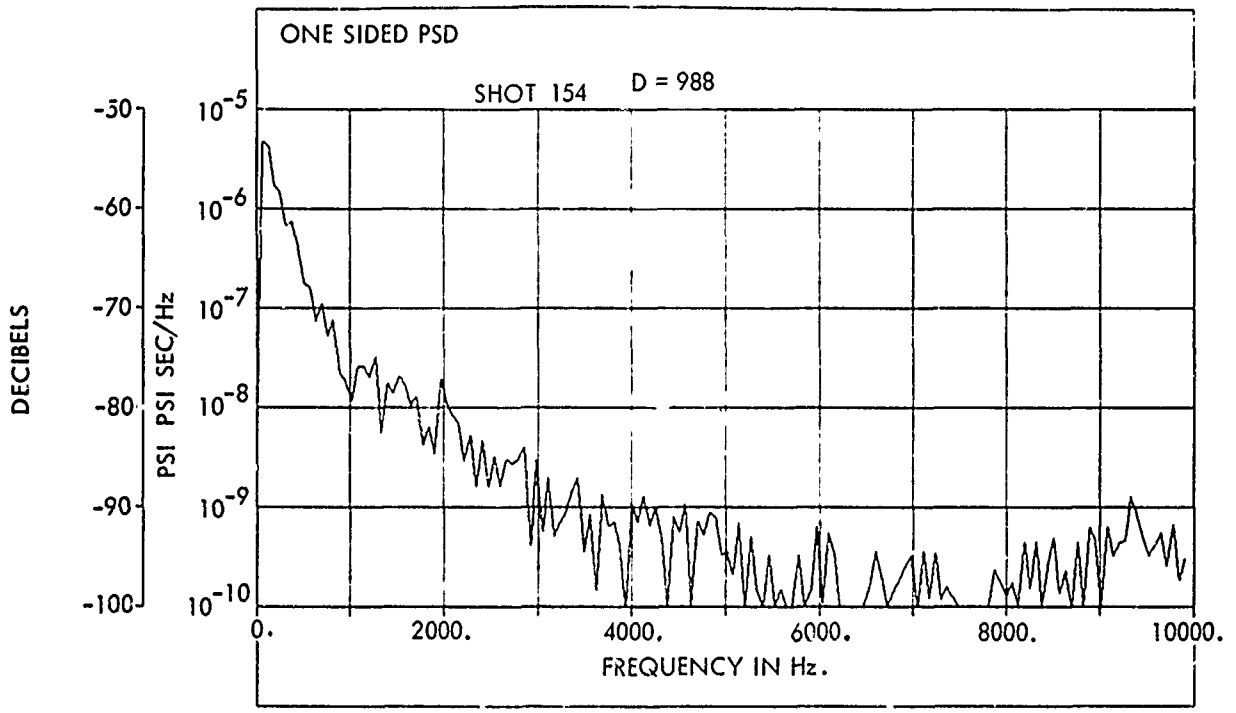

FIG. 117

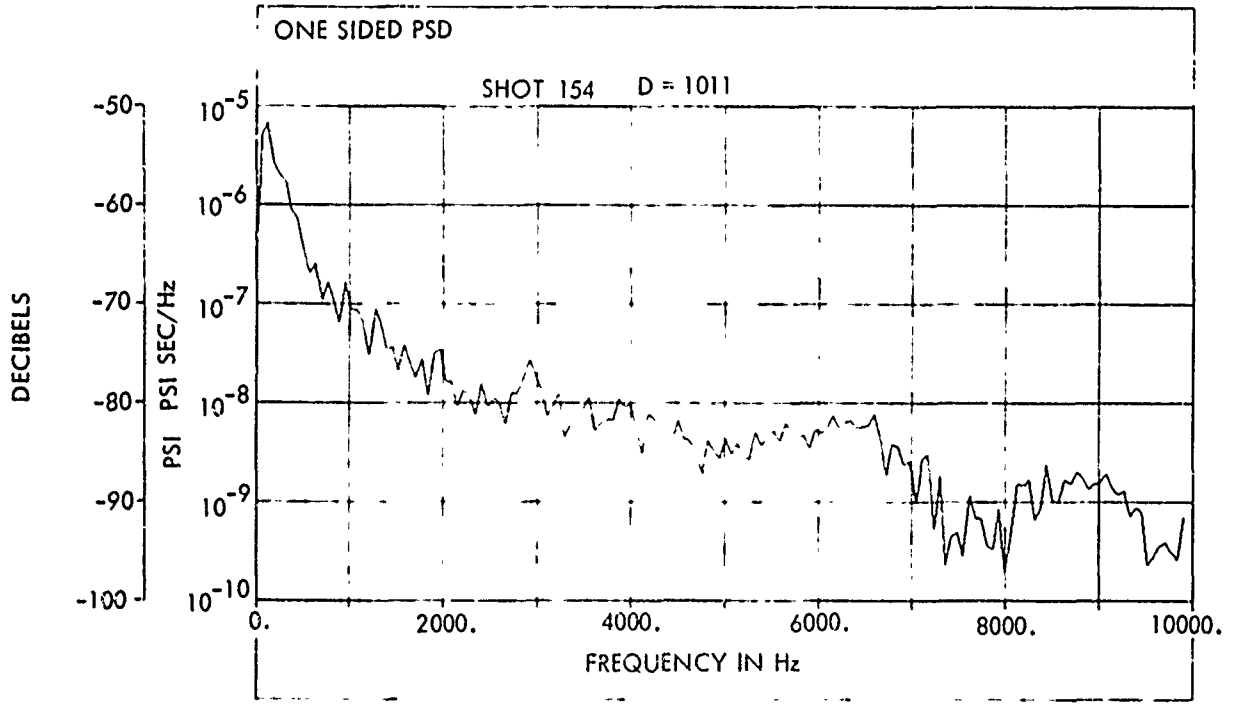

FIG. 118

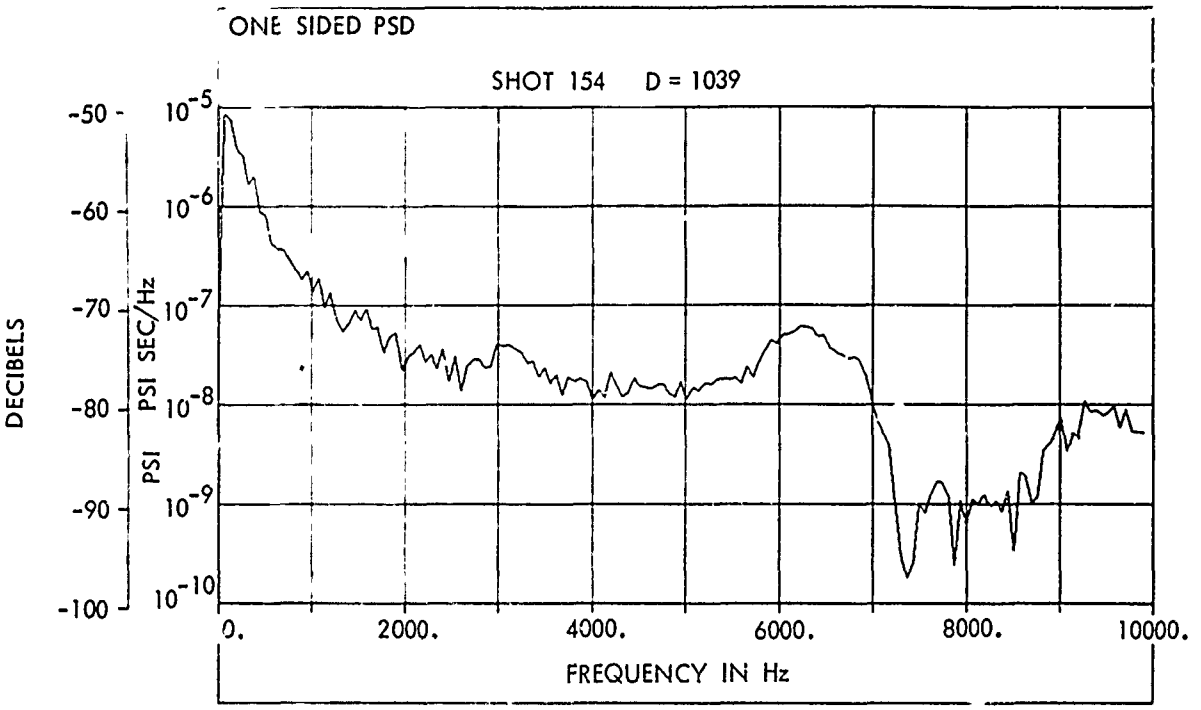

FIG. 119

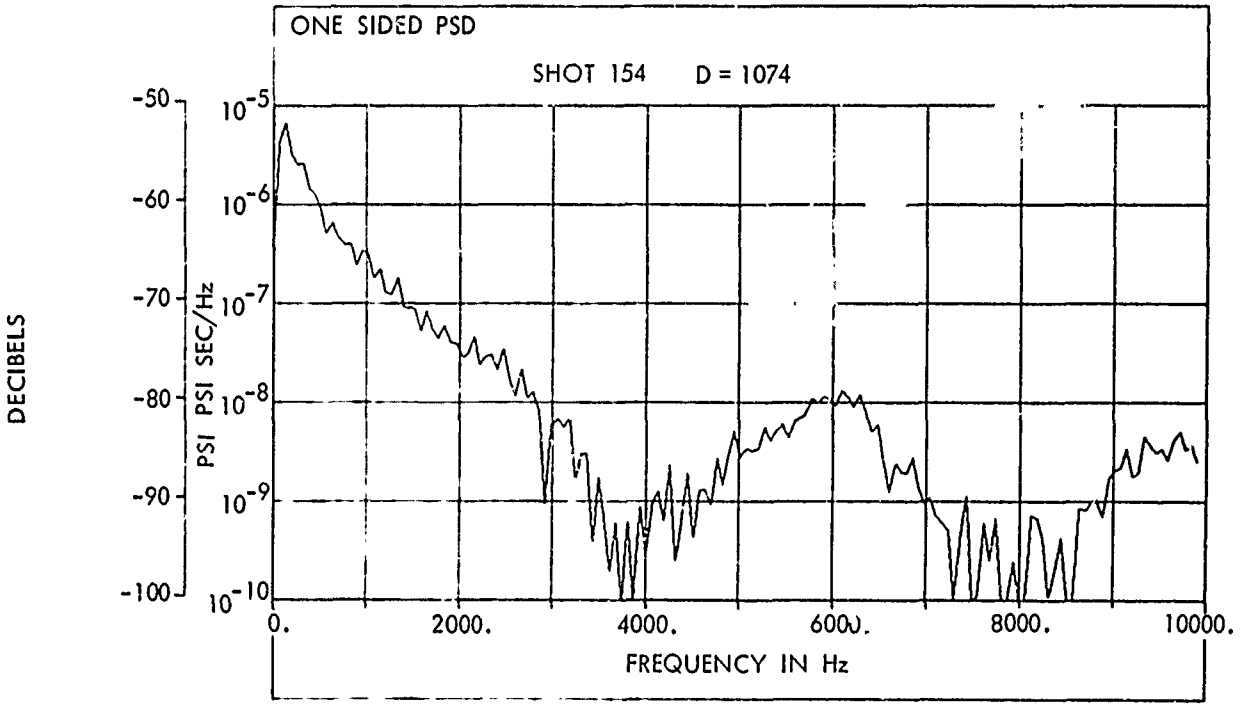

FIG. 120

POWER SPECTRAL DENSITY

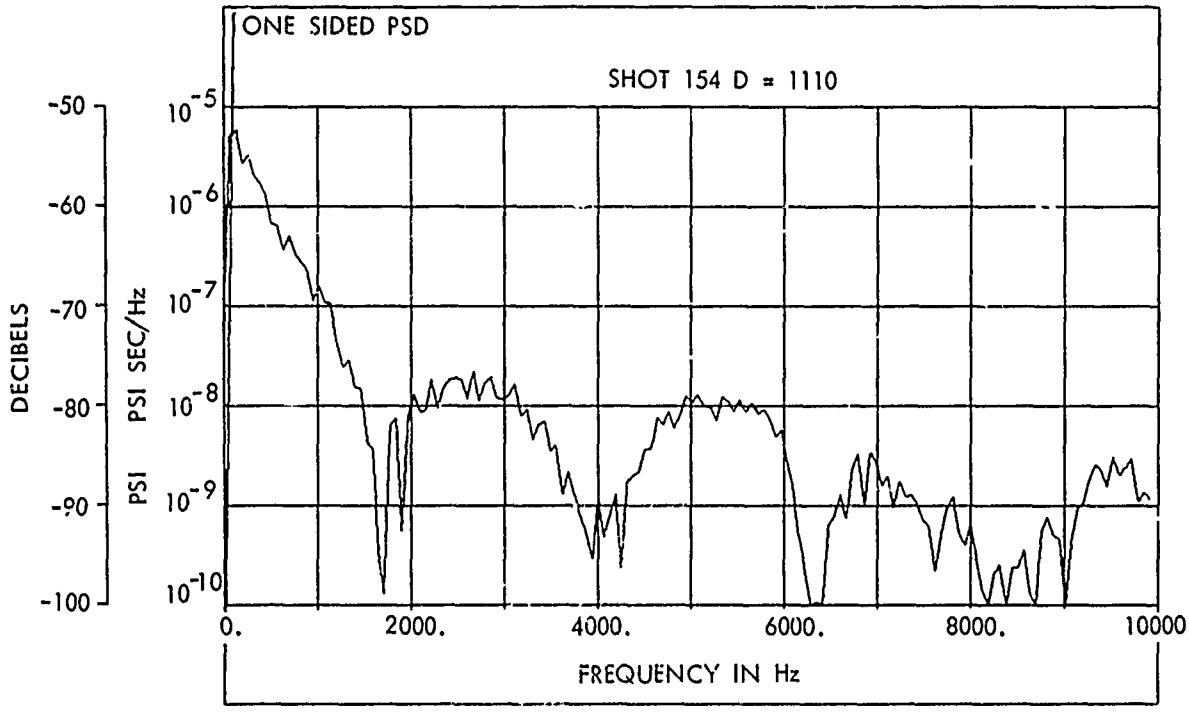

FIG. I 21 POWER SPECTRAL DENSITY